THE ROLE OF PROBABILITY DENSITY FUNCTIONS IN TURBULENT REACTING FLOWS

Pierre Q Gauthier

A Thesis
in
The Department
of
Mechanical Engineering

Presented in Partial Fulfillment of the Requirements
for the Degree of Doctor of Philosophy at
Concordia University
Montreal, Quebec, Canada

May 1996

ISBN 0-612-18391-2

ABSTRACT

The Role of Probability Density Functions in Turbulent Reacting Flows

Pierre Q. Gauthier, Ph.D.
Concordia University, 1996

Computational Fluid Dynamics, for combustion related problems in industry today, is limited to very simple chemistry models due to the size and complexity of the geometry's involved. With these simple models very little quantitative information about the details of the combustion phenomena can be obtained, only general patterns can be found. To investigate important problems such as lean blow-out, engine knock (auto-ignition) and pollutant formation, the details of the chemical kinetics of each individual reaction must be taken into account. Since virtually all combustion related problems are turbulent, the effects of this turbulence must be introduced into the modeling of the chemical kinetics. Probability density functions (pdf's) are used to model the statistical nature of the turbulence in the chemical kinetics. The most accurate method of obtaining the pdf's for this purpose is to solve a modeled transport equation for the pdf, however, very computing intensive Monte Carlo methods are needed for the solution of these equations. An alternative is to assume, a priori, the shape of the pdf and proceed with the calculations. Although this approach is computationally very simple and

requires no extra memory, the trade off is loss in accuracy. New methods are currently being developed to bridge the gap between these two methods. These new methods are far more practical for industrial applications since they require the solution of only one extra equation, which has a very similar form to the existing turbulence equations and can, therefore be easily solved along with the rest of the flow equation. What is missing from the literature, however, is a study of the effects that modifications to the pdf's have on the chemistry calculations under various flow conditions. In the present work a two dimensional, axisymmetric, finite element, turbulent combustion solver has been developed for such a numerical study. The goal of this study is to determine the conditions under which modifications to the assumed pdf become important and when they are not.

ACKNOWLEDGMENTS

First of all I would like to express my gratitude to my thesis supervisors, Dr. Georges H. Vatistas and Dr. T. Bui, for their guidance, support and patience during the completion of this work.

A special thank you is due to Mr. Andy Brankovic of Pratt & Whitney Florida. Through many discussions, and much collaboration, the main ideas of this thesis were first brought out and investigated. The time I spent as member of the CFD group at Pratt & Whitney Canada was also very valuable in making this research very relevant and directly applicable. For these reasons, thanks are due to Dr. M. P. Robichaud, as well as to Mr. M. Peeters. The Turbulent Combustion code developed for the present work was built upon a highly accurate and robust laminar flow solver developed by Dr. Guido Baruzzi. I also owe Dr. Baruzzi many thanks for his help, suggestions and many fruitful discussions.

A special mention should be reserved for my colleagues and students in the Mathematics and Mechanical Engineering departments at Concordia University. Their never-failing faith and support has been a true inspiration to me through the years.

Finally, this work is dedicated to my two sons, Nicolas and Daniel.

TABLE OF CONTENTS

LIST OF FIGURES

LIST OF SYMBOLS

c_v - Specific heat at constant volume

c_p - Specific heat at constant pressure

C_1 - Turbulence model constant

C_2 - Turbulence model constant

C_μ - Turbulence model constant

Da - Damkohler number

D_h - Hydraulic diameter

e - Total energy

F - Balancing term in second order formulation (pressure)

g - Enthalpy variance

G - Balancing term in second order formulation (velocity)

H_o - Total stagnation enthalpy

I - Intermmitancy factor

J_{ij} - Flux vector

k - Turbulence kinetic energy

L - Characteristic length scale

L_o - Turbulence length scale

M_i - Molar mass of species I

N - Number of species participating in a reaction

N_i - Linear shape functions

P	-	Pressure
P_k	-	Kinetic energy source term
Pr	-	Prandlt number
Pr_t	-	Turbulent Prandlt number
Re	-	Reynolds number
Re_t	-	Turbulent Reynolds number
Sc	-	Schmidt number
Sc_t	-	Turbulent Schmidt number
t	-	Time
T	-	Temperature
u	-	Axial component of velocity
v	-	Radial component of velocity
w	-	Swirl component of velocity
y^+	-	Dimensionless wall coordinate
Y_i	-	Mass fraction of Species i

Greek Symbols

α	-	Probability density function parameter
β_1	-	β- Probability density function parameter
β_2	-	β- Probability density function parameter

δ_{ij} - Kronecker delta

Δh_i - Enthalpy of formation of species i

ε - Dissipation of turbulence kinetic energy

γ - Ratio of specific heats

ϕ - General field variable

Γ - Dissipative terms

κ - Von Karman's constant

λ - Relaxation factor

μ - Molecular viscosity

μ_t - Turbulent viscosity

ν_t - Turbulent kinematic viscosity

ρ - Density

σ_{ij} - Total stress tensor

τ_w - Wall shear stress

Ω_{je} - Element domain

ω - Specific dissipation of turbulence kinetic energy

ζ,η - Natural coordinates

CHAPTER 1

INTRODUCTION

Combustion research is motivated by several practical considerations including the quest for more efficient utilization of limited fossil fuel reserves, the introduction of air quality standards backed up by increasingly strict air pollution legislation and the high human and financial costs of accidental fires and explosions. Because of these concerns automobile manufacturers, power generation companies, those involved in the extraction, transportation and storage of fossil fuels, legislators and many others all require and use more or less sophisticated theoretical models of combustion processes. While existing theoretical models have already been found to be useful in all of these applications discerning users find inevitable shortcomings in their performance.

Another strong motivation for the study of combustion comes from the range and complexity of the phenomena which can occur. Practical combustion systems almost always involve turbulent flow. Combustion chemistry and turbulent flow each introduce a range of length and time scales. The spread of these scales is typically so wide that the direct numerical simulation (DNS) of most practical engineering problems by solution of the complete set of equations with full spatial and temporal resolution will

remain impracticable for the foreseeable future. On the other hand DNS can be applied to idealized problems of turbulent combustion and can provide valuable guidance for the development of engineering models like the one presented here.

Consequently most models of turbulent combustion for industrial application use and must continue to use equations which are averaged in a manner similar to that introduced by Osborne Reynolds. Combustion problems typically involve sets of transport equations for scalar variables such as enthalpy and species concentrations, in addition to the equations of motion. The averaging procedure generates unknown Reynolds flux terms, which must be modeled alongside the Reynolds stresses, and which represent the process of turbulent transport or large scale macro-mixing due to the entrainment in turbulent eddying motions.

Instantaneous rates of chemical reaction are highly non-linear functions of composition and temperature and the determination of average values presents a particular problem. Chemical reactions occur at the molecular scale as a result of inter-molecular collisions. Consequently microscale mixing of reactive species is a prerequisite to chemical reactions. Small scale mixing of both composition and temperature variables occurs as a result of molecular diffusion processes and is closely linked to the scalar dissipation terms in the

transport equations for the variance of scalar variables. These terms therefore play an important role in most theoretical models of turbulent combustion.

1.1 Objectives and Overview of the Thesis

The objective of this thesis is the development of a finite element based methodology applicable to the solution of turbulent fluid flows with chemical reactions. In particular, it is intended to demonstrate and compare the effects that two different approaches of using probability density functions have in the calculation of the mean reaction rates of each individual reaction taking place in the given problem. The mathematical model used to describe the fluid flow is the compressible Navier-Stokes equations for multi-component gases along with an energy equation, species equations and chemical kinetic rate equations. Only hydrogen-air mixtures are considered for this comparison study, although one test case presented uses town gas, a derivative of natural gas. The motivation for choosing a hydrogen-air mixture was twofold. In the search for alternatives to our limited supply of hydrocarbon fuels hydrogen has become the most promising new fuel due to its natural abundance and availability. Also, the present work focuses on finite rate chemical reactions and, to date, there are no reaction mechanisms for hydrocarbon fuels used today that are simplified, or reduced, enough to be

handled effectively by today's computers. Two-equation turbulence models are employed for the simulation of turbulent fluid motion in conjunction with the Reynolds averaged Navier-Stokes equations. Another objective of this work was to create a methodology that can be utilized in an engineering environment yielding the most information from the flow field while minimizing the computational time and memory. Each set of equations was solved in a segregated fashion allowing for optimal use of computing resources. Although this results in a slight trade off in speed, since the energy portion of the solver was uncoupled from the Navier-Stokes solver thus resulting in a numerical lag in the density calculations, the resulting savings in memory and solution flexibility make up for this. Computational resource is the most important limitation to the numerical fluid dynamicist. During the last decade, the cost of high speed computing has dramatically decreased since the introduction of the CRAY 1 in the late 1970's, a computer with 10 million floating point operations per second, or 10 Mflops, and with 8 megabytes of memory which cost $15 million. Current workstations perform at up to 25 Mflops and have a minimum 8 megabytes of memory and now cost only $15,000. Projections over the next decade give ever increasing performance for less cost. These cost reductions in computing will help justify the increased use of computational fluid dynamics in designing products. Despite the availability of such workstations

today and the glowing predictions of computing powers in the future, the present computing need of combustion engineers in industry are still far from being satisfied. With the complexity of combustor geometry's and the ever growing need to understand phenomena such as soot and pollutant formation, efficient use of current numerical methods run on today's computing facilities must be a top priority.

The main objective of the present work is to perform an evaluation of a numerical approach to combustion problems currently being developed, so that it may be used most efficiently on industrial scale problems with today's computing power. It has been known for some time that probability density functions can play a very useful role in predicting the behavior of highly statistical phenomena, however their implementation in everyday combustion computational fluid dynamics has yet to be established as a working tool for large industrial problems. The goal of this thesis is to study how different forms of probability density functions influence the resulting calculations and over which ranges of flow conditions does the choice of probability density functions have the most influence. Armed with this information, numerical methods can be developed in which the most efficient form of a probability density functions can be assumed beforehand and used under the given flow condition. As a particular industrial application to focus on, the formation of nitric oxides (NOx) was chosen.

This is a very important consideration given today's concern for the environment and the impact that pollution has on it. The formation of NOx will be calculated as a post processing exercise, completely uncoupled from the rest of the flow equations, since the production of thermal Nox has a negligible effect on the rest of the chemistry of the reacting system. In this way the effects of the probability density functions on the NOx mechanism's reaction rates can be studied for a wide variety of flow conditions.

The rest of chapter 1 presents a background of numerical approaches and considerations when dealing with combustion problems.

Chapter 2 reviews the application of finite element methods to fluid flow problems. Topics include a discussion and presentation of the form of the equations to be solved and the methods of solving the resulting set of algebraic equations. An overview of the averaging technique used is also given. Details of turbulence modeling, specifically the two-equation models used in this study, are given with a presentation of the numerical treatment of solid walls. A list of boundary conditions as well as the wall functions used to complete the turbulence modeling is also presented. A description of the special transition wall logarithmic elements is also provided. The combustion models used in the present work are then described. The very simple Eddy break-up (EBU) model is first presented then the finite rate chemistry equations and kinetic mechanisms are shown. Chapter 2 concludes with a

discussion on reduced kinetic mechanisms and a listing of the mechanisms solved for in the present work and focus then given to the calculation of Nox formation. An introduction of the problems of NOx formation is given then the mechanism used to compare the different pdf approaches is presented. Chapter 3 deals with all of the numerical aspects of the present work. The nondimensionalization of the flow variables is first discussed and the nondimensional form of the equations is presented. The Galerkin finite element approach used to solve all of these equations is then presented. The various types of boundary conditions used for Navier-Stokes, energy and species equations are discussed. The boundary conditions and inlet conditions chosen for the turbulence models is also discussed and presented. Finally, chapter 3 concludes with a detailed discussion of the solution strategy employed to solve the complete reacting flow problem. Numerical methods used to insure stability and accuracy of the solutions are also presented. Chapter 4 introduces the concept of probability density functions and discusses the various approaches in implementing these functions in reacting flow problems. The particular approach of assumed pdf's is discussed in detail along with the presentation of the algorithm used to modify the shapes of these pdf's. Chapter four concludes with a brief discussion of some of the numerical considerations involved in the implementation of the pdf methods.. Chapter 5 lists the results obtained during the present

research. As the finite element flow solver progressed from a simple laminar code to its final version as a multi-species, multi-step, turbulent reacting flow solver, each step in the development was followed by comparison with experimental results to insure that each new model was performing properly. Computational benchmarks like channel flow and flow over backwards-facings step were used to validate the turbulence models. Once the turbulence models were working well results are shown for the simple one-step EBU combustion model using town gas as a fuel. This step was performed to make sure that the chemistry portion of the code was working well. Finally results are given for the multi-step hydrogen air mechanism in which a comparison is made between two pdf approaches used to calculate the reaction rates for each of the steps. Then a similar comparison of pdf's is presented for the NOx postprocessor. Chapter 6 presents the conclusions and recommendations drawn from this comparison study.

1.2 Combustion Regimes

Attention is restricted to the combustion of gaseous fuels which may either be premixed with gaseous oxidizer or alternatively fuel and oxidizer may be supplied separately to form a non-premixed, or diffusion flame.

Combustion and turbulent motion can interact with each other in various ways. Several regimes of turbulent combustion may be identified. In low Mach number flows these regimes are usually described in terms of two parameters which may for example be characteristic values of turbulence Reynolds number 'Re' and Damkohler number 'Da', the latter being defined as the ratio of a turbulence time scale to a chemical time scale. If chemical times are long in comparison with the largest time scales of the turbulent flow, burning takes place in a distributed reaction regime in which the flame structure is influenced mainly by turbulent mixing and chemical reaction. This situation is relatively common in industrial applications .

The other limit, where the longest chemical time scale is shorter than the smallest time scale of the turbulence, leading to so called laminar flamelet combustion, can also be achieved in many practical situations. Here burning takes place exclusively in thin laminar flames whose structure is determined by a balance between molecular transport and chemistry. Such laminar flames are convected and distorted by the turbulent flow. Between these two limits lies a transition regime where the two sets of time scales which describe turbulence and chemistry, respectively, overlap. High and low Reynolds number regimes may also be identified.

1.3 Hierarchy of Approaches

We now identify, in brief outline only, a variety of different approaches to the problem of the prediction of turbulent reacting flows, starting with the most exact (but too computational-intensive) and ending with more approximate but less expensive methods.

Methods which resolve turbulent fluctuations include:

(i) Direct Numerical Simulation (DNS)

All length and time scales associated with both the turbulent flow and the chemical reactions are fully resolved. However the computing requirements are so severe that problems which can at present be solved involve simplified geometry's and chemical reactions schemes. In order to reduce the range of length and time scales, solutions are now restricted to very low values of Re and Da numbers.

(ii) Large Eddy Simulations (LES)

Spatial filtering is applied to the governing equations in such a way that large scale eddying motions are retained while smaller scales are averaged. Sub-grid scale turbulence must therefore be modeled. Chemical reaction occurs at the molecular scale so mean reaction rates must be modeled as well.

(iii) Random Vortex Methods

This is a Lagrangian approach in which turbulence is represented by a random distribution of discrete vortices of finite strength. The cores of these vortices are described empirically. A simple application is to the propagation of reaction sheets in turbulent flows.

Other methods involve the solution of averaged equations in which the effects of turbulent fluctuations are treated in a statistical manner:

(iv) Probability Density Function (PDF) Methods

Using the usual set of conservation equations an exact transport equation may be derived for the joint pdf for a set of scalars such as species mass fractions. The chemical reaction terms in this equation can be evaluated without approximation. However, the equation contains no scale information, so terms describing transport in scalar space due to molecular diffusion require modeling. If velocity components are included as arguments to the joint pdf, turbulent transport is described without modeling, but pressure fluctuation terms must then be modeled.

(v) Second Moment Closure Methods

In these methods the averaged transport equations are solved for first moment mean quantities such as density ρ, velocities u_i and mass fractions

Y_i. The unknown Reynolds stresses and Reynolds fluxes are then obtained from their own transport equations. Models are required for some terms in these equations and for mean chemical source terms.

1.4 Application of the PDF formalism to Jet Diffusion Flames

In moment closures averaging leads to a loss of information with the consequence that various unknown terms, dependent on the fluctuating turbulence field, appear and closure approximations are needed to represent them. In turbulent flames the processes for which closure approximations are required include turbulent transport (diffusion) of heat, mass and momentum and turbulence-chemistry interactions. For turbulent transport, a turbulence model is required but it is the turbulence-chemistry interactions which represent the central difficulty in turbulent flames. More specifically, in moment closures a means must be available to evaluate the average net formation rates which appear in the transport equations for the mass fraction of each chemical species present. If the assumption of 'fast' (Da >>1) reaction can be invoked, then the thermo-chemical state can often be determined uniquely in terms of a single independent scalar variable. In these circumstances it is possible to presume a suitable shape for the pdf in terms of the means and variance of the appropriate scalar with the mean and variance

being obtained from solutions of their respective transport equations. While this approach yields good results in most cases, it is sometimes lacking where chemical reaction rates exert an important influence, for example in the emission of unburned hydrocarbons and formation and emissions of pollutants. In order to reproduce finite rate effects more independent scalars need to be incorporated and a multi-dimensional joint pdf is needed. In this circumstance the presumed shape approach and all of its advantages becomes essentially intractable and the only viable method appears to be the pdf transport equation approach. PDF transport equation modeling is presently being investigated by many researchers and has the potential of becoming a tool for engineering calculations in the future. Due to the large number of variables in a typical joint pdf Monte Carlo type methods must be used to solve their transport equations. In these methods a parallel Lagrangian approach must be developed to simulate the random motion of the fluid particles. To make this method statistically valid many thousands of particles must be used, thus limiting the size and complexity of problems it can handle. The present work offers an alternative in which stochastic methods are used to simulate the effects of turbulent fluctuations while still using assumed pdf's.

1.5 Reduction of Reaction Kinetics for Hydrogen and Hydrocarbon Flames.

The general idea of reducing complex kinetic schemes by the introduction of steady state assumptions has been known to chemists for a long time. However, it has become fruitful for combustion applications only very recently. Steady state approximations for intermediate species can be justified in many different ways. They first were derived for zero dimensional homogeneous systems that depend only on time, and the term 'steady state' was introduced because the time derivative of these species is set to zero. The justification for this approximation is generally provided in physical terms by stating that the rate at which species 'i' is consumed is much faster than the rate by which it is produced. Therefore its concentration always stays much smaller than those of the initial reactants and the final products. Since the concentration always stays small, its time derivative also stays small compared to the time derivatives of the other species. As an example, one may look at the well-known Zeldovich mechanism for thermal production of NO which will be used later in this work. The steady state assumption for species 'i' leads to an algebraic equation between reaction rates. Therefore each of these equations can be used to eliminate rates in the remaining balance equations for the non-steady state species. The stoichiometry of the

resulting balance equations defines the global mechanism between the non-steady state species. Therefore the global mechanism depends on the choice of the reaction rates that were eliminated. The rule is that one should choose for each species the fastest rate by which it is consumed. Although this choice may be arbitrary sometimes, it has no consequences as far as the balance equations for the non-steady state species are concerned. The present work will use such a reduced mechanism for the case of a hydrogen-oxygen mechanism involving only the first 7 reactions. For hydrocarbon flames typically hundreds of elementary reactions are necessary to reproduce the burning velocity over the whole range of equivalence ratios and pressures upto 50 atm with reasonable accuracy. For lean-to-stoichiometric methane flames 'skeletal' mechanism of 25 elementary reactions have shown to yield good results.

CHAPTER 2

EQUATIONS AND MODELS

This chapter reviews the development and the application of the finite element method to the solution of compressible, turbulent fluid flows with chemical reactions. The finite element method is first described as a method for the numerical approximation of partial differential equations. The equations used in the present work are then introduced, including the flow equations, the energy equation, as well as the species equations and the turbulence equations. Details associated with the application of the finite element method to these equations will be discussed in chapter 3. Combustion models and Nox modeling are also discussed.

2.1 Finite Element Method for Fluid Flows

Historically the finite element method was first applied to linear elasticity problems and it has since expanded into many other fields including fluid mechanics. The finite element method when applied to a specific problem can be broken down into the following components: discretization of the domain into elements and selection of interpolating or shape functions to represent the primary unknowns. Next, application of a method for

describing the finite element approximation, such as Ritz method, direct methods or Galerkin weighted residual methods. Assembly of the local elements into a global approximation and application of boundary conditions and, finally, the solution of the resulting system of linearized algebraic equations for the primary unknowns.

The method of weighted residuals is the basis for a large class of approximation techniques used to solve partial differential equations. The method consists of assuming the general functional behavior of the dependent variable in some way so that the given partial differential equation and its boundary conditions are closely satisfied. The use of this method will introduce an error between the exact solution and the solution obtained by using this approximation. This error is commonly called the residual and it is desirable for this residual to vanish in some average sense over the entire domain of the problem. The method of weighted residuals provides a number of ways for choosing the weight functions and each choice of weight function provides a different error distribution principle for the approximation. In the present work, the choice of weighting function is the Galerkin method. This method consists of choosing the weighting functions to be the same as the approximating or shape functions. It may be shown that the Galerkin method produces the same set of integral equations as the application of a variational statement to a set of partial differential equations.

The Navier-Stokes equations in primitive variable form, however, do not have a variational statement. Therefore, the Galerkin method must be employed to derive a set of approximating equations.

The partial differential equations that are of interest in this work are the equations which describe the conservation of mass, momentum and energy. Also needed are the equations conserving the mass fraction of each species participating in a reaction and an extra equation describing the enthalpy variance of the flow field is also presented.

2.2 Equations

2.2.1 Conservation of Mass and the Navier-Stokes Equations

The velocity and pressure fields are governed by the full Navier-Stokes equations which, on their own, are sufficient to describe the entire physics of fluid flow. The conservation of mass or continuity for a general compressible, steady, fluid in axisymmetric form is given by:

$$\frac{\partial(\rho u)}{\partial x} + \frac{1}{r}\frac{\partial(r\rho v)}{\partial r} = 0 \qquad (2.1)$$

The conservation of momentum or Navier-Stokes equations, expressed in terms of stress tensors, for a general compressible fluid also in axisymmetric form, are given by:

$$\frac{\partial(\rho u^2)}{\partial x} + \frac{1}{r}\frac{\partial(r\rho uv)}{\partial r} = -\frac{\partial P}{\partial x} + \frac{\partial(\tau_{xx})}{\partial x} + \frac{1}{r}\frac{\partial(r\tau_{rx})}{\partial r} \tag{2.2}$$

$$\frac{\partial(\rho uv)}{\partial x} + \frac{1}{r}\frac{\partial(r\rho v^2)}{\partial r} = -\frac{\partial P}{\partial r} + \frac{\partial(\tau_{xr})}{\partial x} + \frac{1}{r}\frac{\partial(r\tau_{rr})}{\partial r} - \frac{\tau_{\theta\theta}}{r} \tag{2.3}$$

$$\frac{\partial(\rho uw)}{\partial x} + \frac{1}{r}\frac{\partial(r\rho vw)}{\partial r} + \frac{\rho vw}{r} = \frac{\partial(\tau_{x\theta})}{\partial x} + \frac{1}{r^2}\frac{\partial(r^2\tau_{r\theta})}{\partial r} \tag{2.4}$$

where, based on the usual constitutive assumptions for the isotropic case, we have:

$$\tau_{xx} = 2\mu\frac{\partial u}{\partial x} - \frac{2}{3}\mu(\text{div } v) \tag{2.5}$$

$$\tau_{rr} = 2\mu\frac{\partial v}{\partial r} - \frac{2}{3}\mu(\text{div } v) \tag{2.6}$$

$$\tau_{\theta\theta} = 2\mu\frac{v}{r} - \frac{2}{3}\mu(\text{div } v) \tag{2.7}$$

$$\tau_{rx} = \tau_{xr} = \mu\left(\frac{\partial u}{\partial r} + \frac{\partial v}{\partial x}\right) \tag{2.8}$$

$$\tau_{r\theta} = \tau_{\theta r} = \mu r\frac{\partial\left(\frac{w}{r}\right)}{\partial r} \tag{2.9}$$

$$\tau_{x\theta} = \tau_{\theta x} = \mu\frac{\partial w}{\partial x} \tag{2.10}$$

If isotropy is not assumed, we must then use different values of the above tensors for the different directions under consideration

2.2.2 Energy Equation

To describe how energy is treated in combustion problems, consider the following conservation of energy equation for multi-component fluids, expressed in terms of the total enthalpy, H_o which will include the enthalpy of formation, Δh^f, of each species participating in the reaction:

$$\frac{\partial}{\partial x}\left(\rho u H_o - \mu_{eff}\frac{\partial H_o}{\partial x}\right) + \frac{1}{r}\frac{\partial}{\partial r}\left\{r\left[\rho v H_o - \mu_{eff}\frac{\partial H_o}{\partial r}\right]\right\} = 0 \qquad (2.11)$$

This is a very convenient way of expressing the energy equation for reacting flows since, in this form, combustion does not add energy to the fluid, it simply converts energy stored chemically in the reactants into sensible heat. The total stagnation enthalpy, H_o is then defined as:

$$H_o = \frac{1}{2}\left(u^2+v^2+w^2\right) + \sum_{i=1}^{N} Y_i\left(\Delta h_i^f + \int_{T_{ref}}^{T} C_{pi}\,dT\right) \qquad (2.12)$$

where, Δh^f and C_p denote the enthalpy of formation at T_{ref} °K and the specific heat at constant pressure, respectively, of each species. The values of C_p for different species will be represented by a polynomial of degree three as:

$$C_p = a + bT + cT^2 + dT^3 \tag{2.13}$$

where a, b, c and d are constants for each species which may be determined from tabulated data. If the mixture is assumed to consist of ideal gases, then we may obtain the mixture density through the following equation of state:

$$P = \rho R_u T \sum_{i=1}^{N} \frac{Y_i}{M_i} \tag{2.15}$$

where R_u is the universal gas constant and N is the total number of species in the mixture; Y_i and M_i denote the mass fraction and molar mass of species i, respectively.

2.2.3 Species Mass Fraction Equation

The bulk motion of the fluid is modeled using a single velocity, pressure, temperature and turbulence fields. The influence of the multiple species involved, is felt only through property variations for the various components. Of primary importance is the variation of density, which will affect conservation of mass which, in average form, can also be expressed in the general form as:

$$\frac{\partial(\rho_i u)}{\partial x} + \frac{1}{r}\frac{\partial(r\rho_i v)}{\partial r} = -\frac{\partial(J_{ix})}{\partial x} - \frac{1}{r}\frac{\partial(rJ_{ir})}{\partial r} + \omega_i \tag{2.16}$$

where ρ_i represents the density of fluid component i in the mixture, i.e. the mass of the component per unit volume. J_{ix} and J_{ir} are the relative mass fluxes and, ω_i is the chemical reaction rate of component i. Note that if we sum the above equation over every species, the result is the standard continuity equation (2.1). Since we must have:

$$\sum_{i=1}^{N} \omega_i = 0 \tag{2.17}$$

The terms J_{ix} and J_{ir} account for any differential motion of the individual components. This term may be modeled in a number of ways, to include effects of concentration gradients, a pressure gradient or any external forces that the reacting flow might be subjected to. Of all these possible sources of relative motion among the mixture components, the primary effect is that of concentration gradients. Using Fick's Law, the model for J_{ix} and J_{ir} gives rise to a diffusion-like terms:

$$J_{ix} = -\rho\, \Gamma_i \frac{\partial \rho}{\partial x}$$

$$J_{ir} = -\rho\, \Gamma_i \frac{\partial \rho}{\partial r} \tag{2.18}$$

The diffusion coefficient, ri, must be obtained from experimental data over the range of physical conditions of interest. In fact, this term is commonly expressed in terms of a diffusivity, D_i, where $\Gamma_i = \rho\, D_i$. Now, the mass fraction of component i is defined to be:

$$Y_i = \frac{\rho_i}{\rho_{mix}} \tag{2.19}$$

Substituting all of the above assumptions and models into (2.14) we obtain:

$$\frac{\partial}{\partial x}(\rho u Y_i) + \frac{1}{r}\frac{\partial}{\partial r}(r\rho v Y_i) = -\frac{\partial}{\partial x}\left(\Gamma_{eff}\frac{\partial Y_i}{\partial x}\right) - \frac{1}{r}\frac{\partial}{\partial r}\left(r\left[\Gamma_{eff}\frac{\partial Y_i}{\partial r}\right]\right) + \omega_i \tag{2.20}$$

where:

$$\Gamma_{eff} = \Gamma_i + \frac{\mu_{eff}}{Sc_t} \tag{2.21}$$

Here S_{ct} is the turbulent Schmidt number and we have used the usual eddy viscosity type assumption for the fluctuating terms that result from averaging, which will be discussed in more details later.

2.2.4 Enthalpy Variance Equation

The ß-probability density function used in the present work, and introduced later, requires knowledge of the mean temperature, T, as well as the variance of this temperature, $\widetilde{T''T''}$. The mean temperature is supplied by solving the Navier-Stokes equations along with the energy equation. We now introduce another partial differential equation for the enthalpy variance, from which the needed temperature variance may be calculated. The temperature variance is obtained from the enthalpy variance by noting that:

$$H = \int_{T_{ref}}^{T} C_p \, dT + H_o \tag{2.22}$$

We may now write $H = \widetilde{C_p} T + H_o$ where:

$$\widetilde{C_p} = \frac{\int_{T_{ref}}^{T} C_p \, dT}{T} \tag{2.23}$$

And, assuming that $H'' = \widetilde{C_p} T''$ we may write:

$$\widetilde{T''T''} = \frac{\widetilde{H''H''}}{\widetilde{C_p}^2} \tag{2.24}$$

An equation for the enthalpy variance, $\widetilde{H''H''}$, can be derived in a manner similar to the derivation of Reynold's stresses. As with the Reynolds stress equations, the enthalpy variance equation is complicated and involves extra terms which must be accounted for by models. As a result, various terms in the equation are grouped together according to the type of physical behavior they share and are thus modeled as a unit. The modeled equation has a form very similar to the turbulent kinetic energy equation encountered in the k-ε turbulence model, which will be discussed in some detail later. The resulting modeled equation has the following form:

$$\frac{\partial}{\partial x}(\rho u g) + \frac{1}{r}\frac{\partial}{\partial r}(r \rho v g) + 2 C_g g \frac{\varepsilon}{k} - \frac{\partial}{\partial x}\left(\Gamma_{eff}\frac{\partial g}{\partial x}\right) - \frac{1}{r}\frac{\partial}{\partial r}\left(r\left[\Gamma_{eff}\frac{\partial g}{\partial r}\right]\right) - 2\Gamma_{eff}\left(\left[\frac{\partial h}{\partial x}\right]^2 + \left[\frac{\partial h}{\partial r}\right]^2\right) = 0 \tag{2.25}$$

where the viscous coefficient this time is given by:

$$\Gamma_{eff} = \frac{\mu_{eff}}{Pr_t} \tag{2.26}$$

where Prt represents the turbulent Prandtl number.

Equations (2.23) and (2.22) were implemented into the present work and solved as an integral part of the baseline flow field calculation. Modified reaction rate coefficients for each participating reaction are then calculated based on the ß-probability density function constructed from these equations, completing the turbulent combustion model which will be described in a later chapter.

2.3 Second Order Solution Method of The Navier-Stokes Equations

The numerical solution of the compressible Navier-Stokes equations in primitive variable form requires the use of some form of upwinding or artificial viscosity. If a first order accurate method is used then too much numerical diffusion will follow resulting in a solution for a much lower effective Reynolds number. The present work uses a finite element approach for second order accuracy, developed by Baruzzi (1995). Global second order accuracy is achieved by introducing fourth order operators to replace the Laplacian operators used in a more standard pressure dissipation type artificial viscosity formulation.

For example, a pressure dissipation term may be introduced into the continuity equation as follows:

$$\frac{\partial(\rho u)}{\partial x} + \frac{1}{r}\frac{\partial(r\rho v)}{\partial r} = \varepsilon \nabla^2 P \tag{2.27}$$

This new fourth order operator is recast as the difference of two Laplacian operators and balancing terms are introduced to guarantee that fourth order artificial dissipation is maintained. Thus the continuity equation would now take on the following form:

$$\frac{\partial(\rho u)}{\partial x} + \frac{1}{r}\frac{\partial(r\rho v)}{\partial r} = \varepsilon \nabla \cdot (\nabla P - F) \tag{2.28}$$

Where F is the balancing term and it may be shown that, in discretized form:

$$\nabla \cdot (\nabla P - F) = \frac{-1}{4} \nabla^4 P \tag{2.29}$$

The second order accuracy of this scheme has been formally demonstrated by comparison with an exact solution and its robustness has been proven through many applications in the present work.

2.4 Solution Algorithm

The final step in the application of the finite element method is the solution of a large system of algebraic equations. When explicit methods are used to solve these large systems the problem becomes one of reducing the number of

matrix manipulations. There are many very well understood direct and iterative methods that could be implemented at this stage. A brief discussion on both approaches will be given, however the present work implements a direct solver.

For direct methods the number of matrix operations required scales as the number of equations solved for, therefore any advantage given by the matrix's structure must be taken into account to reduce computing time. There are two main ways of taking advantage of the structure of a matrix in storage and solution procedure. The first scheme uses the size of the maximum bandwidth of the matrix and stores only the maximum, nonzero length of the column or row for all equations. The second approach, called the skyline method, stores only the nonzero length of the column or row for each equation. In this scheme only the nonzero elements of the matrix are stored with pointers providing the location of the entry in the expanded matrix.

Iterative methods for general nonsymmetric matrices have enjoyed limited success. Currently, however, there is an algorithm growing in popularity for use in symmetric finite element matrices and is known as the conjugate gradient method (CGM). This method leads to convergence problems for any type of application where the matrix is ill-conditioned, such as the primitive variable formulation of the finite element fluid flow analysis. Some of these

convergence problems were overcome with the introduction of the generalized minimum residual algorithm (GMRES). This method has been applied to large, nonsymmetric and nonlinear problems with good success. An advantage to using iterative methods for solving nonlinear problems is that the solution to these problems often require multiple iterations themselves. Hence, by using an iterative solver, optimal convergence may be achieved by using only approximate solutions at each global iteration of the solution scheme and as the nonlinear scheme starts to converge more and more accurate solutions can be obtained from the matrix solver.

2.5 Turbulence Modeling

It is generally accepted that the Navier-Stokes equations are sufficient to describe the motion of a viscous, compressible fluid under all flow conditions ranging from laminar to fully turbulent. However, analytical solutions to these highly non-linear equations are not possible and there are only a few analytical solutions to special cases of the Reynolds-averaged version of the equations. The development of turbulence modeling is an engineering attempt to approximate the effects of turbulence on the fluid flow without having to resolve all of the spatial and temporal time scales associated with the instantaneous Navier-Stokes equations. This section will provide a brief

overview of turbulence modeling, with special attention given to the two equation models used in the present work. Also, a special treatment of the wall conditions within the finite element method is presented.

In general, the turbulent equations of fluid flow cannot be solved numerically in their exact form due to the difficulties of resolving all of the various scales involved in the motion. These limitations are especially felt when flows from nature or industry are being considered. In order to proceed with the analysis of flow with real engineering interests, it becomes necessary to simplify the set of governing equations, as was described in chapter 2, and introduce models to handle the extra terms that appear after the equations have been modified. Turbulence modeling can, in general, be put into three distinct categories. The first category includes models that are based on the Bossinesq assumption for the eddy viscosity, hence they are usually referred to as eddy viscosity models. Eddy viscosity models are further sub-classified based on the number of extra equations that are used to obtain this turbulent viscosity. So far, there are zero-equation, one-equation and two-equation models. Zero equation models add no extra partial differential equations to the problem and are thus referred to as algebraic models. One-equation models add one partial differential equation for the turbulence kinetic energy of the flow. Two-equation models also solves an equation for the turbulence kinetic energy and adds a second transport equation which models the

dissipation of this energy. It is these two-equation models which have enjoyed the most success resolving flows of industrial interest and are the main subject of this chapter. The second category of turbulence models do not assume an eddy viscosity but rather attempts to solve the extra Reynolds stress terms, that appear in the averaged Navier-Stokes equations, directly. These models are generally referred to as second moment closures and have not enjoyed the popularity of eddy viscosity based models. Second moment models use transport equations to describe the evolution of each of the Reynolds stress and, although theoretically more accurate than eddy viscosity approaches, are thus too prohibitive to use for large scale industrial flows. The third category includes all models that do not rely on solving the Reynolds averaged Navier-Stokes equations. Most common in this category are large eddy simulations and direct numerical simulations. Since these models solve the instantaneous version of the governing equations they remain, as yet, impractical for industrial applications as the same problem of capturing all time and length scales returns and very fine numerical grids are required.

2.5.1 Reynolds Averaging

The conservation equations for mass, momentum and energy are the basis for the formation of the mean flow equations. Using Reynolds averaging, a statistical approach is used to recast the instantaneous values of velocity, pressure and temperature, as well as any other scalar quantity, as a mean value plus a fluctuating value:

$$\begin{aligned} u &= \tilde{u} + u' \\ P &= \tilde{P} + P' \\ T &= \tilde{T} + T' \\ &\vdots \\ \phi &= \tilde{\phi} + \phi' \end{aligned} \tag{2.30}$$

The mean or average quantities are obtained by integrating the instantaneous values over a very long length of time, much larger that the time scales of the turbulent motion:

$$\tilde{\phi} = \lim_{\Delta t \to \infty} \frac{1}{\Delta t} \int_{t}^{t+\Delta t} \phi(t)\, dt \tag{2.31}$$

When this form of the instantaneous quantities are substituted back into the governing equations we recover basically the same equations as before but for the mean values and we also obtain some extra terms or correlation's which must be accounted for by models. These additional terms introduced by the averaging process, appear as products of fluctuating velocities $\widetilde{u'u'}$ and velocity

and scalar values, for example: $\widetilde{u'T'}$. The first attempt at modeling these fluctuating velocity terms was given by Boussinesq in his eddy viscosity concept for the so called Reynolds stress tensor $\widetilde{u'u'}$.

2.5.2 Eddy Viscosity

The concept of eddy viscosity is based on the analogy between the molecular motion in laminar flows and the eddying motion seen in turbulent flows. Stoke's viscosity law, for laminar fluid flows, relates viscosity to the average velocity gradients of the molecules and the mean free paths between collisions of the fluid molecules. The Boussinesq assumption is to likewise characterize a turbulent viscosity based on the length scales of the eddies in the flow. Zero-equation models are based on a mixing length used to characterize the turbulent viscosity. Here it is assumed that turbulence quantities are not transported by the flow and that turbulence is always in local equilibrium, i.e. turbulence energy is dissipated at the same rate that it is being produced. The Prandtl mixing length scale was the first of these zero-equation models and it yield a familiar form of the turbulent viscosity:

$$\mu_t = \rho l_m^2 \left|\frac{\partial u}{\partial r}\right| \tag{2.32}$$

This relationship only introduces a single unknown parameter, the Prandtl mixing length l_m Although this approach has enjoyed some success in industrial applications, the need to recalibrate the mixing length every time the geometry changes and the limited validity of the equilibrium condition, have made this a poor engineering tool.

One-equation models are rarely encountered and were primarily a stepping stone to the very popular two-equation models. Two-equation models are presently the furthest refinement of the eddy viscosity concept. In these models, two partial differential equations are introduced, one is to calculate the turbulent kinetic energy of the flow and the second is used to obtain information about the length scale along which the dissipation of this turbulent kinetic energy takes place. To this day the general working form of the two-equation model is based on the work introduced by Launder and Spalding in 1974. In general, it is this k-ε form of the two-equation model that is used, where k represents the turbulent kinetic energy and ε the dissipative length scale. Another, more recent, approach is to replace the ε-equation with an equation for the specific rate of dissipation w resulting in the k- ω form of the two-equation model. Both of these models have been implemented in the present work.

2.5.3 The k-ε Turbulence Model

The k- ε model employs the following eddy viscosity concept:

$$\mu_t = C_\mu \tilde{\rho} \frac{k^2}{\varepsilon} \tag{2.33}$$

which relates the eddy viscosity to k and ε. The kinetic energy transport equation is used to determine k:

$$\frac{\partial}{\partial x}(\rho u k) + \frac{1}{r}\frac{\partial}{\partial r}(r\rho v k) = \frac{\partial}{\partial x}\left(\frac{\mu_t}{\sigma_k}\frac{\partial k}{\partial x}\right) + \frac{1}{r}\frac{\partial}{\partial r}\left(r\left[\frac{\mu_t}{\sigma_k}\frac{\partial k}{\partial r}\right]\right) + P_k - \rho\varepsilon \tag{2.34}$$

and the kinetic energy dissipation rate transport equation is used to find ε:

$$\frac{\partial}{\partial x}(\rho u \varepsilon) + \frac{1}{r}\frac{\partial}{\partial r}(r\rho v \varepsilon) = \frac{\partial}{\partial x}\left(\frac{\mu_t}{\sigma_\varepsilon}\frac{\partial \varepsilon}{\partial x}\right) + \frac{1}{r}\frac{\partial}{\partial r}\left(r\left[\frac{\mu_t}{\sigma_\varepsilon}\frac{\partial \varepsilon}{\partial r}\right]\right) + \frac{C_1 \varepsilon P_k}{k} - \frac{C_2 \rho \varepsilon^2}{k} \tag{2.35}$$

where P_k represents the production of turbulent kinetic energy, and is given by

$$P_k = \mu\left[2\left\{\left(\frac{\partial u}{\partial x}\right)^2 + \left(\frac{\partial v}{\partial r}\right)^2 + \left(\frac{v}{r}\right)^2\right\} + \left(\frac{\partial u}{\partial r} + \frac{\partial v}{\partial x}\right)^2 + r\frac{\partial}{\partial r}\left(\frac{w}{r}\right)^2 + \left(\frac{\partial w}{\partial x}\right)^2\right] \tag{2.36}$$

and C_1 and C_2 are model constants.

2.5.4 The k-ω Turbulence Model

Using dimensional analysis combined with physical reasoning Kolmogorov was the first researcher to postulate using a specific dissipation rate, ω, to describe how turbulence kinetic energy is dissipated. Recognizing the key role played by large eddies and the relative unimportance of viscosity, at least explicitly, Kolmogorov combined this knowledge to postulate and equation for ω. The dimensions of eddy viscosity, ν_t, are $(\text{length})^2/(\text{time})$ while the dimensions of k are $(\text{length})^2/(\text{time})^2$, consequently ν_t /k must have dimensions (time). Turbulence dissipation, ε, has dimensions $(\text{length})^2/(\text{time})^3$, therefore, ε /k has dimension 1/ (time). We may, therefore, close both the constitutive relation and the equation for k by introducing a variable with dimensions 1/(time), or (time). The variable representing this time scale must be representative of large eddy motions. Kolmogorov call C_3 the "rate of dissipation of energy in unit volume and time", and tied it to both dissipative and diffusive processes. In the present work, the most thoroughly tested version of the k-ω model is used, the Wilcox version of the model introduced in 1988.

In this model we must solve a slightly modified version of the turbulence energy equation and introduce a new partial differential equation for the new

time scale, ω, to obtain the eddy viscosity for the flow field. The following is basically the same equation for k given by (3.3) but with ω introduced into it:

$$\frac{\partial}{\partial x}(\rho uk)+\frac{1}{r}\frac{\partial}{\partial r}(r\rho vk)=\frac{\partial}{\partial x}\left(\frac{\mu_t}{\sigma^*}\frac{\partial k}{\partial x}\right)+\frac{1}{r}\frac{\partial}{\partial r}\left(r\left[\frac{\mu_t}{\sigma^*}\frac{\partial k}{\partial r}\right]\right)+P_k-\beta^*\rho k\omega \tag{2.37}$$

and the new equation needed to obtain w also has a very similar form:

$$\frac{\partial}{\partial x}(\rho u\omega)+\frac{1}{r}\frac{\partial}{\partial r}(r\rho v\omega)=\frac{\partial}{\partial x}\left(\frac{\mu_t}{\sigma_\omega}\frac{\partial \omega}{\partial x}\right)+\frac{1}{r}\frac{\partial}{\partial r}\left(r\left[\frac{\mu_t}{\sigma_\omega}\frac{\partial \omega}{\partial r}\right]\right)+\alpha\frac{\omega}{k}P_k-\beta^*\rho\omega^2 \tag{2.38}$$

These equations are solved segregated from the Navier-Stokes equations to obtain the eddy viscosity which is, in turn, fed back into the other flow and combustion equations.

2.5.5 Logarithmic Wall Elements

The above described two-equation turbulence models are the classical high Reynolds number k-ε and k-ω models, That is, they are only physically valid when the flow Reynolds number is high, or when the effects of molecular viscosity are very low. For best accuracy a low Reynolds number turbulence model should be used in the near wall region where viscous effects are more important, but this approach would require an additional 10 to 20 grid points to resolve the high flow gradients and turbulence quantities in that region. This would be very costly in terms of speed and memory on any computer,

making a Navier-Stokes code a less practical tool. The wall function approximation therefore excludes the high gradient region near walls and, instead, imposes a linear behavior in the vicinity of the wall:

$$u+ = y+ \quad ; \quad O < y+ < 6 \tag{2.39}$$

and a logarithmic behavior near the first grid point away from the wall:

$$u^+ = \frac{1}{\kappa} \ln y^+ + C \quad ; \quad y^+ \geq 20 \tag{2.40}$$

with smoothing between these two regions. The constants and variables in (2.38) are defined as:

$$k = 0.4184 \; ; \; C = 5.1$$

$$y^+ = \rho y \frac{u_\tau}{\mu} \; ; \; u_\tau = \sqrt{\frac{\tau_w}{\rho \, Re}} \tag{2.41}$$

To obtain the boundary conditions imposed on the k-ε or k-ω models, the production and dissipation of the turbulence energy at the wall are assumed to be equal. The turbulent shear stress at the wall: τ_w is obtained from the wall function assumption and is used to compute new values for k and ε or ω.

The wall function approach is known to be inaccurate for three-dimensional and separated flows and a considerably more accurate approach, yet far cheaper than implementing a low-Reynolds number turbulence model, is used in the present work. As proposed by Manouzi and Fortin as well as Haroutunian and Engelman, th ⁝ near-wall element incorporates into its

shape function the partially logarithmic behavior of the velocity in the direction normal to the wall, while retaining the strictly linear behavior in the direction tangent to the wall, as shown in figure 1. Thus, for the elements adjacent to a wall, the velocity shape function reflects the flow behavior in this region, characterized by a viscous sublayer, a transition layer and a logarithmic outer layer. For example, the element shown in figure 1., assuming that the bottom face to lie on a wall, the shape function $F_2(\eta)$ for nodes off the wall is re-expressed as $F_2\ (y^+/y^+_{edge})$ to reflect the assumed behavior.

Due to the large gradients associated with $F_2\ (y^+/y^+_{edge})$ the velocity variation in the near-wall element cannot be integrated accurately using a standard two-point Gauss quadrature as the elements in the rest of the flowfield. Through numerical experimentation, it has been found that nine Gaussian points are needed in the direction normal to the wall to adequately integrate the behavior, including the logarithmic part.

As the k-ε or k-ω equations are integrated up to one grid point away from the wall, the turbulent viscosity in the near wall region is interpolated as follows: a linear behavior starting at the edge of the near-wall region, where y^+ is assumed to be less than 300, to a y^+ value of 30, and a quadratic variation between $y^+ = 30$ and the wall, i.e. $y^+ = 0$. The k-ε or k- ω equations are solved in a segregated manner from the rest of the flow equations and the turbulent

viscosity is then updated. Furthermore, the highly non-linear source terms that appear in the k-ε equations are loaded into the solution progressively to allow for better overall convergence. The source terms in the k-ω equations on the other hand do not require such a loading procedure and may be fully solved for without adverse effects on overall convergence.

2.6 Combustion Modeling

In this section the combustion models used in the present work are presented. The first model shown assumes equilibrium chemistry and gives no details of the individual kinetics involved in the combustion process. This model is used as a numerical stepping stone toward solving the more complicated finite rate model shown later in this section.

2.6.1 The Eddy Breakup Model

The eddy breakup model is based on the concept that chemical reaction is fast relative to the transport processes in the flow. When reactants mix at the molecular level, they instantaneously form products. The model assumes that the reaction rate may be directly related to the time required to mix the reactants at the molecular level. In turbulent flows, i.e. all industrial flows,

the mixing time is dominated by the turbulence properties, and therefore, the reaction rate is proportional to a mixing time define by the turbulence kinetic energy: k and its dissipation: e (or the specific dissipation : ω).

$$\text{rate} \approx \frac{\varepsilon}{k} \quad \text{or} \quad \text{rate} \approx \omega \tag{2.42}$$

This concept of mixing dominated reaction control is applicable to a wide range of industrial problems, where the flame temperatures and reaction rates are fast when compared to the reactants mixing rates.

The model, as it is implemented in the present work, is based on a single reaction in which fuel and oxidant react together to form products and release heat. The chemistry of the combustion reaction may be represented on a molar basis by:

$$V_f \text{ fuel} + v_O \text{ oxidant} \dashrightarrow v_p \text{ products} \tag{2.43}$$

where Vf represents the number of moles of fuel, vO represents the number of moles of oxidant required to combust the Vf moles of fuel and vp is the number of moles of products generated in the reaction. The fuel, oxidant and products mass fractions are scalar variables that are obtain through solving the species transport equations presented earlier. Equation (2.43) is therefore expressed on a mass basis to coincide with the treatment of multi-component fluids in term of mass fractions:

$$\text{fuel} + r_f \text{ oxidant} \dashrightarrow (1 + r_f) \text{ products} \tag{2.44}$$

where r_f is now the stoichiometry, i.e. the mass of oxidant required to combust a unit mass of fuel.

The species transport equations presented above require the knowledge of the reaction rates for each species. This reaction rate appears as source terms wi which, in a first instance, will be calculated using an eddy breakup model. The model requires that fuel, oxidant and products all be available at a given grid point before any reaction will occur. The fuel and oxidant are needed as components of the forward reaction. products are not necessary as part of the forward reaction but their presence implies that there is heat available due to reaction. Therefore, since any one of these components may limit the reaction rate at a given grid point, the minimum concentration of fuel, oxidant or products is used to calculate the reaction rate. The reaction rate for the fuel, ω_f, is obtained from the product of the minimum concentration of the species and a turbulent mixing rate according to:

$$\omega_f = -A_{ebu}\,\rho\,\frac{\varepsilon}{k}\,\mathrm{Min}\left\{ Y_f,\ \frac{Y_o}{r_f},\ B_{ebu}\,\frac{Y_p}{1+r_f} \right\} \qquad (2.45)$$

where A_{ebu} and B_{ebu} are model constants. The corresponding source terms for the oxidant and product mass fraction transport equations are given by:

$$\omega_o = r_f\,\omega_f \qquad \text{and} \qquad \omega_p = (1+r_f)\,\omega_f \qquad (2.46)$$

2.6.2 Finite Rate Chemistry and Kinetic Modeling

The eddy breakup model for obtaining the reaction rates for each species participating in the reaction is well suited for most industrial applications when details of the individual reactions taking place in forming the 'products' are not necessary. That is, if you are only interested in global values of product concentrations an eddy breakup model will work well under most conditions. If, however, one is interested in the details of the chemical kinetics taking place during the reaction, the simple model described above gives no such details. In many industrial applications it becomes necessary to know about the intermediate steps and species participating in a reaction. In the study of soot formation or engine knock, the individual chemical steps must be know in order to predict or correct these conditions. One of the most important applications today is in pollution control and, in particular the formation of NOx [NO, NO_2]

The instantaneous production rate of a species i due to n chemical reactions involving N different scalar species can be represented, from the law of mass action, in the following most general form [Kuo]:

$$\omega_i = M_i \sum_{j=1}^{N} \left(\nu''_{ij} - \nu'_{ij}\right) \left\{ k_{fj} \rho^{m_j} \prod_{s=1}^{N} [C_s]^{\nu'_{sj}} - k_{bj} \rho^{n_j} \prod_{s=1}^{N} [C_s]^{\nu''_{sj}} \right\} \qquad (2.47)$$

where:

$$m_j = \sum_{s=1}^{N} \nu'_{sj} \quad \text{and} \quad n_j = \sum_{s=1}^{N} \nu''_{sj} \tag{2.48}$$

In the above equations, the number of molecules of the scalar s involved in the j-th forward reaction is ν'_{sj} and the corresponding backward reaction is ν''_{sj}. The forward and backward rate constants of the reaction j are given by k_{jf} and k_{bj} respectively. Typically the forward reaction rates are functions of the temperature based on an Arrhenius expression of the form:

$$k_f = C_f T^{\eta_f} e^{\frac{-K_f}{RT}} \tag{2.49}$$

How this rate coefficient is treated numerically is one of the central themes of the present work. The role that probability density functions will play in the calculation of these rate coefficient will be discussed in more detail later in Chapter 4.

2.6.3 Reduced Mechanisms

The general idea of reducing complex kinetic schemes by the introduction of steady state assumptions has been known to chemists for a long time. However, it has become fruitful for combustion applications only very recently. Interestingly enough, it was the application to hydrocarbon flames rather than to the much simpler hydrogen flames that first showed the full

potential of the methodology. Steady state approximations for intermediate species can be justified in many different ways. They were first derived for zero dimensional homogeneous systems that depend only on time, and the term 'steady state' was introduced because the time derivative of these species is set to zero:

$$\frac{d[C_i]}{dt} = \sum_{j=1}^{N} \nu_{ij}\, \omega_j = 0 \qquad (2.50)$$

Here, t denotes the time, and w_j the reaction rate. The justification for this approximation is generally provided in physical terms by stating that the rate at which species i is consumed is much faster than the rate by which it is produced. Therefore its concentration always stays much smaller than those of the initial reactants and the final products. Since this concentration, C_i, stays small, its time derivative also stays small compared to the time derivatives of the other species, as (2.50) implies.

The reduced mechanism for the H_2-air reaction set utilized in the present work has been calibrated by comparison to a more complex H_2-air mechanism involving 9 species and 19 reactions. The calibration has been performed using a perfectly stirred reactor code. The code computes equilibrium static temperatures at various residence times and equivalence ratios, at given static pressures, assuming instantaneous mixing of the reactants. The extended 19 reaction mechanism used in the calibration is listed below:

Reaction			C_f	n_f	K_f
$H + O_2$	<-->	$O + OH$	3.73E+17	-1,0	17500.0
$H_2 + O$	<-->	$H + OH$	1.80E+10	1,0	8900.0
$OH + H_2$	<-->	$H + H_20$	1.08E+O9	1.3	3650.0
$O + H_20$	<-->	$OH + OH$	4.58E+O9	1.3	17100.0
$H + O_2 + M$	<-->	$H0_2 + M$	2.00E+18	-0.8	0.0
$H + H0_2$	<-->	$OH + OH$	1.69E+14	0.0	874.0
$H + H0_2$	<-->	$H_2 + O_2$	6.63E+13	0.0	2130.0
$OH + H0_2$	<-->	$H_20 + O_2$	1.45E+16	-1.0	0.0
$H_20 + O$	<-->	$H0_2 + M$	5.75E+ll	0.5	57000.0
$H + H + M$	<-->	$H_2 + M$	9.70E+16	-0.6	0.0
$H + OH + M$	<-->	$H_20 + M$	2.16E+22	-2.0	0.0
$O + O + M$	<-->	$O_2 + M$	l.OOE+17	-1.0	0.0
$H0_2 + O$	<-->	$O_2 + OH$	1.81E+13	0.0	-3970
$H0_2 + H0_2$	<-->	$H_2O_2 + O_2$	l.OOE+13	0.0	1000.0
$OH + OH + M$	<-->	$H_2O_2 + M$	1.30E+22	-2.0	0.0
$H_2O_2 + H$	<-->	$H0_2 + H_2$	1.70E+12	0.0	3750.0
$H + H_2O_2$	<-->	$H_20 + OH$	l.OOE+13	0.0	3590.0
$H_2O_2 + O$	<-->	$H0_2 + OH$	9.55E+06	2,0	3970.0
$H_2O_2 + OH$	<-->	$H_20 + H0_2$	7.00E+12	0.0	1430.0

This mechanism is itself a reduced mechanism which results from truncation of the complete 28 reaction hydrogen oxidation kinetic mechanism. The criteria for eliminating reactions was whether a given reaction contributes less than 1% to the species mass fraction being computed. For consistency, the units used are expressed in cm^3, g-mol and seconds, in the computation for

the given chemical equation. The final, reduced, combustion model used in the present work is the following 7-species, 8-reaction mechanism. The rate equations, coefficients and activation energies used are given below:

Reaction			C_f	n_f	K_f
OH + O	<-->	H + H_2O	1.80E+13	0.0	960.0
OH + H	<-->	H_2 + 0	8.40E+O9	1.0	700.0
OH + OH	<-->	H_20 + 0	6.00E+12	0.0	1100.0
OH + H_2	<-->	H_20 + H	2.10E+ll	0.0	5180.0
H + H + M	<-->	H_2+M	1.80E+06	-1.0	0.0
H + O+ M	<-->	OH+M	6.00E+06	-1.0	0.0
O + O + M	<-->	O_2 + M	1.80E-10	0.0	-1800.0
H + OH + M	<-->	H_20 + M	6.00E-02	-2.0	0.0

In this model, atmospheric nitrogen, N_2, is considered inert with no dissociation even at high temperatures. Computationally, its mass fraction is held constant during the chemistry calculations. NOx modeling is discussed in greater detail later in this chapter.

The H_2-air mechanism represented above is a significantly reduced mechanism, the extended mechanism is considered to be more accurate, capable in principle of predicting the details of combustion from cold to hot portions of the flame. This reduced mechanism may result in a decreased ignition delay relative to that predicted by the extended model. A primary reason for this is the absence of important species in the reduced mechanism

including the hydrogen peroxides H_2O_2 and $H0_2$, which are considered important for low temperature calculations. In the present work, however, the incoming air is at a temperature of 810 °K which is well below the auto-ignition temperature of between 1000 °K and 1200 °K required by the extended mechanism.

2.6.4 NOx Modeling

Simplified models for predicting the rate of production of NOx in combustors are presented. These models are based on chemical reactor modeling and are strongly influenced by the nitrous oxide mechanism, which is an important source of NOx. The later have been developed for use in an NOx postprocessor for CFD codes. Whatever model for chemical reactions and for nitric oxide in diffusion flames is employed, two facts are always going to be true. Only a small percentage of the combustor volume (or computing grid points) produces almost all of the total amount of NOx. The typical length scale associated with Nox formation is far below the smallest possible numerical grid size.

The calculation of NO is a two step process in the current formulation. One first calculates a fully converged flow field solution for the aerodynamics and the H_2-air reaction set, including solution of the enthalpy and temperature

variances needed for the standard ß - probability density function approach. Flow field variables are then 'frozen', including velocity components, density, pressure, temperature, mass-fraction of species in the H_2-air reaction set, and the enthalpy and temperature variances. Next, the three equation NOx reaction set, described in the next section below, is calculated, with iterations performed until convergence is achieved for the NO and N variables. This procedure is a reasonable approximation in terms of the enthalpy release into the flow field and for calculation of 'thermal' NOx. For increased accuracy, however, the two-step procedure must eventually be integrated into a single step in which the H_2-air and the NOx kinetics mechanisms are coupled during the baseline flowfield calculation in order compute the additional production mechanisms for NOx, including 'prompt' and 'fuel' NOx. These forms of NOx production currently cannot be calculated due to the decoupling of the three mechanisms.

For thermal NOx, the principle reactions are recognized to be those proposed by the following three extended Zel'dovich mechanisms:

Reaction			C_f	n_f	K_f
$O + N_2$	<-->	NO + N	7.00E+13	0.0	76000.0
$N + 0_2$	<-->	NO + 0	6.40E+09	-1.0	6300.0
N + OH	<-->	NO + H	6.30E+ll	-0.5	0.0

Despite being linked to the H_2-air mechanism, discussed in chapter 4, through the provision of oxygen atoms in the first two reactions, it is possible to decouple the calculation of NO formation rate from that of the combustion rate because the oxygen atom consumption during the formation of NO is much less than that consumed during the combustion reaction. In addition, the heat of reaction associated with nitric oxide formation may be neglected in the calculation of the temperature and concentration fields.

2.6.5 PDF Comparison Mechanism

An analytical study of the forward rate coefficient is undertaken to evaluate the net effects on the flow field due to the modeling of turbulence/chemistry interactions. To this end, an amplification factor is introduced to quantify the net effect of the probability density function on the rate coefficients. The reaction rate coefficient is first calculated from the Arrhenius expression described above, then stored before being modified, or integrated, by a pdf. The amplification factor is the ratio of the modified reaction rate to the unmodified one and is given by:

$$\Lambda = \frac{\widetilde{k_f}}{k_f} = \frac{\int_{T_1}^{T_2} k_f \, P(T) \, dT}{k_f} \qquad (2.51)$$

This is done by examining the reaction rate amplification factor over a range of different 'thermal intensities' or temperature fluctuation levels expected in the flow field and over the temperature limits imposed on the probability density function, as described in chapter 4. We refer to the numerator as the 'turbulent' reaction coefficient and the denominator as the 'laminar rate coefficient. The term laminar here means that turbulent fluctuations are not being taken into account when computing the reaction rate coefficient. It does not mean that the flow is laminar. It will be shown in chapter 4 that the probability density function is completely specified by the mean temperature and its variance, or intensity. Amplification factors depend largely on the local curvature of the rate coefficient curve, which we have seen are primarily functions of the exponential and power terms in the Arrhenius expression (2.49). Rate coefficients which vary strongly with temperature tend to have amplification, or suppression, of larger magnitudes than rate coefficients which are only weak functions of temperature. This is because integration of the 'turbulent' reaction rate over a symmetric or nearly symmetric functional variation with temperature results in negligible modifications to the laminar rate coefficients. Amplification or suppression is determined by the sign of the slope of the rate coefficient curve, i.e., convex or concave. Typically, in the present work, amplification or suppression occur near the low and high extremes of the temperature range, with an

amplification factor close to one over much of the range. The magnitude of the amplification is greatest at high temperature variances, a result which held true at all mean temperature values. Further results are discussed in chapter 5.

CHAPTER 3

NUMERICAL METHODS

This chapter deals with the development of the finite element numerical model used to approximate the Navier-Stokes equations, energy equation, species equations and turbulence models, allowing for the solution of reacting flow problems. First the nondimensionalization of the variables is presented. The second section demonstrates the use of the Galerkin finite element form of the method of weighted residuals used to obtain an algebraic approximation to the governing partial differential equations. Also discussed in this section is the choice of interpolating functions used within each element of the discretized domain. The third section discusses the boundary conditions applied to the governing equations at the time of solution. The final section presents the solution methods used to obtain the results to be discussed in chapter 5.

3.1 Nondimensionalization

In order to provide the correct scaling of all the equations, it is required to recast the variables in a nondimensional form. For the present work there is a well defined characteristic velocity and length scale which are used to

establish the flow Reynolds number. We may introduce these characteristic scales: the characteristic velocity U_o, length L_o and reference temperature T_{ref} and the following nondimensionalizations can be made:

$$x^* = \frac{x}{L_o} \qquad y^* = \frac{y}{L_o} \qquad u^* = \frac{u}{U_o} \qquad v^* = \frac{v}{U_o} \qquad P^* = \frac{P}{\rho U_o^2} \qquad \rho^* = \frac{\rho}{\rho_{ref}} \tag{3.1}$$

and,

$$T^* = \frac{T - T_{ref}}{\Delta T} \tag{3.2}$$

Nondimensionalization will also be introduced to the turbulence modeling as follows:

$$k^* = \frac{k}{U_o^2} \qquad \varepsilon^* = \frac{\varepsilon L_o}{U_o^3} \qquad \omega^* = \frac{\omega L_o}{U_o} \qquad \mu_t^* = \frac{\mu_t}{\mu} \tag{3.3}$$

This leads to the following nondimensional form of the governing equations, continuity:

$$\frac{\partial(\rho^* u^*)}{\partial x^*} + \frac{1}{r^*}\frac{\partial(r^* \rho^* v^*)}{\partial r^*} = 0 \tag{3.4}$$

and the u,v and w momentum equations:

$$\frac{\partial(\rho^* u^{*2})}{\partial x^*} + \frac{1}{r^*}\frac{\partial(r^* \rho^* u^* v^*)}{\partial x^*} = -\frac{\partial P^*}{\partial x^*} + \frac{1}{Re}\left(\frac{\partial(\tau_{xx}^*)}{\partial x^*} + \frac{1}{r^*}\frac{\partial(r^* \tau_{rx}^*)}{\partial r^*}\right) \tag{3.5}$$

$$\frac{\partial(\rho^* u^* v^*)}{\partial x^*} + \frac{1}{r^*}\frac{\partial(r^* \rho^* v^{*2})}{\partial r^*} = -\frac{\partial P^*}{\partial r^*} + \frac{1}{Re}\left(\frac{\partial(\tau_{xr}^*)}{\partial x^*} + \frac{1}{r^*}\frac{\partial(r^* \tau_{rr}^*)}{\partial r^*} - \frac{\tau_{\theta\theta}^*}{r^*}\right) \tag{3.6}$$

$$\frac{\partial(\rho^* u^* w^*)}{\partial x^*} + \frac{1}{r^*}\frac{\partial(r^*\rho^* v^* w^*)}{\partial r^*} + \frac{\rho^* v^* w^*}{r^*} = \frac{1}{Re}\left(\frac{\partial(\tau_{x\theta}{}^*)}{\partial x^*} + \frac{1}{r^{*2}}\frac{\partial(r^{*2}\tau_{r\theta}{}^*)}{\partial r^*}\right) \quad (3.7)$$

and the energy equation:

$$\frac{\partial}{\partial x^*}\left(\rho^* u^* H_o^* - \frac{\mu_{eff}^*}{Re\, Pr_t}\frac{\partial H_o^*}{\partial x^*}\right) + \frac{1}{r^*}\left(r^*\left[\rho^* u^* H_o^* - \frac{\mu_{eff}^*}{Re\, Pr_t}\frac{\partial H_o^*}{\partial r^*}\right]\right) = 0 \quad (3.8)$$

The k-ε turbulence model is also shown in nondimensional form. The other turbulence model, the k-ω model, follows this nondimensional form very closely and will not be presented. The nondimensional turbulent kinetic energy transport equation is given by:

$$\frac{\partial}{\partial x^*}(\rho^* u^* k^*) + \frac{1}{r^*}\frac{\partial}{\partial r^*}(r^*\rho^* v^* k^*) = \frac{1}{Re}\left(\frac{\partial}{\partial x}\left(\frac{\mu_t{}^*\partial k^*}{\sigma_k{}^*\partial x^*}\right) + \frac{1}{r^*}\frac{\partial}{\partial r^*}\left(r^*\left[\frac{\mu_t{}^*\partial k^*}{\sigma_k{}^*\partial r^*}\right]\right) + P_k{}^*\right) - \rho^*\varepsilon^* \quad (3.9)$$

The nondimensional dissipation transport equation is given by:

$$\frac{\partial}{\partial x^*}(\rho^* u^* \varepsilon^*) + \frac{1}{r^*}\frac{\partial}{\partial r^*}(r^*\rho^* v^* \varepsilon^*) = \frac{1}{Re}\left(\frac{\partial}{\partial x}\left(\frac{\mu_t{}^*\partial \varepsilon^*}{\sigma_k{}^*\partial x^*}\right) + \frac{1}{r^*}\frac{\partial}{\partial r^*}\left(r^*\left[\frac{\mu_t{}^*\partial \varepsilon^*}{\sigma_k{}^*\partial r^*}\right]\right) + \frac{C_1\varepsilon^* P_k{}^*}{k^*}\right) - \frac{C_2\rho^*\varepsilon^{*2}}{k^*} \quad (3.10)$$

In addition, the turbulent eddy viscosity and turbulent Reynolds number then become:

$$\mu_t^* = C_\mu \rho^* Re \frac{k^{*2}}{\varepsilon^*} \quad \text{and} \quad Re_t = Re\frac{k^{*2}}{\varepsilon^*} \quad (3.11)$$

The following dimensionless groups are introduced through this process. The ratio of the inertial forces to the viscous forces give rise to the Reynolds

number Re. It determines the behavior and characteristics of viscous flows in general. Its value indicates whether the flow is laminar or turbulent. This ratio may be expressed as follows:

$$Re = \frac{\rho L_o U_o}{\mu} \tag{3.12}$$

The ratio of the diffusivity of momentum to the diffusivity of heat is referred to as the Prandtl number Pr. The value of the Prandtl number indicates the behavior of the thermal diffusion relative to the momentum diffusion. When Pr < 1, the thermal boundary layer is thicker than the viscous velocity boundary layer and develops more quickly. For values of Pr > 1 the thermal boundary layer is thinner than the velocity boundary layer and develops more slowly. We may express the Prandtl number as follows:

$$Pr = \frac{C_P \mu}{\kappa} \tag{3.13}$$

For the combustion model the species mass fraction equations may be expressed in the following nondimensional form:

$$\frac{\partial}{\partial x^*}\left(\rho^* u^* Y_i\right) + \frac{1}{r^*}\frac{\partial}{\partial r^*}\left(r^* \rho^* v^* Y_i\right) = -\frac{\partial}{\partial x^*}\left(\frac{\mu_{eff}^*}{Re\, Sc_t}\frac{\partial Y_i}{\partial x^*}\right) - \frac{1}{r^*}\frac{\partial}{\partial r^*}\left(r^*\left[\frac{\mu_{eff}^*}{Re\, Sc_t}\frac{\partial Y_i}{\partial r^*}\right]\right) + \omega_i^* \tag{3.14}$$

The ratio of the rate of momentum transport to the rate of mass transport is referred to as the Schmidt number Sc, and may be defined for each pair of species in a multicomponent mixture.

3.2 Galerkin Finite Element Approximations

Now that the equations of interest have been introduced and properly scaled the Galerkin method will be applied in order to obtain a set of approximating algebraic expressions. The first step in the finite element method is to approximate each variable over each of the elements using interpolating shape functions, for example:

$$u(x,y) = \sum_{i=1}^{4} N_i \, u_i \tag{3.15}$$

$$v(x,y) = \sum_{i=1}^{4} N_i \, v_i \tag{3.16}$$

$$w(x,y) = \sum_{i=1}^{4} N_i \, w_i \tag{3.17}$$

$$P(x,y) = \sum_{i=1}^{4} N_i \, P_i \tag{3.18}$$

$$H_o(x,y) = \sum_{i=1}^{4} N_i \, H_{oi} \tag{3.19}$$

These expressions for the dependent variables are substituted into the governing equations and the application of the Galerkin method with weighting functions being the same as the above interpolating functions, leads to the following set of integral equations, for continuity:

$$\int_{\Omega_{ie}} N_j \left\{ \frac{\partial(\rho u)}{\partial x} + \frac{1}{r} \frac{\partial(r\rho v)}{\partial r} \right\} dA = 0 \tag{3.20}$$

and the momentum equations:

$$\int_{\Omega_{ie}} N_j \left\{ \frac{\partial(\rho u^2)}{\partial x} + \frac{1}{r} \frac{\partial(r\rho uv)}{\partial r} + \frac{\partial P}{\partial x} - \frac{\partial(\tau_{xx})}{\partial x} - \frac{1}{r} \frac{\partial(r\tau_{rx})}{\partial r} \right\} dA = 0 \tag{3.21}$$

$$\int_{\Omega_{ie}} N_j \left\{ \frac{\partial(\rho uv)}{\partial x} + \frac{1}{r} \frac{\partial(r\rho v^2)}{\partial r} + \frac{\partial P}{\partial r} - \frac{\partial(\tau_{xr})}{\partial x} - \frac{1}{r} \frac{\partial(r\tau_{rr})}{\partial r} + \frac{\tau_{\theta\theta}}{r} \right\} dA = 0 \tag{3.22}$$

$$\int_{\Omega_{ie}} N_j \left\{ \frac{\partial(\rho uw)}{\partial x} + \frac{1}{r} \frac{\partial(r\rho vw)}{\partial r} + \frac{\rho vw}{r} - \frac{\partial(\tau_{x\theta})}{\partial x} - \frac{1}{r^2} \frac{\partial(r^2\tau_{r\theta})}{\partial r} \right\} dA = 0 \tag{3.23}$$

A similar set of integral equations are obtained for the energy equation and the turbulence and combustion equations. Note that the nondimensional '*' notation has been omitted for clarity of presentation, although all of the above equations refer to nondimensional quantities.

Integration by parts is then applied to these integrals thus reducing the constraints on the shape functions and introducing the natural boundary conditions via a boundary integral. Since the constraints have been weakened on the interpolating functions, this approach is often referred to as the weak-Galerkin method. The resulting set of algebraic equations are then solved for,

once boundary conditions have been applied. Each entry in the matrix is thus obtain by integrating the equations, multiplied by the appropriate weights, over each element. Gaussian quadrature is used to perform this integration and to accomplish this each element is transformed into a standard element over which the integration may be carried out. In this standard element the shape functions have the following form:

$$N_1 = \frac{1}{4}(1-\xi)(1-\eta)$$
$$N_2 = \frac{1}{4}(1+\xi)(1-\eta)$$
$$N_3 = \frac{1}{4}(1+\xi)(1+\eta)$$
$$N_4 = \frac{1}{4}(1-\xi)(1+\eta) \qquad (3.24)$$

These are linear interpolating functions for four node quadrilateral elements.

3.3 Boundary Conditions

The boundary conditions possible for fluid flow problems include inlet, outlet, solid wall and symmetry conditions. The boundary conditions for each of these possibilities is described for each of the flow variables. Inlet boundary conditions for velocity usually consists of an imposed value or Dirichlet boundary condition. The outflow or outlet boundary conditions are specified by applying a normal derivative value or Neumann boundary condition. For solid walls, the no-slip condition is applied to the velocity variables. For

symmetry conditions the radial velocity component is set to zero and the other velocities are left free. Pressure boundary conditions are applied through the contour or boundary integrals obtained through the weak-Galerkin formulation at the exit of the domain. The boundary conditions on temperature consist of Dirichlet conditions on all walls and inlets.

The level of turbulence at the inlets is established by Dirichlet conditions based on the intensity of the turbulence and the length scale of the dissipation of this turbulence:

$$k_{in} = I\, u_{in}^2 \tag{3.25}$$

and

$$\varepsilon_{in} = \frac{k_{in}^{1.5}}{L_d D} \tag{3.26}$$

and $\omega_{in} = \varepsilon_{in}/k_{in}$. Here I represents the turbulence intensity at the inlet, where $0.01 < I < 0.1$ with a value $I = 0{,}03$ yielding the best results for most cases. L_d represents the length scale of the energy containing eddies in the flow and D is the hydraulic diameter of the apparatus. A value of 0.005 worked best for L_d. Wall functions are used to specify the turbulent quantities at the solid walls as Dirichlet boundary conditions. The turbulent kinetic energy at a solid wall is zero, due to the no-slip condition for the velocities. The boundary condition for the dissipation ε is set to a finite value using the wall functions discussed above.

The values for the combustion model were all set as Dirichlet boundary conditions at the inlets. Here the appropriate mass fraction of each species was set to specific values. 3.4 Solution Strategy

The solution strategy consists of the details of steps followed in obtaining a converged solution for each case that was run. Strategies for solving laminar and turbulent flows differ. The strategy must address what is used as an initial guess for each of the variables, linearization methods and any relaxation applied. The initial guess of the unknowns must be within the radius of convergence of the linearization scheme. Often a zero velocity, or Stoke's flow, condition is used as an initial starting point. This usually provides a good starting point for subsequent iterations. Another approach which is very useful in obtaining solutions to high Reynolds number problems is to start the solution at a lower Reynolds number as the initial guess. In this fashion, the solution is advanced from a low Reynolds number to the final desired level by a finite number of steps. In general laminar flow solutions are easy to obtain using this approach when using a Newton linearization scheme. Turbulent flows, however, are not so well behaved. Turbulent flows requires additional steps not needed in laminar flows due to the added nonlinearities. In the present work a segregate solution strategy has been adopted to reduce

the amount of core memory needed in solving the full problem. This strategy is especially useful in the present work since, not only are turbulence equations added to the system but combustion and enthalpy variance equations are also need. A segregated solution strategy uncouples the Navier-Stokes and energy equations and turbulence model equations and solves them separately. The combustion model equations and the enthalpy variance equation, needed for the pdf calculations are also solved separately. This approach increases the number of overall iterations to full convergence of the solution, but the added flexibility in getting converged solutions more than makes up for this loss in efficiency. The first step for any test case was to obtain a laminar non-reacting solution for as high a Reynolds number as possible and use this solution as a first best guess for a turbulent non-reacting solution for the desired flow Reynolds number. Once these two steps were accomplished and a turbulent flow field was established a simple chemistry model, the EBU model discussed in chapter 2, was used to obtain a rough first solution for the temperature and density fields. Once that the Navier-Stokes and energy equations have converged a few orders of magnitude the full finite rate chemistry model is turned on. Underrelaxation is used on the density calculations until steady convergence has been re-established. When all of the equations are converging steadily the probability density function model starts working. As this work is intended to compare modified and un-

modified assumed pdf's, the flow field solution is frozen at this point and stored in a restart file. Once the flow field has been saved, calculations may proceed with either an un-modified pdf or a modified pdf. The reason thatthe flow field is stored prior to any pdf applications is that a one to one comparison is to be made between the effects of both kinds of pdf's, so it is desired that each case start from exactly the same initial flow field. The convergence criterion on each of the flow variables makes use of a standard relative error norm. This relative error norm is simply the Euclidean norm and is verified as follows:

$$\text{Error} = \frac{\left[\sum_{i=1}^{N} \left(\phi_i^n - \phi_i^{n+1}\right)^2\right]^{1/2}}{\left[\sum_{i=1}^{N} \left(\phi_i^{n+1}\right)^2\right]^{1/2}} \tag{3.27}$$

where ϕ_i^n represents any one of the flow variables at node I at the end of the nth iteration.

A Newton linearization method is used on the variables. Using this method the desired solution is a combination of the previous iteration value and the change in this value:

$$\phi^{n+1} = \phi^n + \Delta\phi^n \tag{3.28}$$

In the present work it is this change in the variables value that is actually solved for. The above solution strategy is shown schematically in figure 2.

Additional difficulties associated with the turbulence equations are centered around the nonlinear source terms that appear in these equations. One main requirement is that the turbulence variables remain positive throughout thecalculations. During the iterative process, it may become possible that negative turbulence quantities appear. If such negative values occur they cannot be used in subsequent calculations as divergence of the whole system will follow within a few short iterations. In order to maintain positive valued turbulence quantities, a clipping method may be used when the values become negative. In this approach the values of k, ε and ω are set to predetermined minimum values whenever they become negative. This method works if there are only a few nodal values which become negative, however, clipping often distorts the solution and leads to erroneous values for the turbulent viscosity. A much better approach, that is adopted in the present work, is a linearization of the source terms in the turbulence equations. Following suggestions by Patankar (1980) for what he calls always-positive variables, the source term in the k transport equation is linearized as follows:

$$\mu_t P_k - \rho\varepsilon \Rightarrow \mu_t P_k - \rho \frac{\varepsilon^n k^{n+1}}{k^n} \tag{3.29}$$

The source term in the ε transport equation is linearized as follows:

$$C_1 \mu_t \frac{\varepsilon}{k} P_k - C_2 \rho \frac{\varepsilon^2}{k} \Rightarrow C_1 C_\mu k^n P_k - C_2 C_\mu \rho \frac{k^n \varepsilon^{n+1}}{\mu_t} \tag{3.30}$$

The ω transport equation source term is also liniarized in a similar fashion:

$$C_1 \mu_t P_k - C_\mu \rho \omega k \Rightarrow C_1 C_\mu \rho P_k - C_2 \rho \omega^n \omega^{n+1} \tag{3.31}$$

Note that the definition of the turbulent eddy viscosity for the given turbulence model has been used in the linearizations shown above.

CHAPTER 4

PROBABILITY DENSITY FUNCTIONS

Probability density function (pdf) methods provide an alternative approach to turbulence and turbulent combustion modeling that requires fewer modeling assumptions and, hence, in principle, should be more accurate and general. The most attractive feature of pdf methods in particular, are their ability to overcome the chemistry closure problem in turbulent reacting flow computations. Much progress has been made in both pdf theory and application during the past decade, however, the development of such models as quantitative, predictive tools for engine design and analysis, and other industrial applications, remains an important task. In the first part of this chapter the basic definitions of pdf's are given and some examples are presented. The various numerical approaches being developed for pdf's is then briefly discussed, then particular attention is given to the focus of the present work: assumed pdf methods and variations of this approach. Numerical methods used in performing calculations with the pdf's used in the present work are then addressed.

4.1. Definitions

Consider some fluctuating quantity, Θ We can define a function, $P(\theta)$, called the probability density function, such $P(\theta)\Delta\theta$ is the fraction of time that Θ is in the interval $\Delta\theta$ during a time interval ΔT, i.e.,

$$P(\theta)\,\Delta\theta = \frac{\Delta t_1 + \Delta t_2 + \ldots + \Delta t_n}{\Delta T} \tag{4.1}$$

Then:

$$P(\theta) = \lim_{\Delta\theta \to 0} \frac{1}{\Delta\theta} \frac{\sum_{n=1}^{N} \Delta t_n}{\Delta T} \tag{4.2}$$

This function can be used to determine the probability that, at any particular time the value of Θ will be between two given values, a and b:

$$\text{Prob}(a \le \theta \le b) = \int_a^b p(\theta)\, d\theta \tag{4.3}$$

Note that we also have the following property:

$$\int_{-\infty}^{\infty} p(\theta)\, d\theta = 1 \tag{4.4}$$

The probability density function can also be used to determine the average of any function of the variable Θ. If we have $F = F(\Theta)$, then:

$$\widetilde{F} = \int_a^b F(\theta)\, P(\theta)\, d\theta \tag{4.5}$$

It will be this feature of probability density functions that we will exploit the most. In particular, we may obtain the average forward rate coefficient for a reaction, which is a function of temperature, by integrating it with respect to a probability density function in temperature:

$$\widetilde{k_f} = \int_{T_1}^{T_2} k_f\, P(T)\, dT \tag{4.6}$$

In the present work, the backward rate coefficient, k_b, becomes amplified (or suppressed) by the same factor as the forward rate coefficient.

There are several forms of pdf's that have been used in turbulent combustion calculations. The most commonly used ones are the Gaussian distribution:

$$P(\theta) = \left\{ \begin{array}{ll} \displaystyle\int_{-\infty}^{0} \frac{1}{\sigma(2\pi)^{1/2}} \exp\left[\frac{-1}{2}\left(\frac{\theta-\mu}{\sigma}\right)^2\right] d\theta & , \quad \theta = 0 \\ \displaystyle\frac{1}{\sigma(2\pi)^{1/2}} \exp\left[\frac{-1}{2}\left(\frac{\theta-\mu}{\sigma}\right)^2\right] & , \quad 0 < \theta < 1 \\ \displaystyle\int_{1}^{\infty} \frac{1}{\sigma(2\pi)^{1/2}} \exp\left[\frac{-1}{2}\left(\frac{\theta-\mu}{\sigma}\right)^2\right] d\theta & , \quad \theta = 1 \end{array} \right\} \tag{4.7}$$

It should be noted that the standard Gaussian distribution has infinite tails which would represent serious numerical problems, which is why the above

clipped version of the distribution is used. This distribution is then represented by the standard Gaussian function for $0 < \theta < 1$, but the tails have been clipped and are represented by δ-functions at both $\theta=0$ and $\theta=1$. Another commonly used pdf is the rectangular-wave distribution which is constructed from two δ-functions located at the predetermined values θ^+ and θ^-

$$P(\theta) = \alpha\,\delta(\theta - \theta^+) + (1 - \alpha)\,\delta(\theta - \epsilon^-) \tag{4.8}$$

This form of pdf, however, has been shown to be unsatisfactory for turbulent diffusion flames. An alternate to the Gaussian probability density function is the ß-probability density function. The ß-distribution is defined in terms of gamma functions as follows:

$$P(\theta) = \frac{\theta^{\beta_1 - 1}\,(1-\theta)^{\beta_2 - 1}}{\Gamma(\beta_1)\,\Gamma(\beta_2)}\,\Gamma(\beta_1+\beta_2) \tag{4.9}$$

where $\Gamma(\beta_i)$ is the gamma function and:

$$\beta_1 = \theta\left[\frac{\theta(1-\theta)}{\widetilde{\theta''\theta''}} - 1\right] \tag{4.10}$$

$$\beta_2 = (1-\theta)\left[\frac{\theta(1-\theta)}{\widetilde{\theta''\theta''}} - 1\right] \tag{4.11}$$

This function is defined for $0 < \epsilon < 1$.

The ß-probability density function, while more complicated than the Gaussian distribution, is much more flexible. It has the ability to handle fluctuations which are not symmetric about a mean value, as well as allowing for bi-modal behavior. Bi-modal behavior occurs in the early stages of mixing. As the stages of mixing progress, this bi-modal behavior disappears. The β-probability density function has one other main advantage over the Gaussian distribution in that it already has definite integration limits and no artificial clipping is required. In the present work, the ß-distribution is assumed for the temperature field

4.2. Transport Models, Assumed pdf's and Modified pdf's

The most accurate pdf calculations are based on the Monte Carlo solution of a modeled transport equation for the pdf. In Monte Carlo approaches, Lagrangian solution procedures are used in contrast to the Eulerian formulation that is the basis for most alternative methods. These applications, however, have been limited to relatively simple flow configurations due to the large demands on memory and computing time brought on by the Lagrangian particle tracking needed for these methods. The statistical error involved in using Monte Carlo methods is of the order $N^{-1/2}$, where N represents the number of particles used to represent the flow

field, so it can be readily verified that, for use in industrial combustor design, the number of particles needed to effectively model the fluid dynamics would be too prohibitive.

Instead of solving a transport equation for the probability density function for temperature, it is convenient to assume a form for the probability density function shape. Gaussian distributions are sometimes used to describe the mixing and transport of scalar flow variables. In the present work, however, the Gaussian distribution was rejected for two main reasons: the Gaussian probability density function has 'tails' which extend to plus and minus infinity, which is physically incompatible with the requirement that temperature must be limited to finite positive values. The distribution would then have to be 'clipped' arbitrarily, resulting in a violation of the fundamental property given by (4.4). The second reason is that Gaussian distributions assume that all fluctuations of the quantity are symmetric about its mean value, which is not always true for temperature fluctuations. At lower temperatures, for example, positive temperature fluctuations will be much larger than the negative fluctuations, to avoid arriving at negative temperatures. Therefore, the physics of the problem dictates that the probability density function should be asymmetric or skewed, which is not the case for Gaussian distributions. Since ß- pdf's are much more flexible and there shape may be altered to become asymmetric, they present a much more

attractive choice for turbulent combustion problems. When a static pdf shape is assumed, however, we necessarily introduce errors into the calculations, therefore, in order to minimize this error methods are being developed to bridge the gap between Monte Carlo methods and assumed pdf methods. In the present work one such method is implemented for the purposes of quantifying the benefits and drawbacks of these new methods. The idea is to have the shape of the assumed pdf evolve with the flow calculations without solving transport equations for the pdf's. The method implemented here modifies the shape of the β-pdf using the fluctuating enthalpy of the flow field. An extra equation is required to obtain this fluctuating enthalpy term at each computational grid point, but it has a very similar form to the turbulent kinetic energy equation and may, therefore be solved using standard Eulerian approaches and the segregated solver approach used in the present work means that no extra memory is needed for this equation. This fluctuating enthalpy equation is fully described in chapter 2.

Since the above definitions of the ß-pdf are for values between zero and one, a change of variables is used to normalize the temperature T to the variable θ:

$$\theta = \frac{T - T_{min}}{T_{max} - T_{min}} \tag{4.12}$$

which yields the desired condition $0 < \theta < 1$. Also, we must define the following correlation:

$$\widetilde{\theta''\theta''} = \frac{\widetilde{T''T''}}{(T_{max} - T_{min})^2} \tag{4.13}$$

Therefore, knowing the temperatures: T, T_{max} and T_{min} and the fluctuating temperature correlation: $\widetilde{T''T''}$, obtained from the solution of the fluctuating enthalpy equation, we may calculate the constants $ß_1$ and $ß_2$ and the new shape of the pdf is then determined.

Once the β-probability density function is fully defined, the integrated, probability density function weighted reaction rate coefficient can be computed:

$$\widetilde{k_f} = \int_0^1 k_f \, P(\theta) \, d\theta \tag{4.14}$$

where:

$$k_f = k_f(T(\theta)) \tag{4.15}$$

One difficulty with applying the β-pdf to temperature, is the determination of the maximum and minimum temperatures allowable in the calculations: T_{max} and T_{min}. These are the absolute limits of the temperature fluctuations. In other words, T_{max} = mean temperature + maximum possible fluctuation and T_{min}= mean temperature + maximum negative fluctuations. These extrema are not always known with absolute certainty. One method is to select the maximum and minimum temperatures in the field. The potential problem

with this approach, however, is that the global maxima and minima may have nothing to do with the local maxima and minima. In the present work the following method is used to obtain these limits:

$$T_{min} = \text{Max}\left(T - \alpha\sqrt{\widetilde{T''T''}}\ , T_{low}\right)$$

$$T_{max} = \text{Min}\left(T + \alpha\sqrt{\widetilde{T''T''}}\ , T_{high}\right) \qquad (4.16)$$

Note that by setting T_{min} and T_{max} in this way, we have assumed that the fluctuations are symmetric about the mean when the temperature becomes sufficiently far from T_{low} and T_{high}. When the temperature approaches T_{low} or T_{high}, however, the fluctuations become skewed. In the present work T_{low} was selected to be 540°R which is the injection temperature of the gaseous hydrogen, and T_{high} was selected to be slightly higher than the adiabatic flame temperature, or 4500 °R, of hydrogen in air. The value of the parameter α was chosen to be 4.6 based on numerical experimentation so that:

$$\int_{T_{min}}^{T_{max}} P(\theta)\ d\theta \approx 1 \qquad (4.17)$$

4.3. Numerical Considerations

An important numerical consideration occurs when the statistical variance approaches zero. When this occurs, the pdf behaves very much like a δ-

function and, in theory this is to be expected, however, when this expression is integrated numerically, a singularity results. The present work, which does integrate this term numerically, avoids this problem by computing a fluctuation intensity to monitor for such occurrences. This intensity is defined as follows:

$$I = \frac{\sqrt{\widetilde{T''T''}}}{T} \tag{4.18}$$

The pdf is then only used to compute the reaction rates when the intensity I is greater than 1%. If the intensity is below this value, the reaction rates are computed straight from the Arrhennius expression using only the local temperature T.

As mentioned above the β-pdf must be integrated numerically at each computational grid point to obtain the average reaction rates for each reaction in the mechanism, this reaction rate is in turn used to establish the source terms in the transport equations for each species participating in the reaction. Fortunately this integral may be evaluated analytically to obtain:

$$\widetilde{\omega_i} = M_i \left(\nu_i'' - \nu_i'\right) \widetilde{k_f} \left[\rho^{n_1} \left(\prod_{j=1}^{N} C_j^{-\nu_j'} \right) I_f - \rho^{n_2} \left(\prod_{j=1}^{N} C_j^{-\nu_i'} \right) I_b \right] \tag{4.19}$$

where

$$I_f = \frac{\prod_{i=1}^{N} \prod_{j=1}^{\nu_i'} (\beta_i + \nu_i' - j)}{\prod_{j=1}^{n_1} (B + n_1 - j)} \tag{4.20}$$

and

$$I_b = \frac{\prod_{i=1}^{N} \prod_{j=1}^{\nu_i''} (\beta_i + \nu_i'' - j)}{\prod_{j=1}^{n_2} (B + n_2 - j)} \tag{4.21}$$

with the following values given by:

$$n_1 = \sum_{i=1}^{N} \nu_i' \quad , \quad n_2 = \sum_{i=1}^{N} \nu_i'' \quad \text{and} \quad B = \sum_{i=1}^{N} \beta_i \tag{4.22}$$

This analytical form of the integrals avoids the use of costly numerical integration schemes and thus speeds up considerably the whole solution process.

CHAPTER 5

RESULTS

The results of several test-cases are discussed in this chapter. The test have been chosen to demonstrate the accuracy of the flow solver itself, the turbulence models, the basic combustion modeling added to the flow solver and, finally, the effects of modifying the shapes of probability density functions have on the chemistry model.

5.1 Validation of the Turbulence Models

The first step in the development of this finite element turbulent reacting flow solver was to include the effects of turbulence. This was done by including the two separate two-equation models described, in detail, in chapter 2. To 'adjust' all of the model constants involved, two separate tests cases were run: the first was a simple developing pipe flow with known experimental values. This test case was chosen to make sure that the turbulence models were well calibrated as to predict well known velocity profiles. Results comparing the computed developing radial velocity profiles with experimental values can be seen, for various stations along the pipe, in Figures 3, 4 and 5. Having compared very well on this test case a backward

facing step geometry was chosen next. This test case was used to further calibrate the turbulence models for cases involving recirculation and, since the ultimate goal was to model combustor geometry's, backward facing steps are good models of simple dump combustors. The inlet conditions for the turbulence models were also established at this point. Both k and ε were set as discussed in chapter 2, so as to obtain the best comparison with experimental values for this type of geometry. The backward facing step chosen for the present work has a well known reattachment length. The computed values, for both turbulence models, of this length are tabulated against experimental values in Figure 6. Figure 7 shows the streamlines and reattachment point for the k-ω model. Excellent result were obtained for both the k-ε and k-ω models. Some turbulence quantities are then shown: Figure 8. shows the contours of turbulence kinetic energy (k), Figure 9. shows contours of the dissipation of this turbulence kinetic energy (ε) and finally Figure 10. shows contours of the specific dissipation of turbulence kinetic energy (ω).

5.2 Validation of the Combustion Model

Once it was established that the turbulence models were working well on the backward facing step-type geometry, a multi-component capability and

combustion model were added to the code. Two separate test cases were used to validate the chemistry model used in the present work, one for swirling flames and another for nonswirling flames. It is often difficult to compare the mass fractions of individual species for a given flame since there is no precise definition for the limits of this flame. As is usually done, a mixture fraction is defined to compare with available experimental results. The mixture fraction was defined as the mass fraction of fuel and fuel related products in the mixture divided by the total mass. Since 29% of the mass of the products originates from the fuel, the mixture fraction at any location was given by:

$$f = \frac{1}{1 + (\text{air/fuel mass ratio})} \tag{5.1}$$

5.2.1 Eddy Breakup Model for a Non-Swirling Jet Flame

A test case, which is well documented in the literature was used to insure that the basic multi-component combustion model, which was added to the turbulent flow solver, was working properly. The cylindrical combustion chamber consists of a tube with a 0.21m internal diameter by 1.9m in length, as shown in Figure 11. A double concentric tube jet burner is axially aligned to one end of the chamber. A fairly fine 80X120 finite element grid was used for all cases involving this geometry. This grid allowed for a sufficiently fine

spacing of the nodes near the nozzle and walls where gradients are highest, thus insuring the accuracy of the solution proceedure. The first case run was for a nonswirling town-gas flame. Fuel and air mixed rapidly downstream of the inlet and products began forming at about 0.27m, as can be seen in Figure 13. At about 1.0m downstream the products mass fraction reaches a peak. This peak corresponds to the stoichiometric fuel-air ratio and peak flame temperature as can be seen in Figure 12. At this position, the calculated flame temperature was 2350 K and was within 4% of the adiabatic flame temperature. The close agreement between predicted and measured flame temperature demonstrates that the effects of combustion on gas temperature was properly modeled. Data was available to compare the computed results with experimental values of mixture fraction, as defined above. The overall agreement between measured and predicted mixture fraction along the centerline was good as can bee seen in Figure 14.

5.2.2 Eddy Breakup Model for a Swirling Jet Flame

Results for the geometry described above were also available for swirling flames. A swirl angle of 45° was chosen for the present analysis. The results of the computations demonstrate the influence of swirl on flame properties. There was a substantially faster rise in products mass fraction along the

centerline which started almost immediately after the inlet. In this case the flame was predicted as stabilized at about 0.22m downstream of the inlet, Figure 16., as compared with 1.0m for the nonswirling case. This rapid combustion is largely due to the extra mixing induced by the added turbulence imparted onto the flow by the swirling air. The temperature also rose rapidly near the inlet. reaching a maximum value of 2510 K, which also compares very well with the predicted adiabatic flame temperature Figure 15. Comparison of the mixture fraction along the centerline was also reasonable Figure 17. Although the decrease in mixture fraction near the fuel pipe was overpredicted, results compare very well over the rest of the channel. This discrepancy can be attributed to the coarseness of the computational grid in that region. The general features of both the swirling and nonswirling test cases were in general realistic, thus validating the chemistry portion of the flow solver. Experimental values where obtained from Lockwood and Naguib.

5.3 Hydrogen-Air Reaction Rates for Modified and Unmodified PDF's

The purpose of this section is to perform comparison tests between computed results, at various temperatures, with and without modifications being made

to an assumed probability density functions being applied to the hydrogen-air reaction mechanism described in chapter 2. The geometry used was the same cylindrical combustor used above. Realistic inlet conditions, including air and hydrogen temperatures and pressures were obtained from similar work done by the author at Pratt & Whitney Canada, where various nozzle designs, for hydrogen-air reactions in cylindrical combustors, were to be tested. In order to quantify the comparisons between calculations an amplification function, described in Chapter 4 was developed. The following results will show the effects of two pdf approaches on the 7 reaction rates for the hydrogen-air calculations through plots of this amplification (or suppression) factor over a wide range of temperatures. In all plots the solid line represents pdf's that have been modified using the enthalpy variance method described in chapters 2 and 4 and the dashed lines represent a pdf that remains unmodified throughout the calculations. Figures 18. through 24. show the comparison of the reaction rates for each step of the hydrogen-air mechanism. It can be observed in all of these results that the influence of modifying the pdf is negligible over a fairly wide range of operating temperatures, however, a strong influence at the extreme temperatures, especially at the higher temperatures, is felt by the reaction rates. It can also be seen that the influence felt by the modification to the pdf at higher temperatures varies for each reaction. In some of the cases, reactions 3, 5 and 7 or Figures 20., 22. and 24.,

this influence is not as pronounced as it is for the other steps in the mechanism. For these reactions the difference in amplification factors is less than 20%, whereas this difference can be as much as 109% for the other reactions, Figure 18.

5.4 Nitrogen Oxide Reaction Rates for Modified and Unmodified PDF's

Figures 25. to 27. shows the amplification and suppression of the reaction rate coefficient for the NOx mechanism presented in chapter 2. Once again the shape of the pdf has a strong influence the extreme temperatures. However, it can clearly be seen that this effect is no entirely limited to these extreme temperatures as it is for the hydrogen-air results shown above. In this case, it can be seen that the production of NOx is much more sensitive to the shape of the assumed pdf. This sensitivity is more pronounced in the first two steps of the NOx mechanism, Figure 25. and 26. whereas the third step in the reaction shows similar results as seen for the hydrogen-air reactions, Figure 27., that is there is no marked effect over a wide range of temperatures with a large difference being felt at very high or very low temperatures. For these calculations the effect that pdf shape has on the results cannot be neglected at any temperature.

CHAPTER 6

CONCLUSIONS AND RECOMMENDATIONS

6.1 Summary

A study of the use of probability density functions, in a finite element turbulent reacting flow solver has been completed. An overview of the role that probability density function play in turbulent reacting flows has been presented.

The equations of fluid motion as well as the thermochemical equations need to describe a muti-component reacting flow field were outlined in Chapter 2. A finite element descritization of these equations was implemented into a two-dimensional, axisymmetric flow solver. The finite element code started from a very accurate, second order, laminar flow solver. The first step was to include the effects of turbulence through the addition of, first, a standard k-ε model and then a k-ω model. These models were calibrated and tested on two basic geometry's: developing flow in a straight pipe and flow over a backward facing step. The developing pipe flow was chosen to insure that the turbulent flow solver could reproduce well known flow characteristics such as maximum centerline velocities and development lengths. The backward

facing step was chosen since it has all of the basic characteristics of a typical dump combustor geometry. Also, a well known test for flow solvers is to reproduce accurate reattachment lengths for the separated region. The next major step was to add a multi-component capability to the code. Here, the gas is broken down into its constitutive components, each of which is transported by its own equation of continuity. The treatment of the thermodynamic properties was also modified to that of a mixture thermochemistry. The code was now ready for its first combustion model: the one-step, equilibrium chemistry, eddy breakup model. This model was chosen for two main reasons: firstly, this is the most common model used in industry today and, although it does not give any details of the combustion process itself, the model does a good job of predicting overall temperature fields. The second reason for choosing this combustion model is a purely numerical one. The ultimate goal of solving for the individual chemical kinetics involved in the combustion process, is a computationally very stiff one and much relaxation is need to coax the code to converge at a steady rate. Here the eddy breakup model plays the role of a first approximation to the thermochemical properties, of the given reactions, before implementing the full kinetic mechanism. In this way one is able to achieve satisfactory overall convergence faster and with less under-relaxation of the main variables. To test the eddy breakup model, a well known dump combustor test case was

chosen that has results for both swirling and non-swirling inlet conditions. Once the eddy breakup model was working well for this test case the next step was to include a kinetic model for the reactions as well as the probability density function treatment of the rate coefficients. Here a hydrogen-air reaction mechanism was chosen as the focus of this study. This scheme was chosen because of the relative simplicity of its reaction mechanism and for the growing popularity of this gas as a fuel for automotive and aeronautical applications due to its abundance. The final step in building the finite element code was to add a NOx post-processor. The Nox reactions were also used to judge the effects of different shapes of probability density. Since hydrogen burn at very high temperatures it is feared that, if not properly controlled, these high temperatures would lead to a significant about of atmospheric nitrogen to be converted into nitric oxides. It is therefore necessary to have analytical tools at our disposition to be able to design nozzles and combustors that will burn hydrogen in such a way as to minimize the impact on the environment. And the proper use of pdf's in these applications is of fundamental importance in achieving realistic numerical results. Most of the theoretical development of the turbulent combustion model here has centered around the use of the H_2/Air reaction mechanism presented in Chapter 2. Of concern to gas turbine combustor designers also, however, is applicability of turbulent combustion and NOx

emissions models in particular, to hydrocarbon fuels used in laboratory research combustors and in commercial and military engines. These fuels include methane and propane, and jet fuels such as Jet-A, P-8, etc. Progress in developing these reduced reaction sets has been slow due to the complexity of these fuels and the extended sets of elementary reactions (greater than 300 reactions for propane alone) needed to describe their behavior over the range of temperatures and pressures and equivalence ratios observed over the entire combustion process. The difficult feature of this process is to rigorously analyze each reaction in the mechanism, and systematically eliminate those reactions and species not contributing significantly to the final enthalpy and species concentration values.

The prospects for computation of thermal NOx emissions for hydrocarbon fuels, however, are good, with the post-processing approach described in the present work. Since the NOx reaction mechanism is more closely coupled to the hydrocarbon's reaction mechanism. For example, a reduced reaction mechanism to compute propane/Air combustion with NOx is currently available involving approximately 16 species, and 30 reactions. the CPU requirements for such a large reaction set are formidable. With expected short-term advances in parallel workstation technology and in supercomputing speeds, however, such calculations should prove feasible for use in CFD codes for certain high priority tasks. Clearly, much progress is

needed in several disciplines before finite rate based emissions calculations become a standard analytical tool for combustion designers. As a bridging technology, and a way of obtaining a first good approximation, a good two-dimensional axisymmetric model, using a postprocessor with probability density functions, for NOx emission calculations can be used as a fast engineering tool.

6.2 Conclusions

The first conclusion to be drawn from this work is that using the finite element method to solve turbulent combustion problems by segregating the various models from the main flow solver is a very practical and efficient approach to handling such problems. Although there is always going to be a trade off when equations are solved for in an uncoupled manner, the benefits of added flexibility to the solution strategies far outweigh any extra time needed to converge the problem. Having the energy equation uncoupled from the Navier-Stokes equations allowed for relaxation strategies to be applied to the density calculations. This proved invaluable when a chemistry model was added to the code. The sudden changes in density due to the combustion process were easily handled by allowing the effects of the chemical reactions to be progressively loaded into the density updates. This

approach was especially useful in the early stages of convergence when the changes in density were very large. As the solution began to converge steadily this relaxation could be slowly removed until final convergence was achieved. Also, having the turbulence and species equations solved separately meant that both models could share the same memory allocation and different relaxation strategy could be used on each model to achieve maximum stability. This approach, therefore, removes one of the conceived disadvantages to the finite element method for fluid flow problems, especially with turbulence and combustion, that is of the high impact it has on computer resources.

Both the test cases for validating the turbulence and the simple chemistry models gave good results and agreed well with experimental values. This laid a good foundation for the purpose of this study: to compare reaction rate calculations using modified and unmodified probability density functions. When applied to a reduced hydrogen-air reaction mechanism, the main conclusion to be drawn is that there is little benefit in modifying the shape of an assumed pdf for a wide range of operating conditions. For most of the 7 reactions used there is no significant difference between the reaction rates obtained with modified or unmodified pdf's between temperatures of 555 K and 2200 K. At the extreme temperatures, however some of the reactions in the mechanism showed significant difference for both types of pdf's.

Although some of the reactions showed more sensitivity than others to the change in pdf's, all showed change. This information shows that the type of pdf used to calculate the reaction rates becomes quite important for low temperature phenomena such as engine blow-outs and for very high temperature problems such as autoignition. From a practical and numerical point of view these results suggest that for general calculations of medium and regular operating condition temperatures the extra expense of modifying the shape of an assumed pdf is not needed, very similar results would be obtained if either method were used. However, when specialized problems are being analyzed, where the flow temperatures are at their extremes modifying the shapes of the pdf's as the flow evolves will have a large impact on the results. This can be seen even more clearly for the results obtain for the NOx reactions. The production of NOx is seen to be sensitive to the shape of the pdf used over most temperatures, not only at the extreme values. This sensitivity implies that pdf's used to calculate such reactions must be made to reflect the local flow conditions and that simply using an assumed shape for a pdf will lead to great under or over prediction of the NOx formed, depending on the temperatures involved.

6.3 Recommendations

The present work showed that need to calculate the shape of a pdf only became important, for the hydrogen-air mechanism, when certain temperature ranges are encountered. This work should be extended to hydrocarbon fuels as soon as reduced mechanisms become available which can be handle without difficulty on today's computers. The range of temperatures over which the shape of the pdf has negligible impact on the reaction rates might not be as large and the idea of unmodified assumed pdf's might have to be abandoned all together for these problems. The main recommendation to come out of the present study is to continue research in numerical methods aimed at modeling the evolution of pdf's in problems of pollutant formation, Nox formation in particular. The sensitivity of these phenomena to local temperature fluctuations means that a single assumed pdf could never capture the ever-changing character of the local temperature field. The use of enthalpy variance is one method of modifying the shape of the pdf to suit the local flow conditions. Other methods should be investigated and developed, including the use of fractals and strange attractors from chaos theory. The stretching and folding behavior of such mathematical tools has long been observed in turbulent flows, it remains,

however, to find a suitable way of introducing these concepts into a practical numerical method for solving turbulent reacting flows.

REFERENCES

Ait Ali Yahia, D., Habashi, W.G. and Baruzzi, G.S. (1994) A Finite Element Method for Hypersonic Reacting Flow, Advances in Finite Element Analysis in Fluid Dynamics, ASME.

Anagnostopoulos J.S. and Bergeles G. (!992) Discrete-Phase Effects on the Flowfield of a Droplet-laden Swirling Jet with Recirculation: A Numerical Study, Int. J. Heat and Fluid Flow, Vol. 13, 141-150.

Axelsson O.A. and Baker V.A. (1984) Finite Element Solution of Boundary Value Problems, Academic Press.

Babuska, I. (1971), Error-Bounds for Finite Element Method, Numer. Math., Vol.16, 322-333

Babuska, I. and Aziz A. (1972), Survey Lectures on the Mathematical Foundations of the Finite Element Method, The Mathematical Foundations of the Finite Element Method with Application to Partial Differential Equations, Academic, NewYork.

Baker, A.J. (1973), Finite Element Solution Algorithm for Viscous Incompressible Fluid Dynamics, Int. J. Numer. Meth. Eng., Vol. 6, 89-101.

Baruzzi, G.S., Habashi, W.G. and Hafez, M.M. (1992b) An Improved Finite Element Method for the Solution of the Compressible Euler and NavierStokes Equations, Proceedings of the First European Computational Fluid Dynamics Conference - Volume 2 (ECCOMAS), eds. Ch. Hirsch, J. Periaux, E. Onate, Elsevier, Brussels, Belgium, 643-650.

Bathe, K.J. and Cimento A.P. (1980), Some Practical Procedures for the Solution of Nonlinear Finite Element Equations, Comp. Meth. Appl. Mech. Eng., Vol 22, 59-85.

Baurle R.A., Drummond J.P. and Hassan H.A. (1992) An Assumed PDF Approach for the Calculation of Supersonic Mixing Layers, AIAA Paper 92-0182.

Bestek, H., Thumm, A. and Fasel, H. (1992) Direct Numerical Simulation of Three-Dimensional Breakdown to Turbulence in Compressible Boundary Layers, Proceedings of the 13th International Conference on Numerical Methods in Fluid Dynamics, eds. M. Napolitano and F. Sabetta, SpringerVerlag, Rome, Italy, 145-149.

Boivin, S. and Fortin, M. (1993) A New Artificial Viscosity Method for Compressible Viscous Flow Simulations by FEM, International Journal of Computational Fluid Dynamics, 1, 25-41.

Bowman C.T. (1975) Kinetics of Pollutant Formation and Destruction in Combustion, Prog. Energy Combust. Sci., Vol. 1, 33-45.

Chen H.C. and Patel V.C. (!988) Near-Wall Turbulence Models for Complex Flows Including Seperation, AIAA Journal, Vol. 26, No. 6, 641-648.

Chomiak J. (1990) Combustion A Study in Theory Fact and Application, Gordon and Breach Science Publishers, Gupta A.K. and Lilley D. G. Editors.

Chung T.J. (1993) Numerical Modeling in Combustion, Taylor & Francis, Publishers, Minkowycz W.J. and Sparrow E.M. editors.

Conley J. and Zeman P. (1991) Verification of the PROTEUS Two-Dimensional Navier-Stokes Code for Flat Plate and Pipe Flows, AIAA Paper 91-2013.

Dutto, L.C., Habashi, W.G., Fortin, M. and Robichaud, M.P. (1993) Parallelizable Block-Diagonal Preconditioners for 3D Viscous Compressible Flow Calculations, AIAA Paper 93-3309, Proceedings of the 11th AIAA Computational Fluid Dynamics Conference - Vol. 2, Orlando, Florida, 135-143.

Eickhoff H. and Winandy A. (1985) Visualization of Vortex Formation in Jet Diffusion Flames, Combustion and Flame, Vol. 60, No. 1, 99-101.

Faeth G.M. (1987) Mixing Transport and Combustion in Sprays, Prog. Energy Combust. Sci., Vol. 13, 293-345.

Frohlich A., Immich H., LeBail F., Popp M. and Scheuerer (1991) Three-Dimensional Flow Analysis in a Rocket Engine Coolant Channel of High Depth/Width Ratio, AIAA Paper 91-2183.

Ghaly W.S., Habashi W.G., Peeters M.F., Gauthier P.Q. and Robichaud M.P. (1992) Finite Element Solution of Viscous Compressible Flows in Gas Turbine Components, Proceedings of the 4th International Symposium on Transport Phenomena and Dynamics of Rotating Machinery, Honolulu, April 1992, 641-651.

Girimaji S.S. (1991) A Simple Recipe for Modelling Reaction-Rates in Flows with Turbulent Combustion, AIAA Paper 91-1792.

Givi P. (1989) Model-Free Simulations of Turbulent reactive Flows, Prog. in Energy and Combust. Sci., Vol. 15, 1-107.

Gosman A.D. and Ioannides E. (1983) Aspects of Computer Simulation of Liquid-Fueled Combustors, J. Energy, Vol. 7, 482-490.

Gupta, A.K. and Lilley D.G., Flowfield Modeling and Diagnostics, Abacus Press, 1985.

Habashi, W.G., Fortin, M., Liu, J.W.H., Robichaud, M.P., Nguyen, V-N and Ghaly, W.S. (!991) Large-Scale Computational Fluid Dynamics by the Finite Element Method, AIAA Paper 91-0120.

Habashi W.G. and Youngson G.G. (1983) A Transonic Quasi-3D Analysis for Gas Turbine Engines including Split-Flow Capability for Turbofans, Int. J. Numer. meth. Fluids, Vol. 3, No. 1, 1-22.

Hafez, M.M. and Soliman, M. (1991) Numerical Solution of the Incompressible Navier-Stokes Equations in Primative Variables on Unstructured grids, AIAA paper 91-1561.

Haroutounian, V. and Engelman, M.S. (1991) On Modeling Wall Bound Turbulent Flows Using Specialized Near-Wall Finite Elements and the Standard k- ε Turbulence Model, Advances in Numerical Simulation of Turbulent Flows, ASME, Vol. 117, 95-105.

Hinze J.O. (1975) Turbulence, McGraw Hill, New York.

Hoffmann, K.A. and Chiang, S.T. (1993) Computational Fluid Dynamics for Engineers, Vol. I, Engineering Education Systems, Wichita, Kansas.

Hollander, H. and Ravalason, W. (1986) Resolution des Equations de NavierStokes en Fluide Compressible par Methode Implicite, La recherche Aerospatial, 1, 23-46.

Jaeger, M. and Dhatt, G. (1992) An extended k-ε Finite Element Model, International Journal for Numerical Methods in Fluids, 14, 1325-1345.

Jones, W.P. and Launder, B.E. (1972) The Prediction of Laminarization with a Two-Equation Model of Turbulence, Int. J. Heat Mass Transfer, Vol. 15, 301-314.

Jones, W.P. and Launder, B.E. (1973) The Calculation of Low Reynolds Number Phenomena with a Two Equation Model of Turbulence, Int. J. Heat Mass Transfer, Vol. 16, 1119-1130.

Kennedy, L.A. (1977) Turbulent Combustion, American Institute of Aeronautics and Astronautics, NewYork, New York.

Kim, S.W. (1988) A Fine Grid Finite Element Computation of Two-Dimensional High Reynolds Number Flows, Compt. Fluids, Vol. 16, No. 4, 429-444.

Kuo K.K. (1986) Principles of Combustion, John Wiley & Sons, Publishers.

Kuznetsov V.R. and Sabel'nikov V.A. (1993) Turbulence and Combustion, Hemisphere Publishing Corporation, New York.

Lam, C.K.G. and Bremhorst K. (1981) A Modified Form of the k-ε Model for Predicting Wall Turbulence, J. Fluids Eng., Vol. 103, 456-460.

Laufer J. (1951) Investigation of Turbulent Flow in a Two-Dimensional Channel, NACA Report 1053, 1247-1266.

Launder B.E. (1988) On the Computation of Convective Heat Transfer in Complex Turbulent Flows, J. Heat Transfer, Vol. 110, 1112-1128.

Launder B.E. (1989) Second-Moment Closure and its Use in Modelling Turbulent Industrial Flows, Int. J. Numer. Meth. Fluids, Vol. 9, 963-985.

Launder B.E. and Sharma B.I. (1974) Application of the Energy Dissipation Model of Turbulence to the Calculation of Flow Near a Spinning Disc, Letters Heat Mass Transfer, Vol. 1, 131-138.

Launder B.E. and Spalding D.B. (1974) The Numerical Computation of Turbulent Flows, Comp. Meth. Appl. Mech. and Eng., Vol. 3, 269-289.

Lockwood F.C. and Naguib A.S. (1975) The Prediction of the Fluctuations in the Properties of Free Round-Jet, Turbulent Diffusion Flames, Combustion and Flame, Vol. 24, 109-124.

Magnussen B.F. and Hjertager B.H. (1976) On Mathematical Modelling of Turbulent Combustion with Special Emphasis on Soot Formation and Combustion, Proc. 16th Sympossium (International) on Combustion.

Manouzi H. and Fortin (1991) A Treatment of Wall Boundaries for Turbulent Flows by the Use of a Transmission Finite Element Method. Int. J. Numer. Meth. Eng., Vol. 31, 113-126.

Matthies H. and Strang G. (1979) The Solution of Nonlinear Finite Element Equations. Int. J. Numer. Meth. Eng., Vol. 14, 1613-1626.

McBride B.J., Heimel S., Ehlers J.G. and Gordon S. (1963) Thermodynamic Properties to 6000° K for 210 Substances Involving the first 18 Elements, NASA SP-3001.

Miller J.A. and Bowman C.T. (1989) Mechanism and Modelling of Nitrogen Chemistry in Combustion, Prog. Energy Combust. Sci., Vol. 15, 287-338.

Morgan K., Hughes T.G. and Taylor C. (1979) The Analysis of Turbulent, Free-Shear, and Channel Flows by the Finite Element Method, Compt. Meth. Appl. Mech. Eng., Vol. 19, 117-125.

Myong H.K. and Kasagi N. (1988) A New Proposal for a k-ε Turbulence Model and its Evaluation. 1st Report, Development of the Model, Trans. Japan Soc. Mech. Eng., Series B, Vol. 54, No. 507, 3003-3009.

Nagano Y. and Hishida M. (1987) Improved Form of the k-ε Model for Wall Turbulent Shear Flows, J. Fluids Eng., Vol. 109, 156-160.

Nagano, Y. and Tagawa M. (1990) An Improved k-ε Model for Boundary Layer Flows, J. Fluids Eng., Vol. 112, 33-39.

Narayan J.R. (1991) A Two-Equation Turbulence Model for Compressible Reacting Flows, AIAA Paper 91-0755.

Nonino, C and Del Giudice S. (1988) Finite Element Analysis of Turbulent Forced Convection in Lid-Driven Rectangular Cavities, Int. J. Numer. Meth. Eng., Vol. 25, 313-329.

Oden J.T. and Wellford L.C. jr. (1972) Analysis of Flow of Viscous Fluids by the Finite Element Method, AIAA J., Vol. 10, No. 12, 1590-1599.

Oosthuizen P.H. and Paul J.T. (1990) Laminar Forced Convection Heat Transfer Downstream of a Rearward Facing Step, AIAA paper 90-1726.

Ostrach S. (1988) Natural Convection in Enclosures, J. Heat Transfer, Vol. 110, No. 4(B), 1175-1190.

Pai, S.I. (1953) On Turbulent Flow Between Parallel Plates, J. Appl. Mech., Vol. 20, 109-114.

Patankar S.V. (1980) Numerical Heat transfer and Fluid flow, Hemisphere Publishing Corporation, Washington, New York, London.

Patel V.C., Rodi W. and Scheuerer (1985) Turbulence Models for Near-wall and Low Reynolds Number Flows: A Review, AIAA J., Vol. 23, No. 9, 1308-1319.

Peeters M.F., Habashi W.G., Nguyen B.Q. and Kotiuga P.L. (1992) Finite Element Solutions of the Navier-Stokes Equations for Compressible Internal Flows, AIAA Paper 90-0441, also AIAA Journal of Power and Propulsion, Vol. 8, No. 1.

Pelletier D., Fortin A. and Camarero R. (1989) Are FEM Solutions of Incompressible Flows Really Incompressible? (Or How Simple Flows can Cause Headaches!), Int. J. Numer. Meth. Fluids, Vol 9, 99-112.

Polansky G.F., Lamb J.P. and Crawford M.E. (1984) A Finite Element Analysis of Incompressible Turbulent Backstep Flow with Heat Transfer, AIAA paper 84-0178, 1-6.

Polansky G.F. (1987) Finite Element Simulation of Recirculating Flows with Heat Transfer, Commun. Appl. Numer. Meth., Vol. 3, 17-22.

Pope S.B. (1985) PDF Methods for Turbulent Reactive Flows, Prog. in Energy and Combust. Sci., Vol. 11, 119-192.

Pope S.B. and Chen Y.L. (1990) The Velocity Dissipation Probability Density Function Model for Turbulent Flows, Physics in Fluids, Vol. 2, 1437-1449.

Ramaswamy B. (1988) Finite Element Solution for Advection and Natural Convection Flows, Compt. Fluids, Vol. 16, No. 4, 349-388.

Reddy J.N. (1984) An Introduction to the Finite Element Method, McGraw Hill, New York.

Rizk N.K. and Mongia H.C. (1992) Three-Dimensional Gas Turbine Combustor Emissions Modeling, ASME Paper 92-GT-129.

Rodi W. (1989) Recent Developments in Turbulence Modelling, Refined Flow Modelling and Turbulence Measurements, Universal Academy Press, 3-17.

Savas O. and Gollahalli S.R. (!986) Flow Structure in Near Nozzle Region of Gas Jet Flames, AIAA Journal, Vol. 2, No. 7, 1137-1140.

Segal A. (1979) On the Numerical Solution of the Stokes Equiations Using the Finite Element Method, Compt. Meth. Appl. Mech. Eng., Vol. 19, 165-185.

Shih T.H. and Hsu A.T. (1991) An Improved k-ε Model for Near-Wall Turbulence, AIAA Paper 91-0611.

Silvester D.J. and Thatcher R.W. (1986) The Effect of the Stability of Mixed Finite Element Approximations on the accuracy and Rate of Convergence of Solution when Solving Incompressible Flow Problems, Int. J. Numer. Meth. Fluids, Vol. 6, 841-853.

Smith R.M. (1984a) On the Finite Element Calculation of Turbulent Flow Using the k-ε Model, Int. J. Numer. Meth. Fluids, Vol. 4, 303-319.

Smith R.M. (1984b) A practical Method of Two-Equation Turbulence Modelling Using Finite Elements, Int. J. Numer. Meth. Fluids, Vol. 4, 321-336.

Smith R.M. and Hutton A.G. (1982) The Numerical Treatment of Advection: A Performance Comparison of Current Methods, Num. Heat Transfer, Vol. 5, 439-461.

Speziale C.G., Abid R. and Anderson E.C. (1990) A Critical Evaluation of Two-Equation Models for Near-Wall Turbulence, AIAA Paper 90-1481.

Stephenson P.L. (1976) A Theoretical Study of Heat Transfer in Two-Dimensional Turbulent Flow in a Circular Pipe and Between Parallel and Diverging Plates, Int. J. Heat Mass Transfer, Vol. 19, 413-423.

Sugavanam A. (1985) Evaluation of Low Reynolds Number Turbulence Models for Attached and Seperated Flows, AIAA Paper 85-0375, 1-11.

Takahashi F., Mizomoto M and Ikai S. (1982) Transition from Laminar to Turbulent Free Jet Diffusion Flames, Combustion and Flame, Vol. 48, No. 1, 85-95.

Taylor C., Thomas C.E. and Morgan K. (1981b) Modelling Flow Over a Backward Facing Step Using FEM and the Two-Equation Model of Turbulence, Int. J. Numer. Meth. Fluids, Vol. 1, 295-304.

Taylor C., Hughs T.G. and Morgan K (1977) A Numerical Analysis of Turbulent Flow in Pipes, Compt. Fluids, Vol. 5, 191-204.

Tong G.D. (1982) A treatment of Wall Boundaries for (k-ε) Turbulence Modelling Within an Integral (Finite Element) Formulation, Finite Element Flow Analysis, North-Holland Publishing Co., 227-236.

Utnes T. (1988) Two-Equation (k- ε) Turbulence Computations by the Use of a Finite Element Method, Int. J. Numer. Meth. Fluids, Vol. 8, 965-975.

Van Doormal J.P., Turan A. and Raithby G.D. (1987) Evaluation of New Techniques for the Calculation of Internal Recirculating Flows, AIAA Paper 87-0059.

Van Driest E.R. (1956) On Turbulent Flow Near a Wall, J. Aero. Sci., 1007-1011 and 1036.

Wilcox D.C. (1991) A Half Century Historical review of the k-ω Model, AIAA Paper 91-0615.

Zienkiewicz O.C., Loehner R., Morgan K. and Nakazawa S. (1984) Finite Elements in Fluid Mechanics - A Decade of Progress, Finite Elements in Fluids, Ed. R.H. Gallagher, J.T. Oden, O.C. Zienkiewicz, T. Kawai and M. Kawahara, John Wiley & Sons, Vol. 5, 1-26.

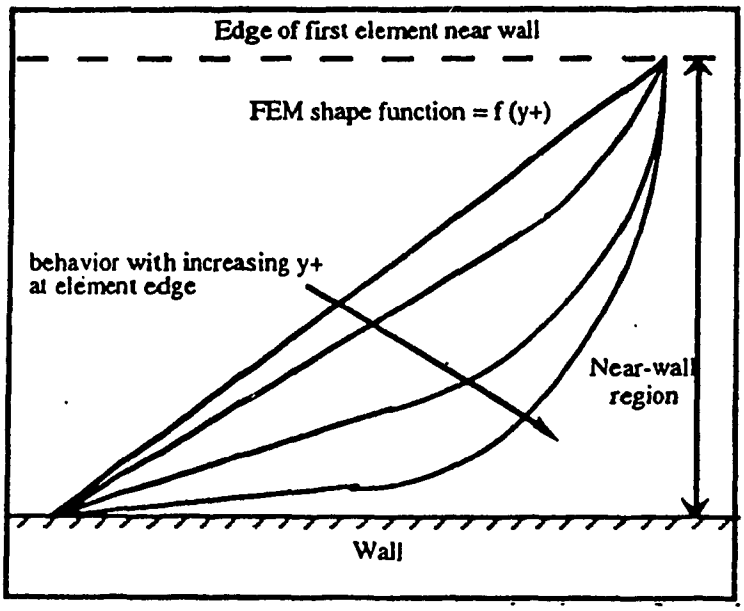

Figure 1. Logarithmic wall element for increasing values of y+

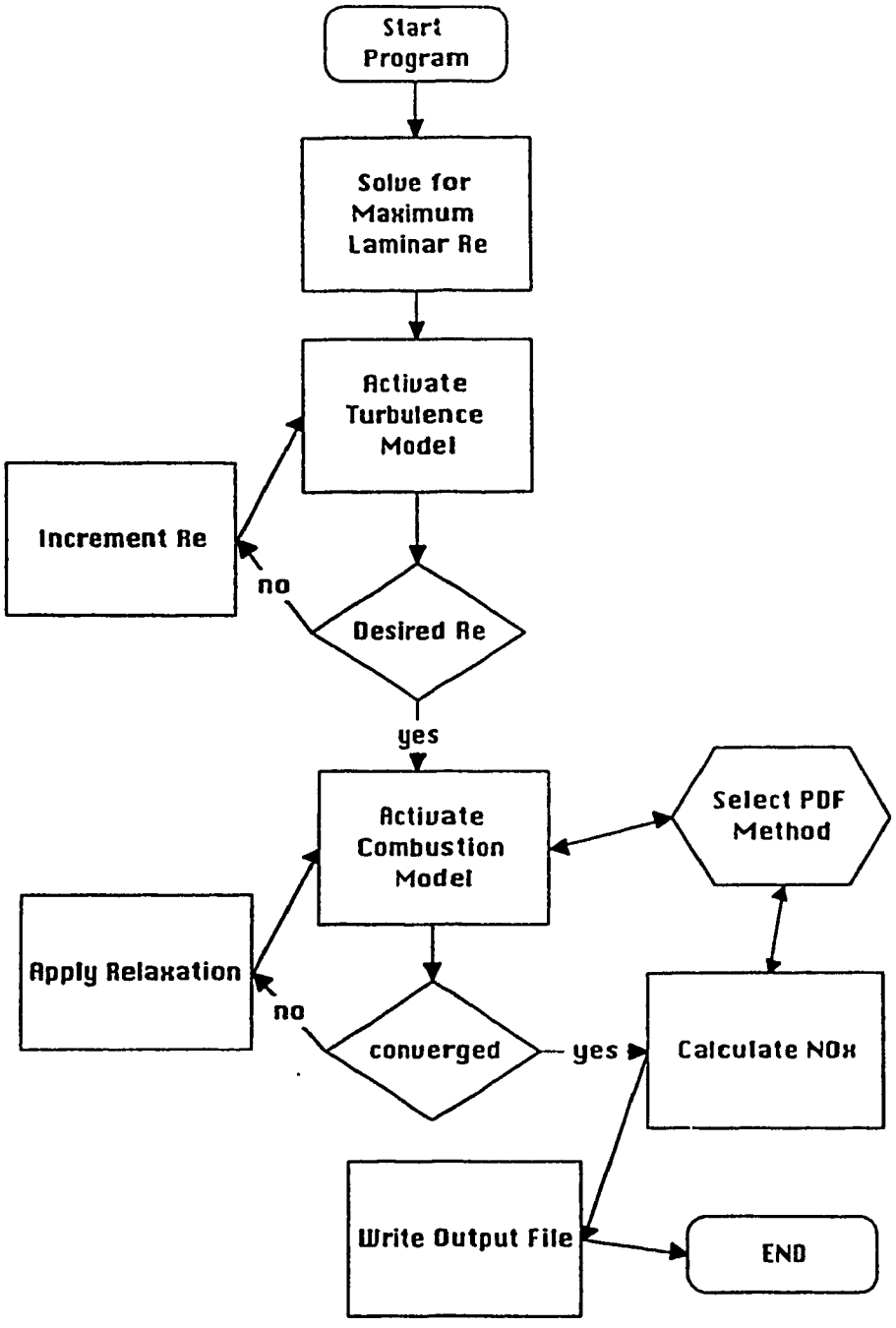

Figure 2. Flowchart of solution strategy

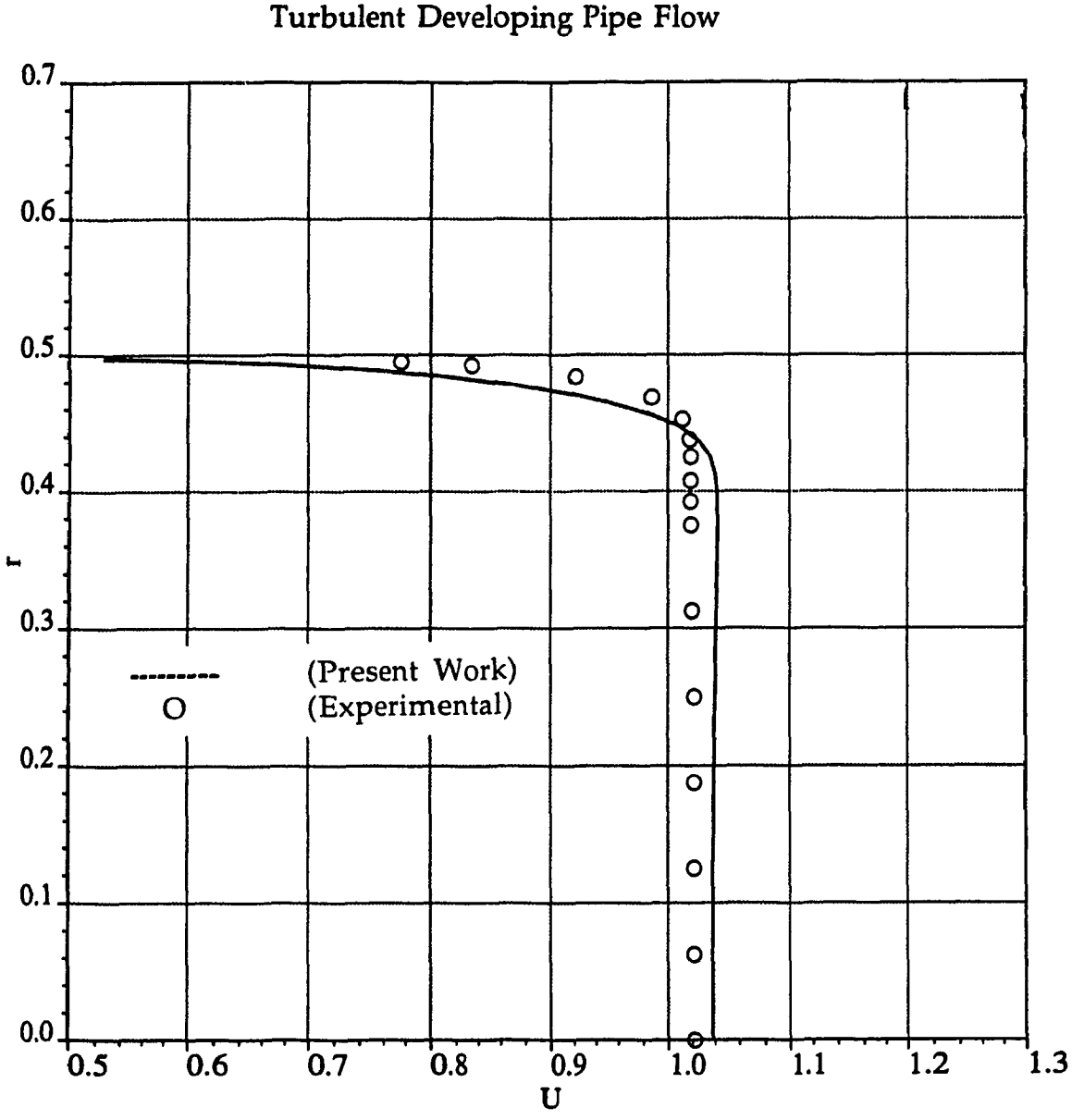

Figure 3. Experimental comparison of radial velocity profiles in a developing pipe flow at axial station x= 1.5.

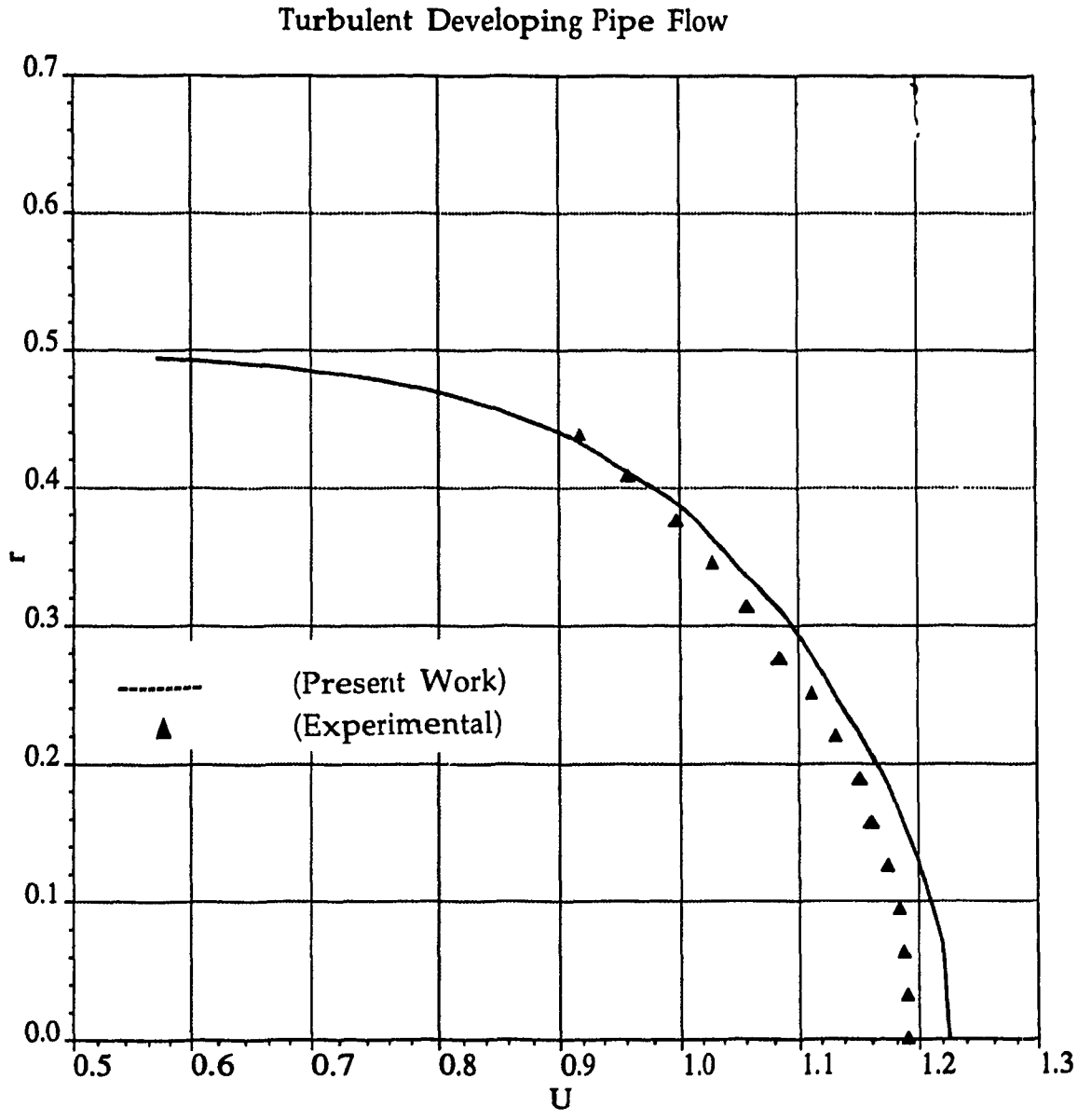

Figure 4. Experimental comparison of radial velocity profiles in a developing pipe flow at axial station x= 28.5.

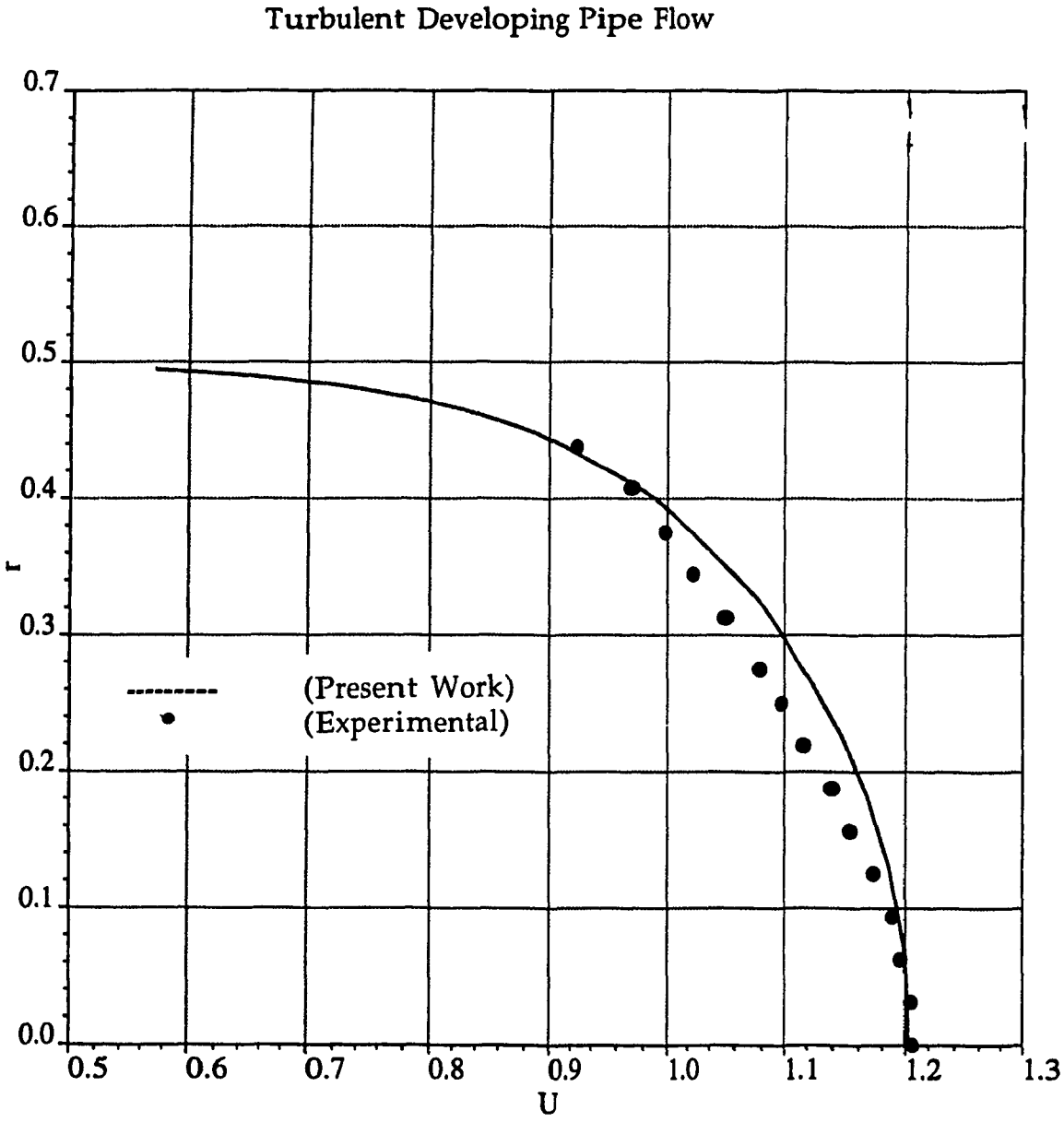

Figure 5. Experimental comparison of radial velocity profiles in a developing pipe flow at axial station x= 40.5.

Model	Reference	Attachment Length
k-ε	Launder (1974)	5.20
k-ω	Wilcox (1988)	6.40
k-ε	Present Work	6.11
k-ω	Present Work	6.32
Measured	Driver-Seegmiller (1985)	6.20

Figure 6. Experimental comparison of reattachment length for turbulent flow over a backward facing step.

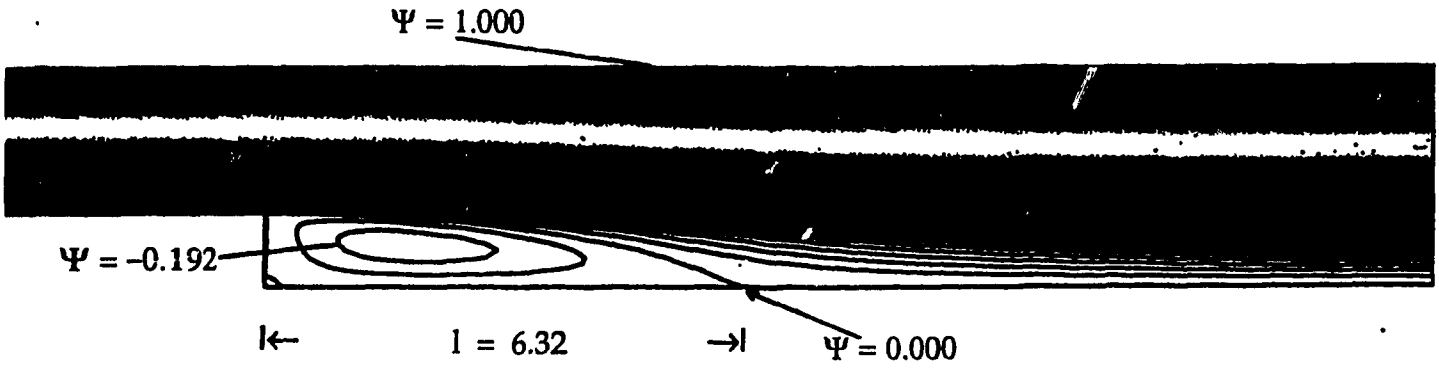

Figure 7. Streamlines (Ψ) showing the location of the reattachment point at Ψ = 0: (Ψ_{min} = -0.192, $\Delta\Psi$ = 0.05)

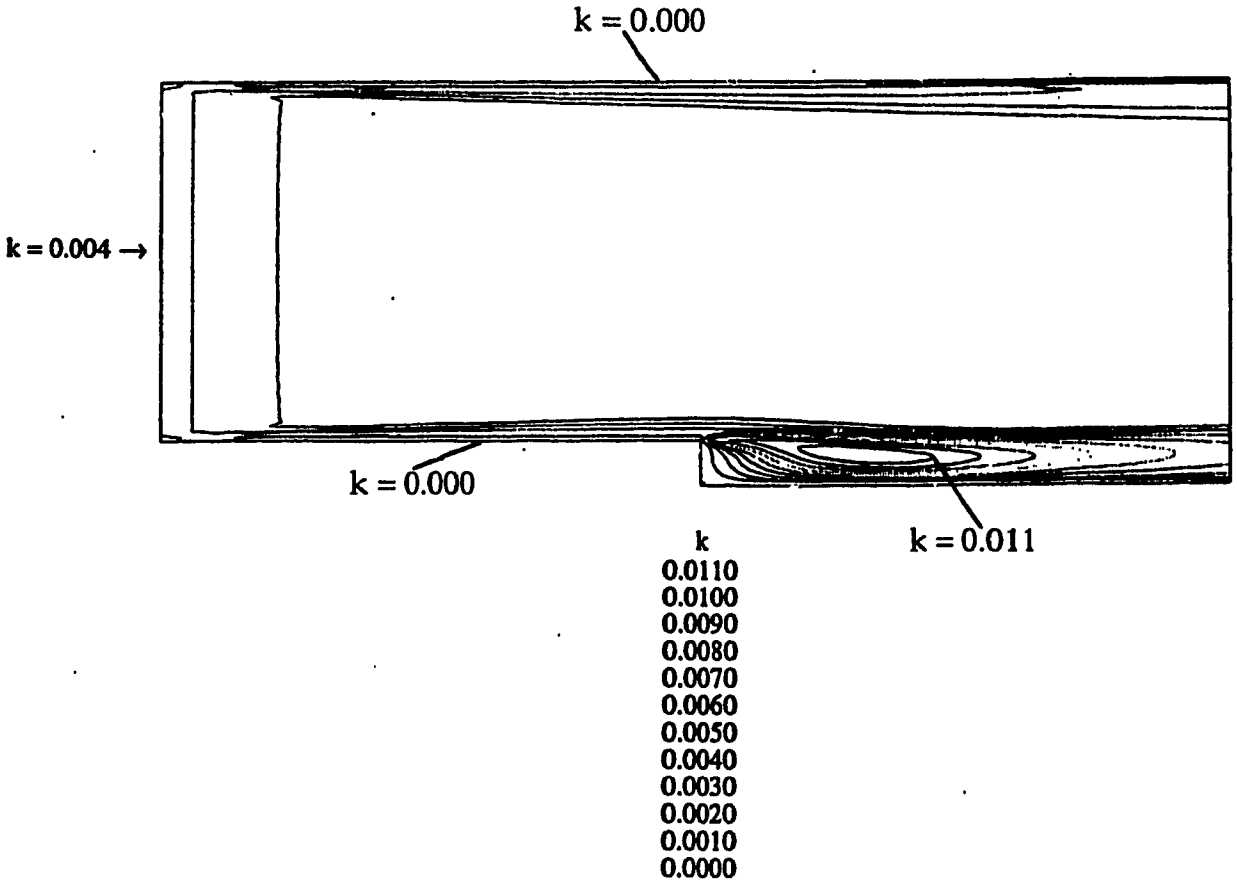

Figure 8. Turbulence Kinetic Energy (k) contours for the backward facing step: ($k_{min} = 0.0$, $\Delta k = 0.001$)

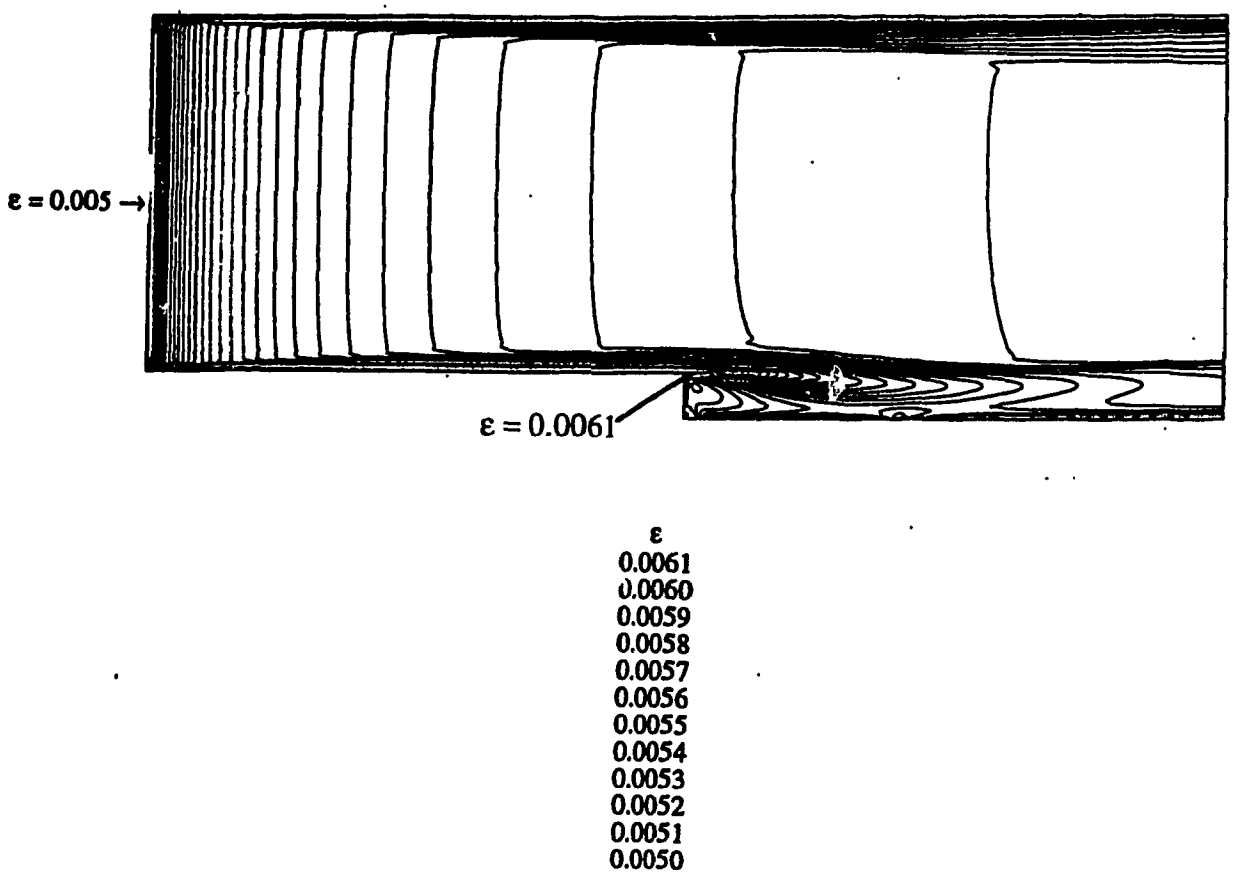

Figure 9. Dissipation of Turbulence Kinetic Energy (ε) contours for the backward facing step: ($\varepsilon_{min} = 0.005, \Delta\varepsilon = 0.0001$)

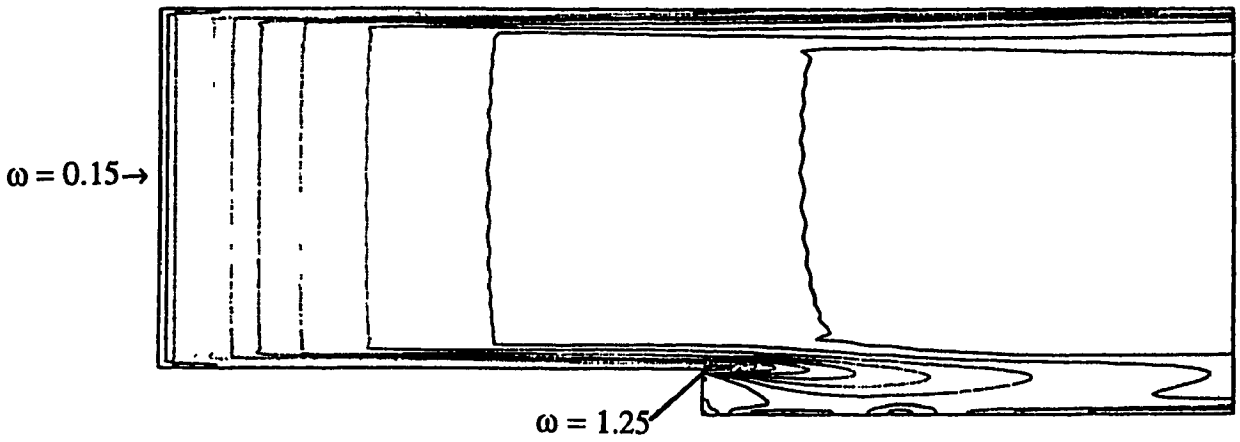

ω
1.2500
1.1500
1.0500
0.9500
0.8500
0.7500
0.6500
0.5500
0.4500
0.3500
0.2500
0.1500
0.0000

Figure 10. Specific dissipation of Turbulence Kinetic Energy (ω) contours for the backward facing step: ($\omega_{min} = 0.0, \Delta\omega = 0.1$)

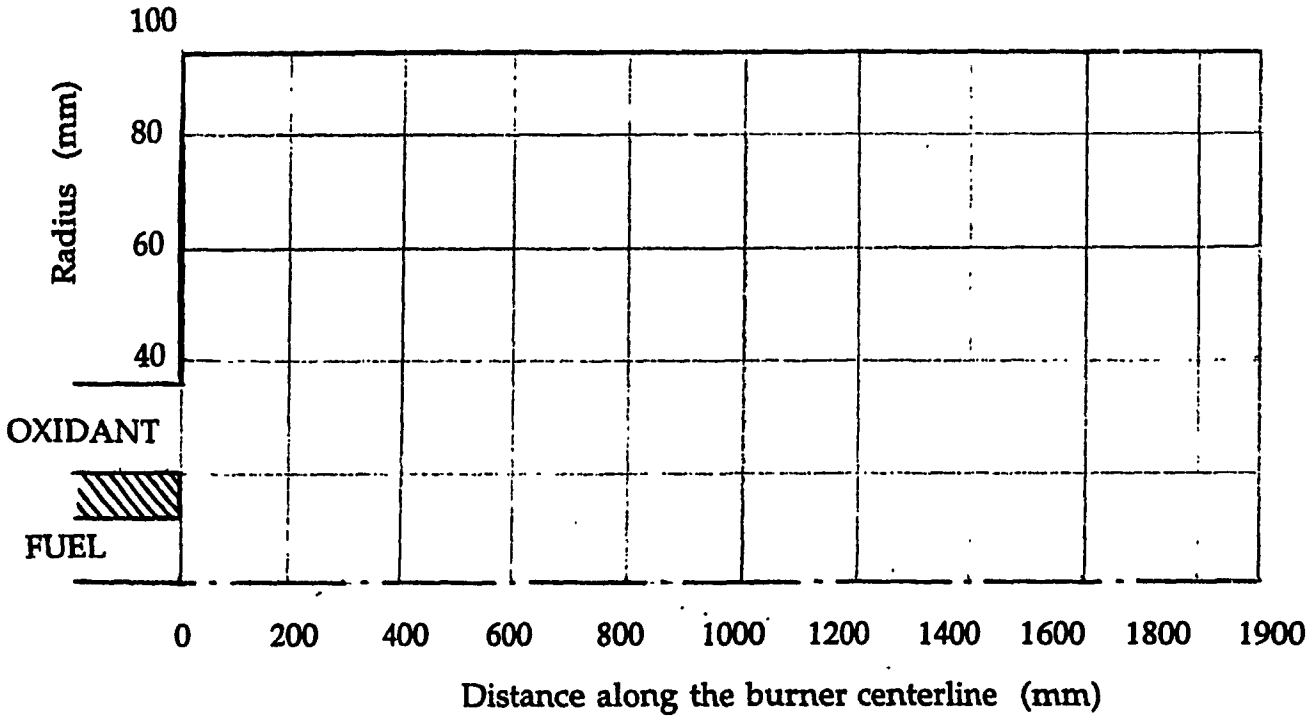

Figure 11. Sketch of the Flame Jet geometry

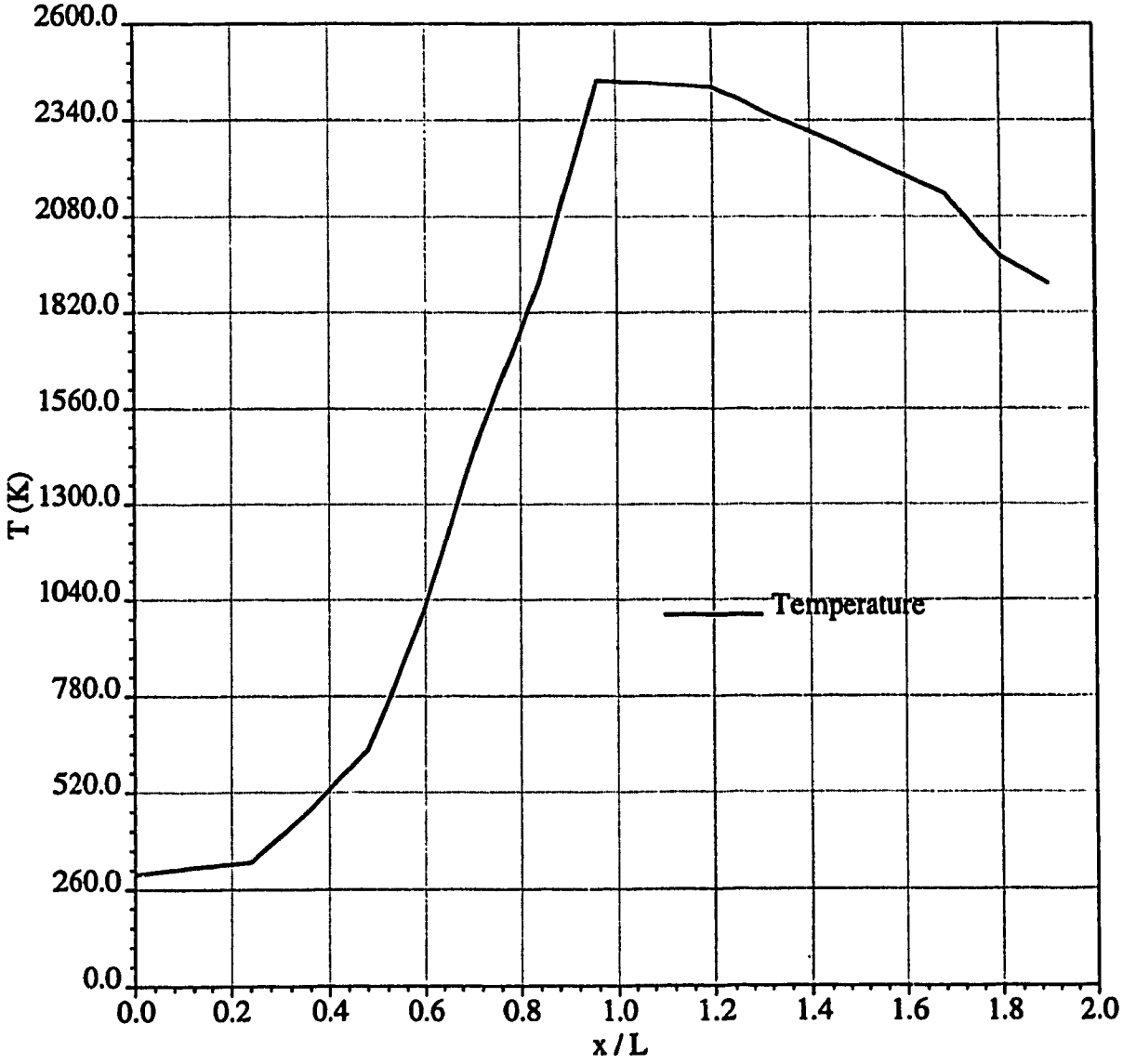

Figure 12. Temperature distribution along the centerline for a nonswirling jet flame

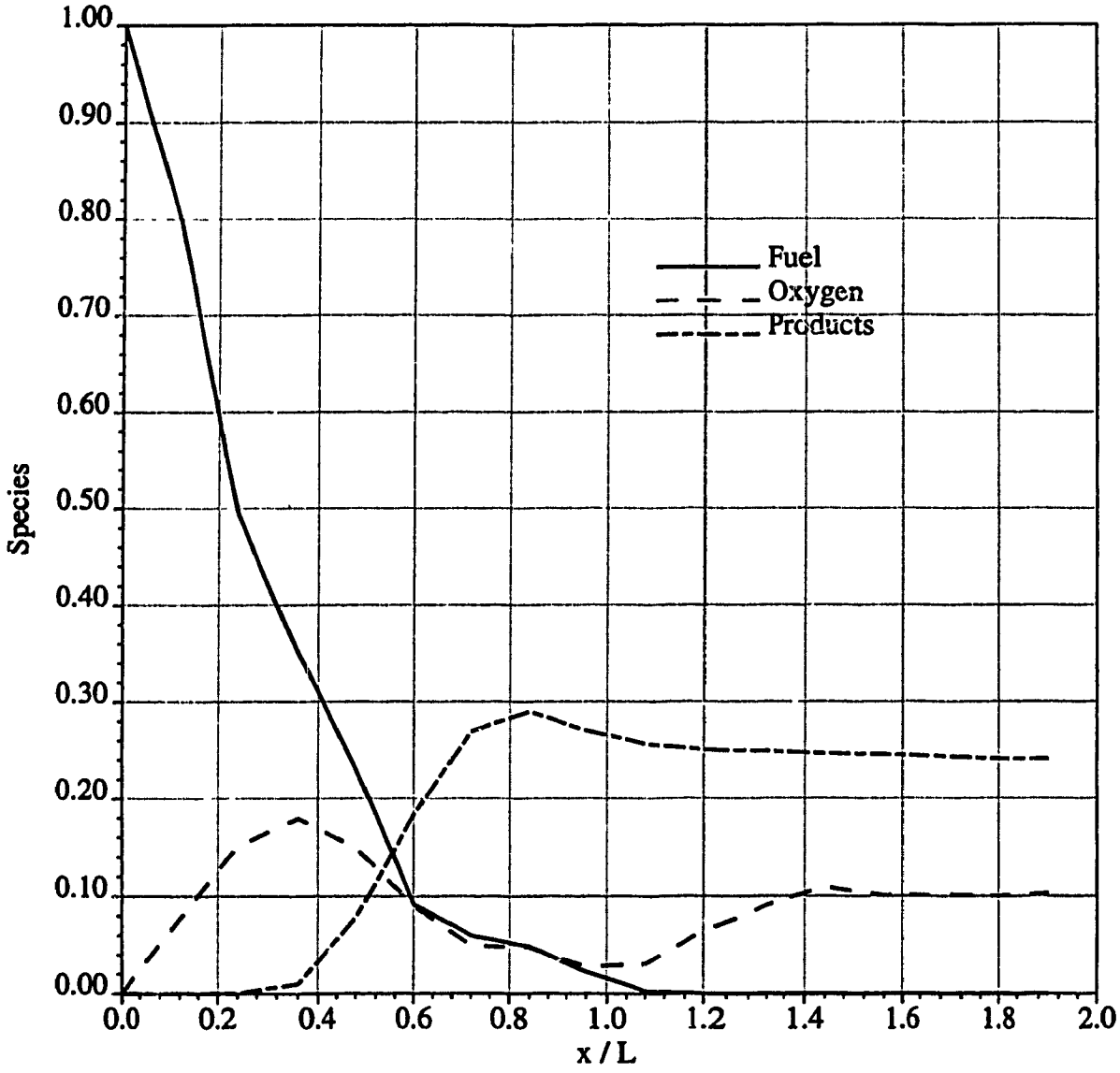

Figure 13. Species distribution along the centerline for a nonswirling jet flame

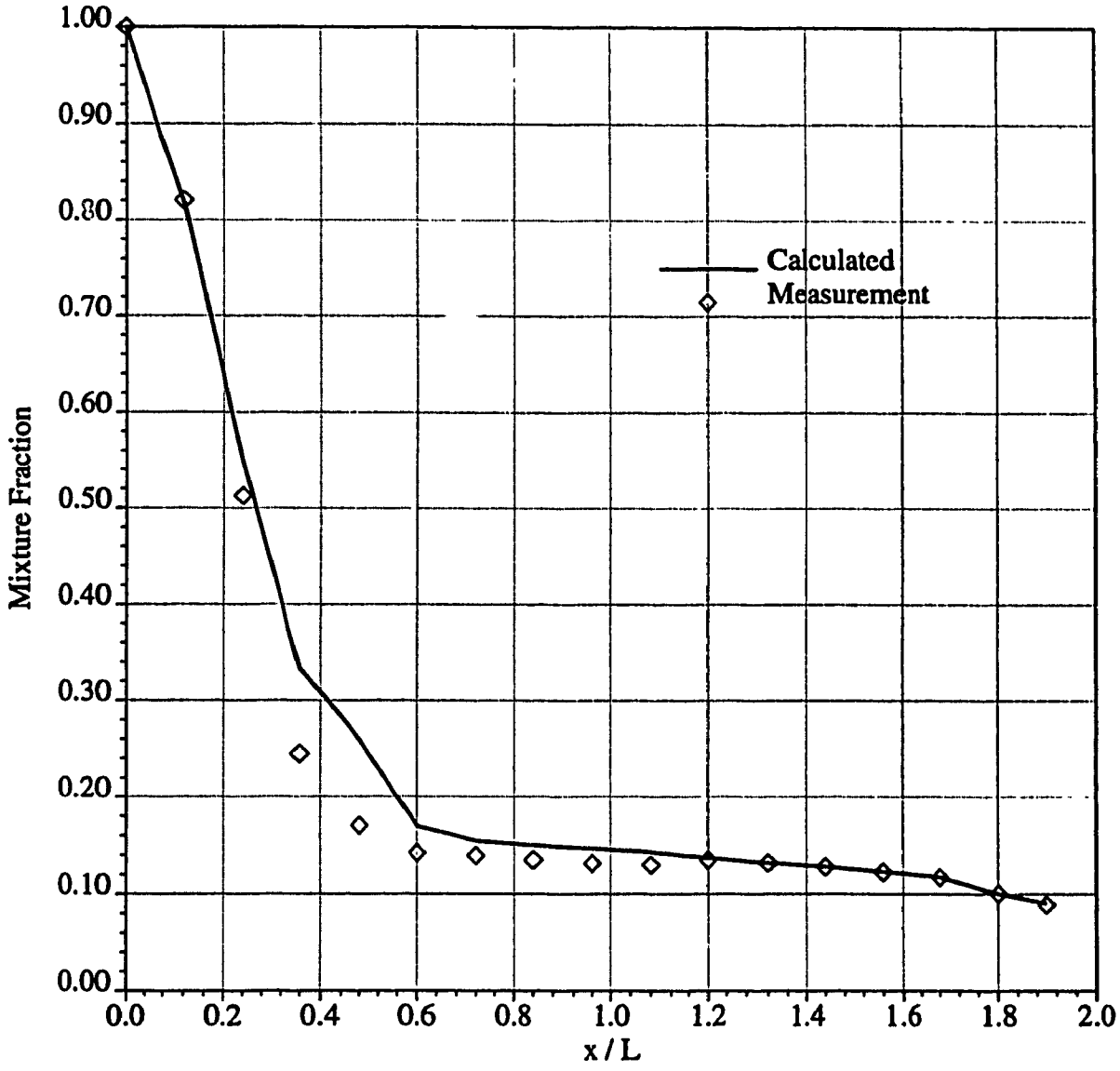

Figure 14. Experimental comparison of mixture fraction for a nonswirling jet flame.

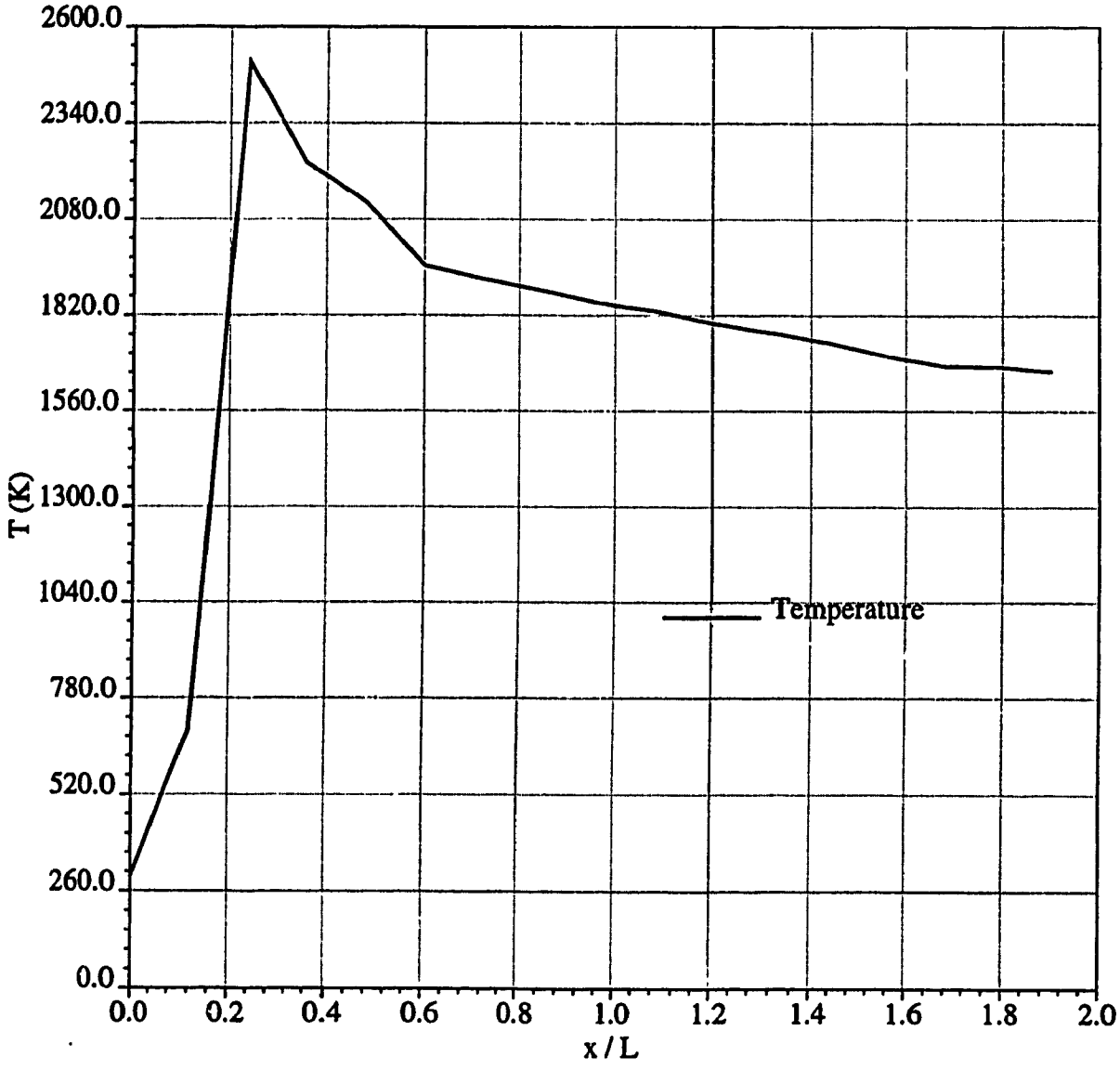

Figure 15. Temperature distribution along the centerline for a swirling jet flame.

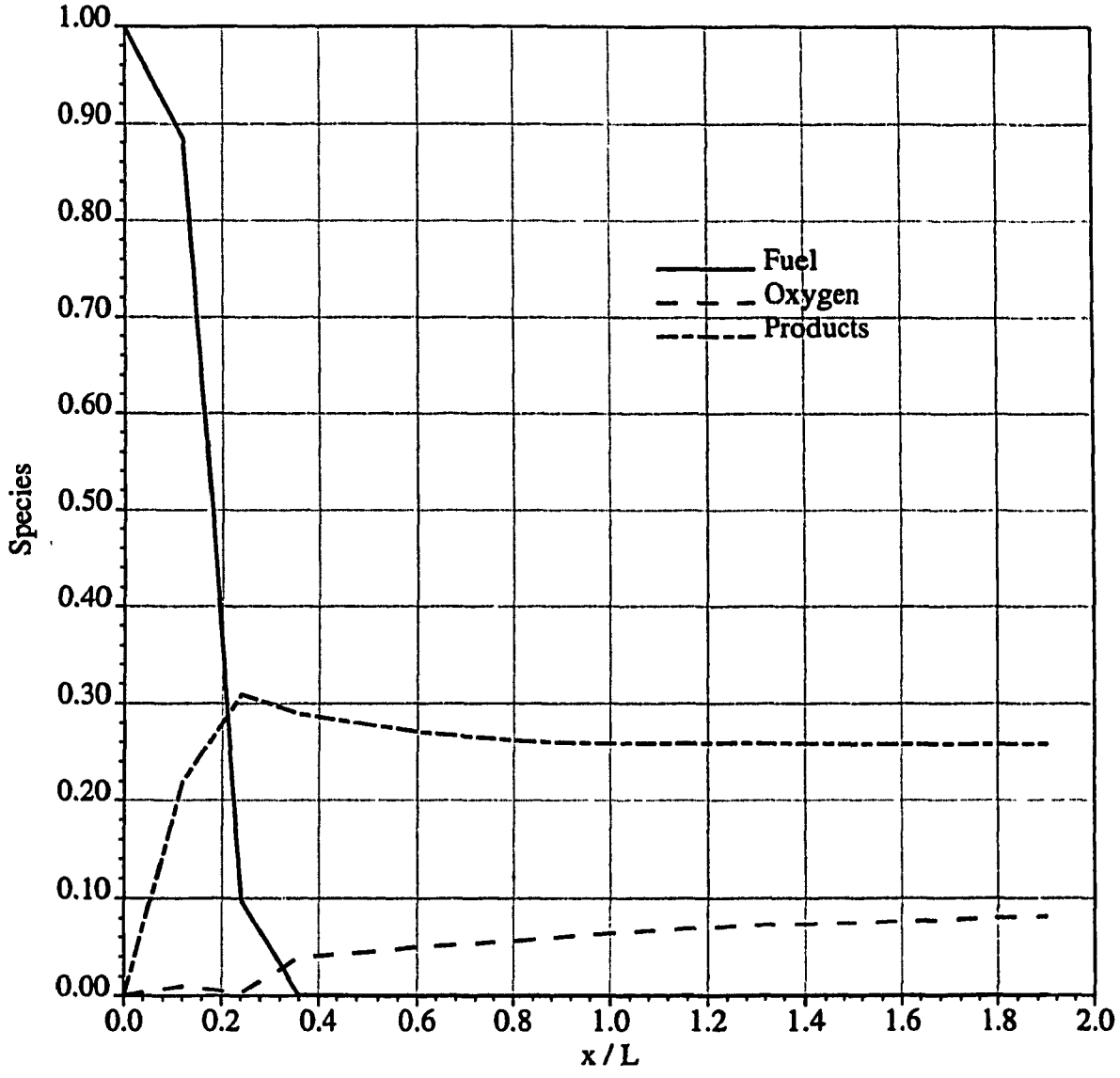

Figure 16. Species distribution along the centerline for a swirling jet flame.

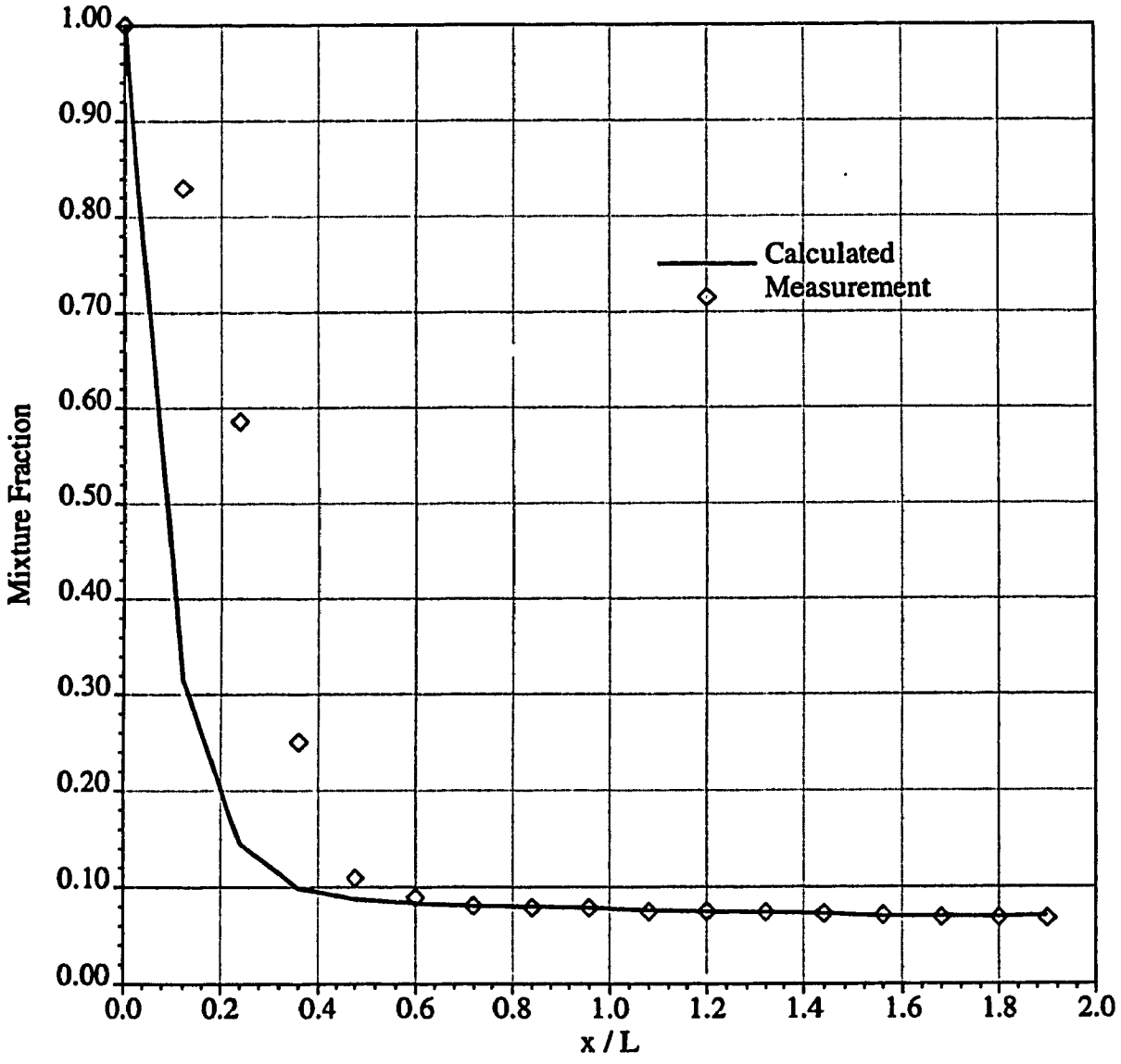

Figure 17. Experimental comparison of mixture fraction for a swirling jet flame.

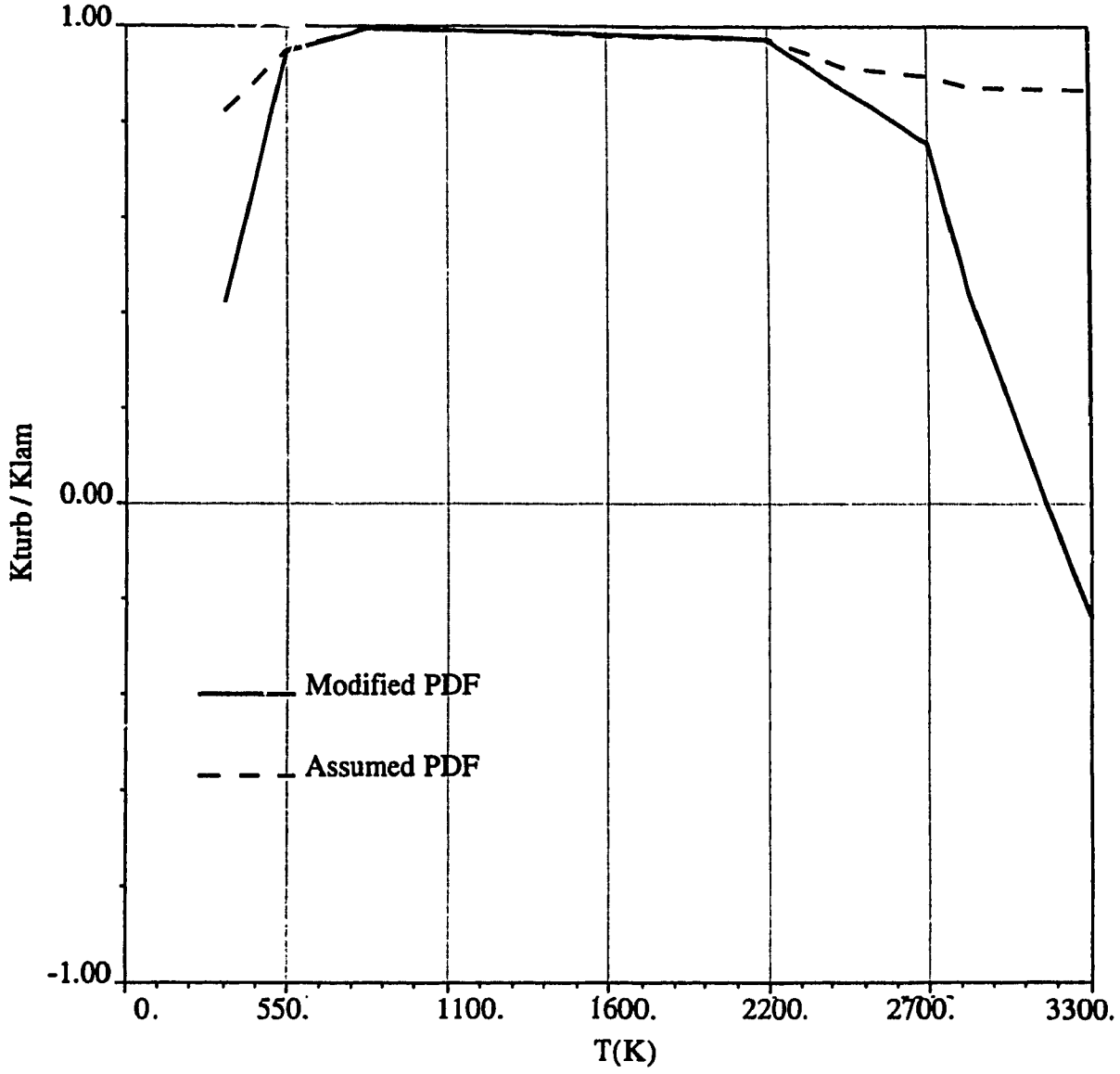

Figure 18. Comparison of modified and unmodified assumed pdf treated reaction rate for hydrogen-air reaction 1: $OH + O \leftrightarrow H + H_2O$.

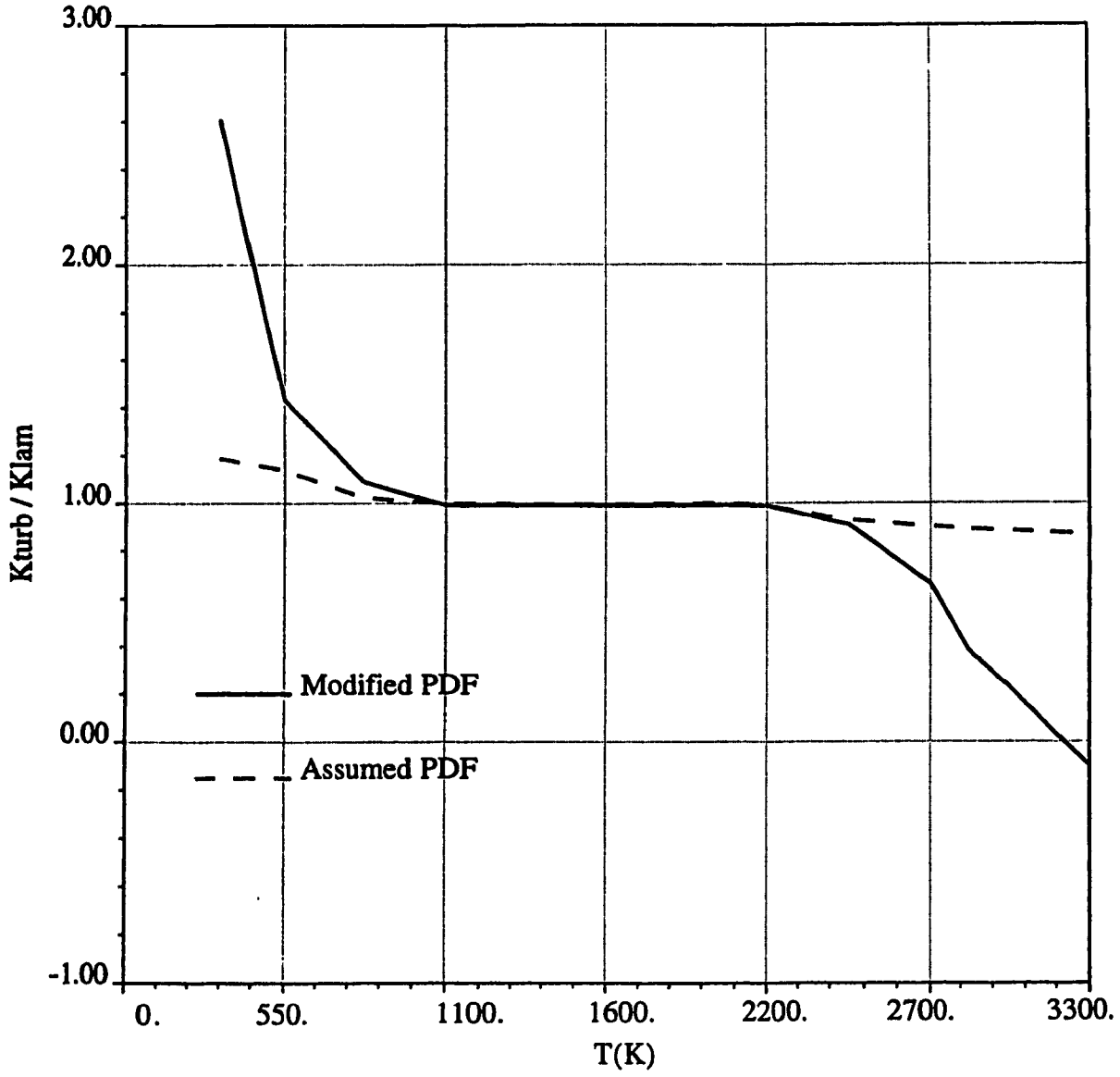

Figure 19. Comparison of modified and unmodified assumed pdf treated reaction rate for hydrogen-air reaction 2: $OH + H \leftrightarrow H_2 + O$.

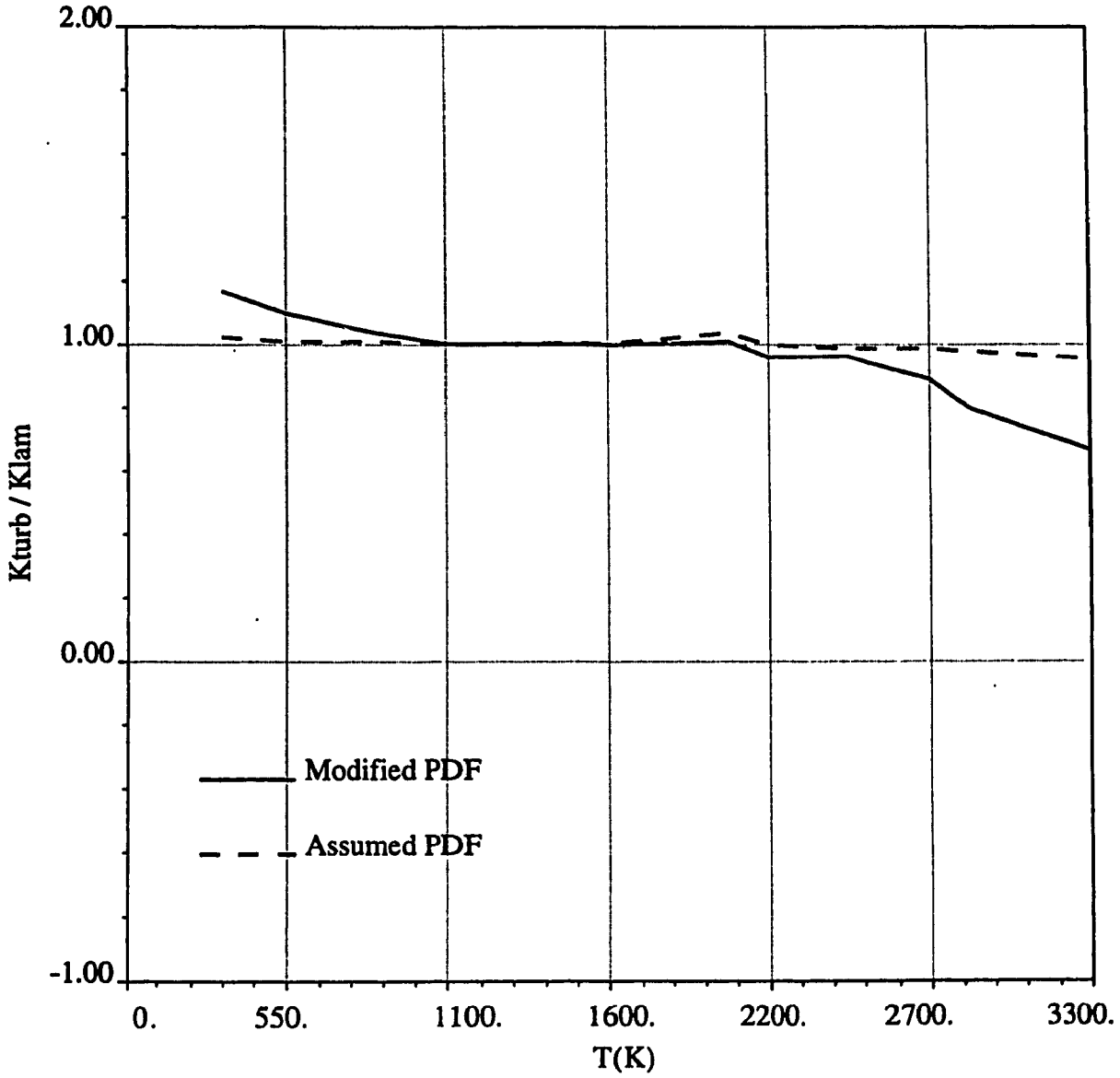

Figure 20. Comparison of modified and unmodified assumed pdf treated reaction rate for hydrogen-air reaction3: OH + OH <---> H_2 O+ O.

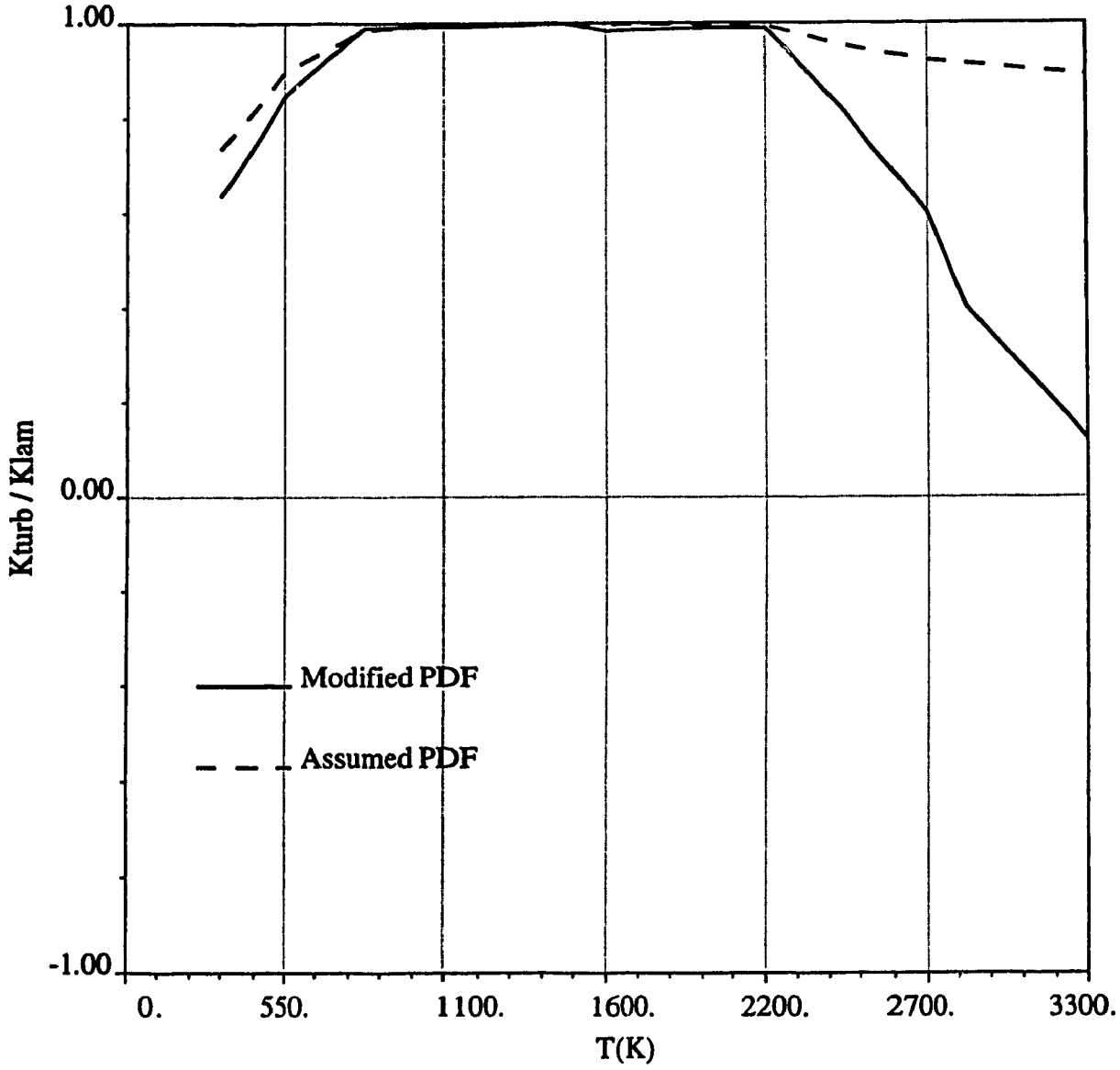

Figure 21. Comparison of modified and unmodified assumed pdf treated reaction rate for hydrogen-air reaction4: $OH + H_2 <---> H_2O + H$.

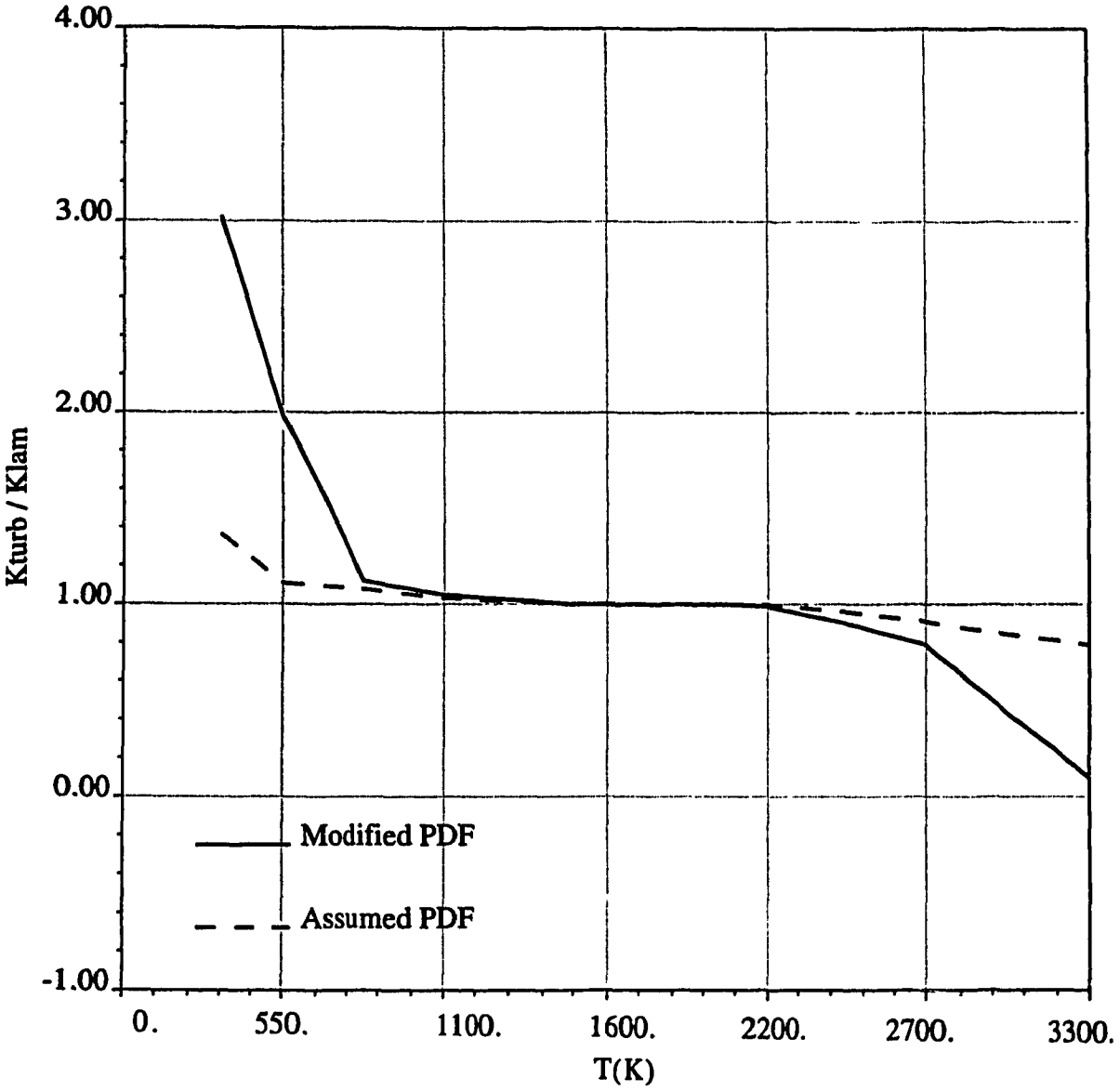

Figure 22. Comparison of modified and unmodified assumed pdf treated reaction rate for hydrogen-air reaction5: H+H+M <---> OH+ M.

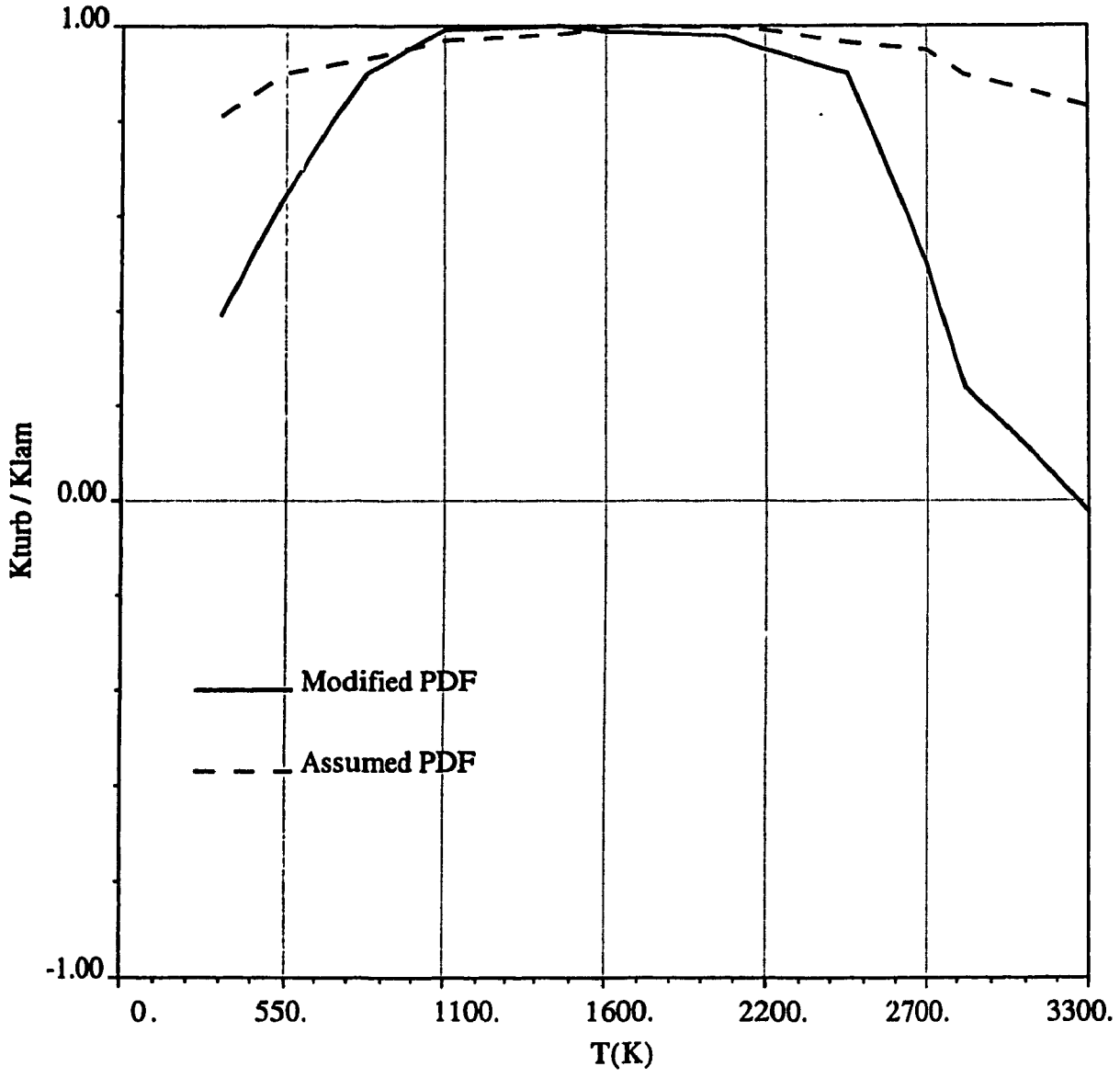

Figure 23. Comparison of modified and unmodified assumed pdf treated reaction rate for hydrogen-air reaction6: H+O+M <---> OH+ M.

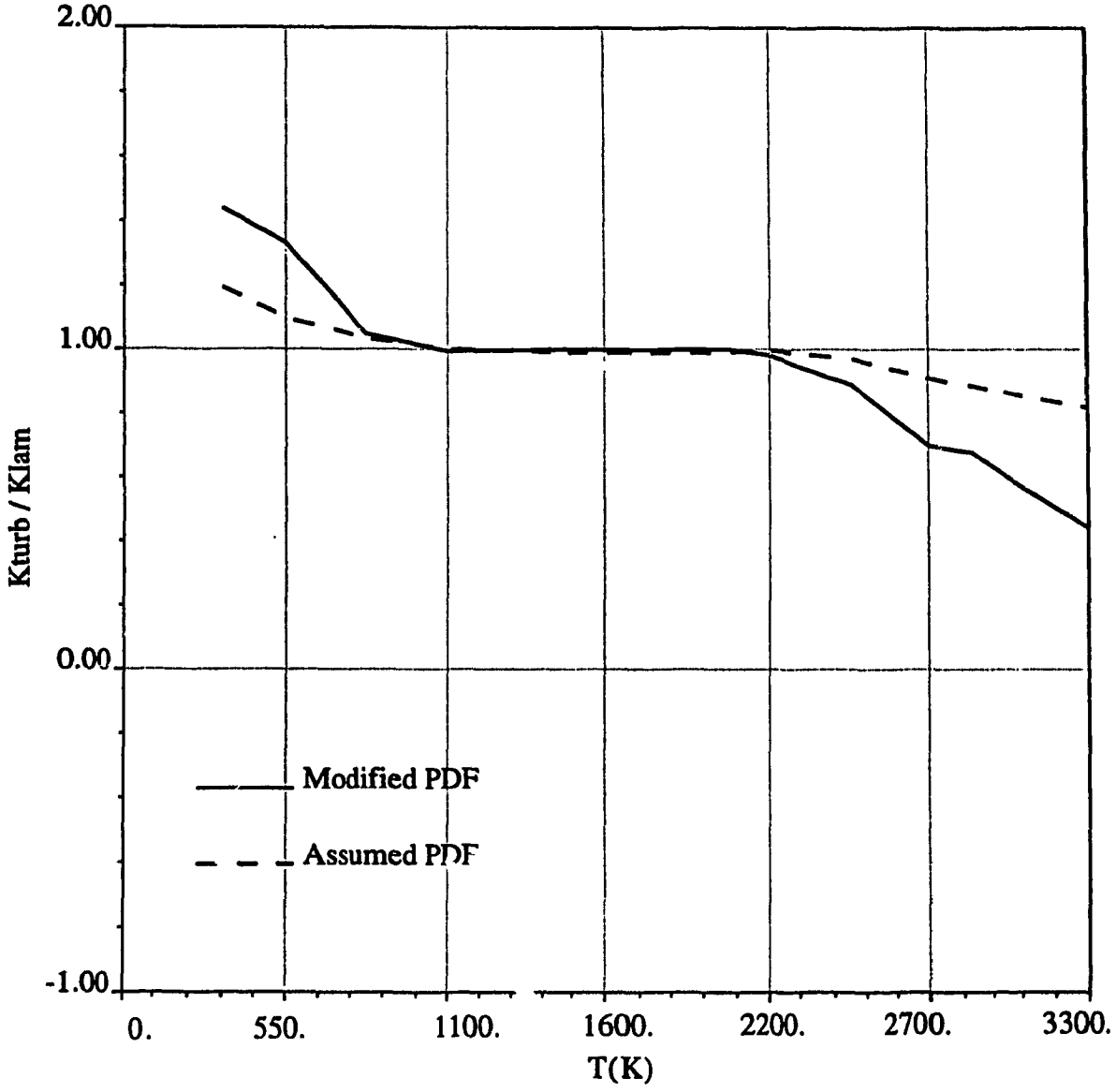

Figure 24. Comparison of modified and unmodified assumed pdf treated reaction rate for hydrogen-air reaction7: O+O+M <---> O_2+ M.

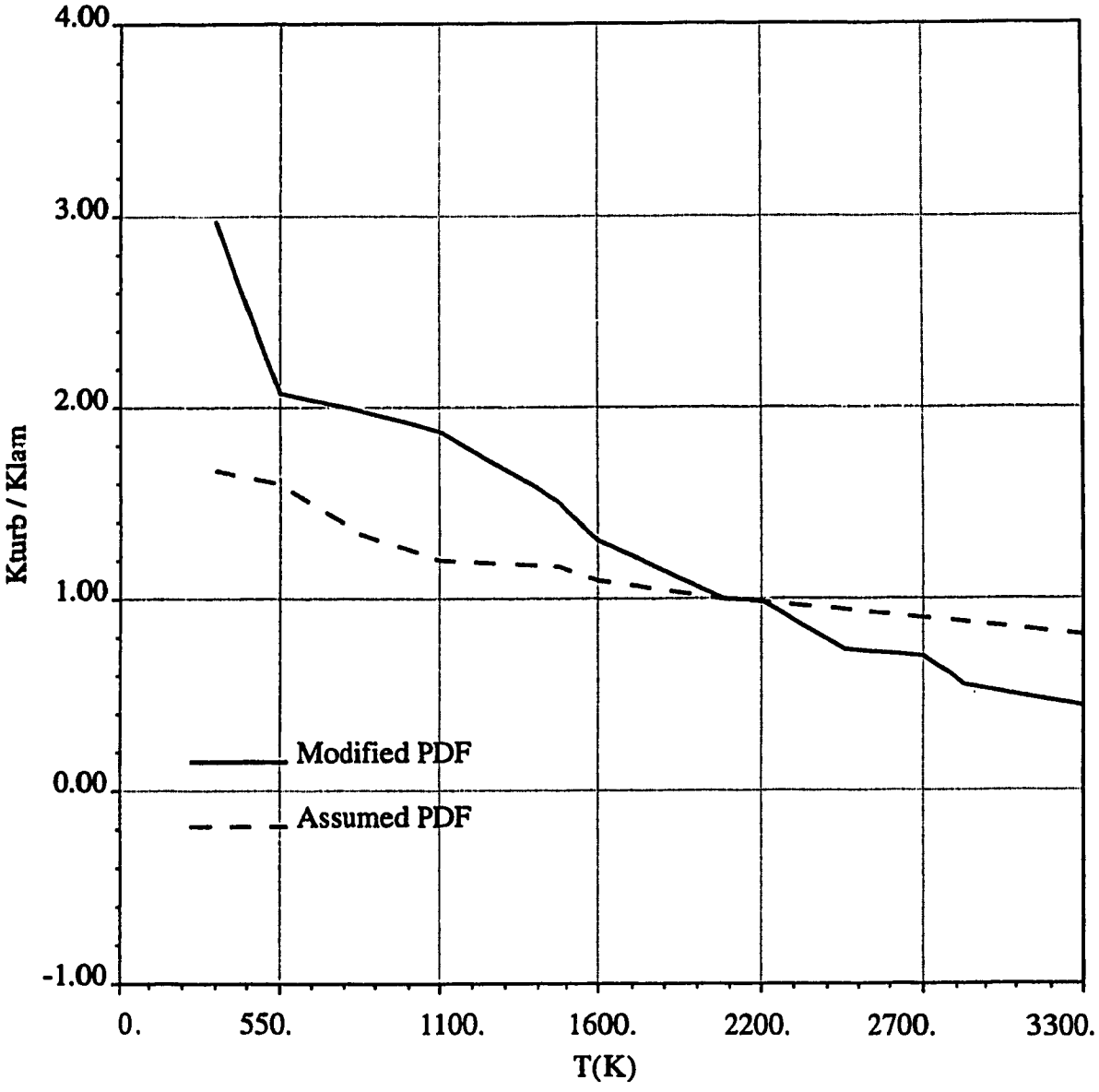

Figure 25. Comparison of modified and unmodified assumed pdf treated reaction rate for NOx reaction 1: O+ N_2 <---> NO+N.

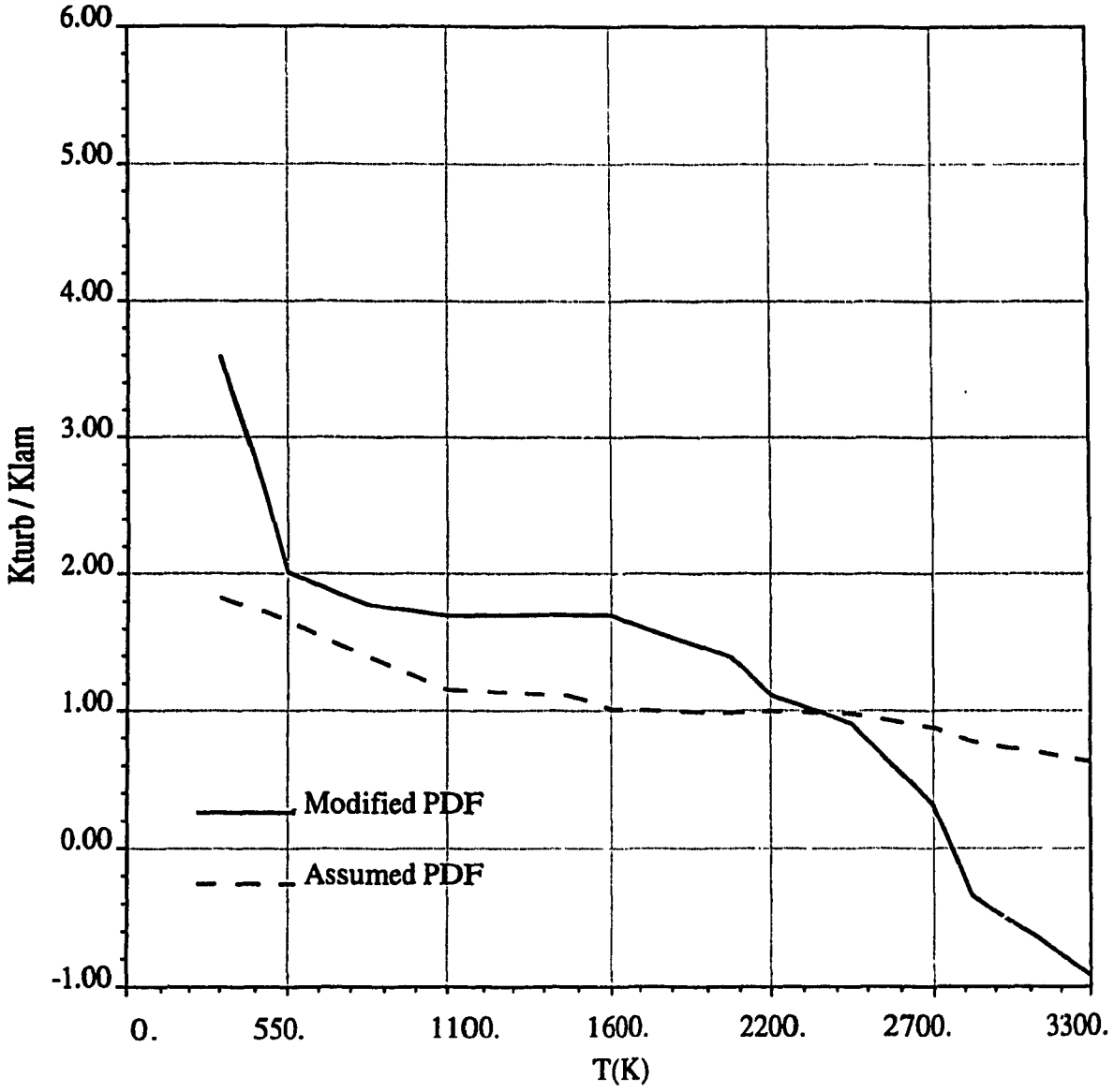

Figure 26. Comparison of modified and unmodified assumed pdf treated reaction rate for NOx reaction 2: $N+O_2$ <---> NO+O.

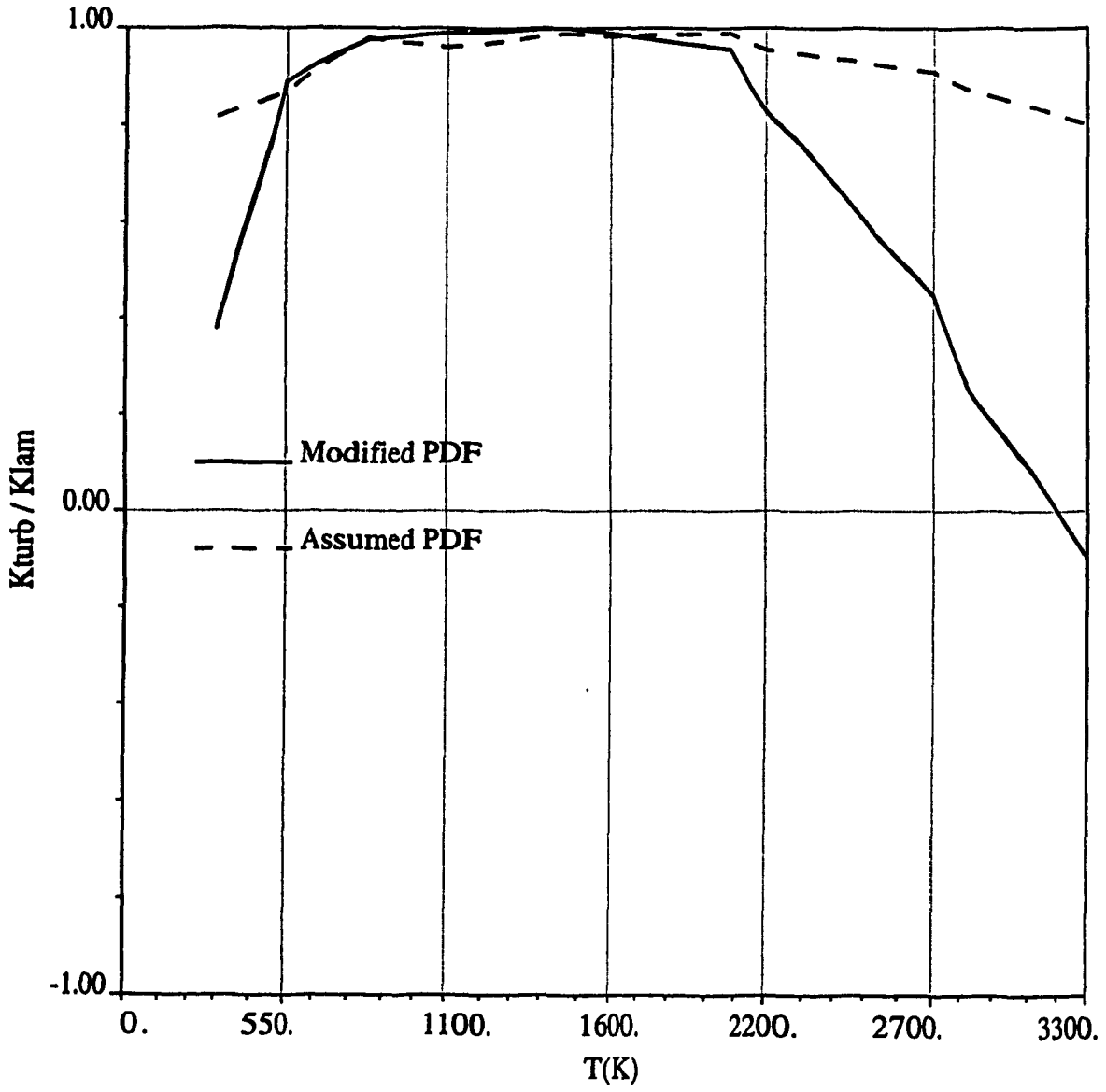

Figure 27. Comparison of modified and unmodified assumed pdf treated reaction rate for Nox reaction 3: N+OH <---> NO+H.